2001

Study of the Cross Sections of Fast Neutron Induced (n,2n), (n,p) and (n, a) Reactions on the Isotopes of Zinc, Germanium, Scandium and Zirconium

Rakib-uz-Zaman, Md.

University of Rajshahi

Study of the Cross Sections of Fast Neutron Induced (n,2n), (n,p) and (n, α) Reactions on the Isotopes of Zinc, Germanium, Scandium and Zirconium

A Dissertation
Submitted to the University of Rajshahi, Bangladesh
In Partial Fulfilment of the Requirements for the
Degree of Master of Philosophy

Examination Roll No. : 53 (Batch July'99)
Registration No. : 12181

Department of Applied Chemistry
and Chemical Technology
University of Rajshahi
Rajshahi, Bangladesh

November, 2001

DECLARATION

We the undersigned declare that the research work presented in this dissertation has been carried out by Md. Shuza Uddin under the joint supervision of Dr. Md. Rakib-uz-Zaman, Professor, Department of Applied Chemistry and Chemical Technology, University of Rajshahi, Rajshahi and Dr. Nurul Islam Molla, Chief Sci entific Officer, Bangladesh Atomic Energy Commission. The research work presented here is original. No part of this work has been used by anybody for the award of any degree previously.

Dr. Nurul Islam Molla
Co-supervisor
Chief Scientific Officer
Bangladesh Atomic Energy Commission
Dhaka

(Ex-Member, Physical Science)

(Dr. Md. Rakib-uz-Zaman)
Supervisor
Professor
Department of Applied Chemistry
and Chemical Technology
University of Rajshahi
Rajshahi

DEDICATED

TO

MY PARENTS

ABSTRACT

The fast neutron induced reaction cross sections were studied systematically in the energy range of 13.82 to 14.71 MeV using the neutron generator facility under identical conditions in order to provide real nuclear data required in the fusion reactor design and in developing semiconductor technology. In the present investigation, the activation cross section data for $^{64}Zn(n,2n)^{63}Zn$, $^{64}Zn(n,p)^{64}Cu$, $^{70}Zn(n,2n)^{69m}Zn$, $^{70}Ge(n,2n)^{69}Ge$, $^{74}Ge(n,\alpha)^{71m}Zn$, $^{76}Ge(n,2n)^{75m+g}Ge$, $^{45}Sc(n,2n)^{44m}Sc$ and $^{90}Zr(n,2n)^{89}Zr$ reactions in the energy range of 13.82 to 14.71 MeV were measured in an unified experimental condition. High purity samples of natural isotopic compositions were used. Each sample was irradiated separately by neutrons. Monoenergetic neutrons were produced via $^{3}H(d,n)^{4}He$ reaction at J-25 neutron generator facility of the Institute of Nuclear Science and Technology, AERE, Saver, Dhaka by the bombardment of the solid tritium target with deuteron. The different energies of the neutrons were obtained as a function of emission angle to the direction of incoming deuteron beam. The neutron activation technique in combination with high resolution HPGe-detector γ-ray spectrometry was used to measure the activities of the reaction products and to identify them. Peak area analysis was done using Multi Channel Analyzer (MCA) system based on personal computer. The effective neutron flux densities at the energies of interest were determined by the irradiation of monitor Al-foil with sample. The neutron flux obtained in the present work was in the range of 7.366×10^{5} to 1.855×10^{6} $ncm^{-2}s^{-1}$ using known cross section data obtained from H.Vonach. To determine the cross sections of the desired reactions, the well known activation equation was used. The total uncertainty in cross section was obtained by considering both the statistical errors and possible major sources of systematic errors. The overall uncertainties observed in our experiment were in the range of 7- 15 %.

The measured reaction cross section values along with the available literature data have been plotted as a function of neutron energy to get the excitation functions of the reactions. The theoretical cross section calculations using statistical code SINCROS-II in the energy range of 13 to 15 MeV were performed to validate the experimental data theoretically. In most cases, the calculated values agree fairly well with the experimental results. In the present experiment, it has been observed that the cross section values of all the (n,2n) reactions increase with increasing neutron energy. The value of (n,α) reaction cross section also increases with the increase of neutron energy whereas the value of cross section of (n,p) reaction decreases with increasing neutron energy. The measured data showed significant improvement in accuracy in comparison with literature value. The obtained data, therefore, will offer substantial nuclear data base for fusion reactor design, current evaluations of neutron activation cross section and nuclear model calculations for nuclear technology applications.

CONTENT

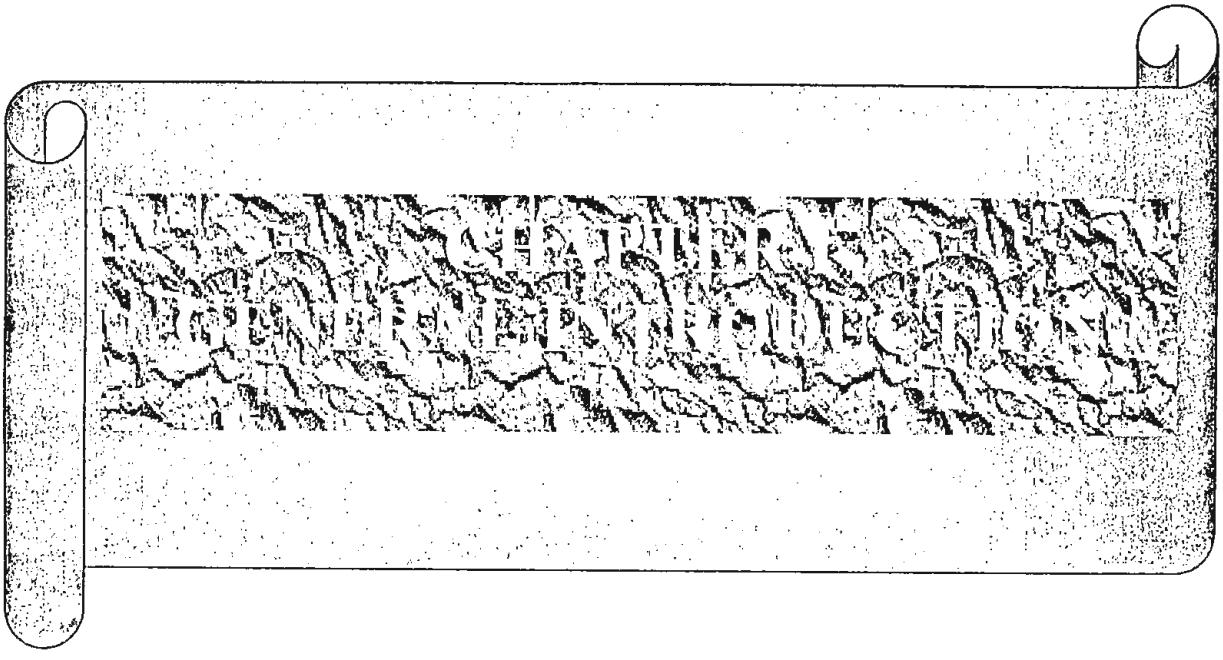

CHAPTER I

GENERAL INTRODUCTION

One of the characteristic features of our time is the emergence of nuclear science and the utilization of the results achieved in the field. The discovery of neutron by Chadwick (in 1932) and the invention of particle accelerators thereafter had given an enormous impetus to the development of nuclear reaction studies. Wherever radioactivity and nuclear reactions are concerned, energetic atom and transmutation effects are at work. The study of the reactions of energetic atoms is of interest mainly for two reasons : i) to identify new reactions that are not common with thermal atoms and ii) to acquire quantitative information on the reaction cross section as a function of energy and on the reaction threshold for new reactions.

Radioactivities produced in structural materials with neutrons as well as with charged particles are of immense importance in the whole range of nuclear applications. A particular structural material may be consisted of many stable isotopes. Fast neutrons, therefore, lead to the formation of many radioactive products. Therefore an accurate knowledge of their formation cross sections is important for estimating the total induced activity. A study of (n, charged particle) reactions on the structural materials is of great importance since such reactions give rise on the one hand to transmutation products which might strongly influence the development of damage microstructure and thereby lead to property changes and on the other to hydrogen and helium gases which may cause high temperature embrittlement of structural materials[1]. The experimental data, generally obtained via the activation technique, are rather discrepant [2-4].

In figures 1.1 and 1.2 are shown two possible designs of future Tokamak-type fusion reactors. Figure 1.1 shows plasma composed of deuterons and tritons surrounded by a first wall of toroidal shape which in turn is surrounded by a shielding blanket in which, through interaction of the neutrons produced in the plasma with lithium, tritium is produced. Figure 1.2 shows a complete design of a possible fusion reactor along with

heat exchanger and other components. It also shows how tritium is fed back into the plasma.

Developing a material suitable for the first wall and similar critical locations is one of the most difficult problems of fusion. Present materials fail in their resistance to radiation damage, creep and other things to meet the lifetime requirements of a fusion reactor by about an order of magnitude; ingenious considerations for frequent replacement present cost penalties. Thus materials development will be a critical pacing item in the future fusion programe[5].

The deuterium and tritium in the plasma react according to the scheme $D + T \rightarrow (^4He + 3.25\ MeV) + (n + 14.1\ MeV)$. The helium ion deposits its energy in the plasma thereby keeping the plasma hot. The neutron deposits its energy in the blanket that surrounds the discharge plasma. The blanket not only absorbs the 14 MeV neutron energy, but produces an additional 9.2 MeV of energy per incident neutron. In addition the neutron reactions with the natural lithium in the flibe, together with the neutron multiplication reactions in the beryllium[6], easily produce a tritium breeding ratio of 1.04.

The details of compilation of several types of cross sections used in the nuclear heating calculation are described elsewhere[7]. The distribution of tritium production reaction rates i.e., the tritium breeding ratio by $^6Li(n,\alpha)$ t reaction is 0.80 and the tritium breeding ratio by $^7Li(n,n'\alpha)$ t reaction is 0.36. The neutron flux at the first wall was calculated as 6.3×10^{13} n cm^{-2} s^{-1} for 14 MeV; 1.96×10^{14}n cm^{-2} s^{-1} for E >0.1 MeV and 2.7×10^{14} n cm^{-2} s^{-1} for total neutron. Difference of reaction rates between the plasma and coolant sides of the first wall are about 10% for both (n,α) and (n,p) reactions[8]. Since radiation damage can cause reduction in strength and ductility, appropriate evaluation of the irradiation behavior of the wall material is of major importance in the design study.

The interaction of radiation with crystalline solids has been studied extensively in the last two decades, mainly as a result of the development of nuclear energy. For non-fissionable metals major attention must be paid to those types of radiation that are able to

displace atoms from their normal lattice positions. In this respect irradiation with high energetic particles such as fast electrons, neutrons, protons, deuterons and ions are to be considered. More indirectly, thermal neutron irradiation and α-irradiation may also cause atomic displacements. Transmutation elements resulting from nuclear reactions may in some cases be important too[9]. In recent years increasing attention has also been paid to the effect of spontaneous recombination between vacancies and interstitials, occurring even at very low temperature. Theoretical and experimental work, as well as computer work in this field, have contributed to a better understanding of the damage production mechanisms[10-16].

The most important individual particle interactions with the first wall have been briefly surveyed by G.M. McCRACKEN[17], with a view to estimating erosion rates. For this purpose particle fluxes, energy spectra and yields are required. Experimental data pertaining to the fatigue failure of irradiated metals are almost non-existent. What data do exist are usually from post-irradiation tests where the damage state is not the same as it would be during cyclic stress in a reactor. The theoretical explanations for the effect of radiation-produced defects on the mechanical properties of metals are not very well developed, nor are they in sufficiently good shape to allow extrapolation from the present fission reactor data to 14 MeV neutron damage.

G.L.KULCINSKI[18] has described that the followings are the main requirements for future work in radiation damage of first-wall materials.

a) Comparison of 14 MeV neutron displacement damage to fission reactor and heavy ion damage. It is of paramount importance to determine if 14 MeV neutron displacement damage is simply an extension of fission reactor damage when appropriate interaction cross sections are taken into account.

b) Investigation of the synergistic effects of helium and hydrogen on displacement damage produced by neutrons should be pursued. It is important that such studies be carried out properly, i.e., gas atoms should be added to the solid in a direct proportion to the displacement damage predicted by theory in a fusion reactor.

c) The effect of displacement rate on the microstructural distribution of defects must be understood.

d) It is necessary to understand the effect of non-gaseous transmutation products on the microstructure of the damage state. The concern here stems from the fact that in metals like niobium the concentration of the major transmutation product, zirconium, may actually exceed the solubility limit in the host metal.

e) A concerted effort must be mounted towards the theoretical understanding of the effects of 14 MeV neutrons on the mechanical properties of materials. For example, most of the present fusion reactor designs are sorely lacking in the assessment of the fatigue lifetime that might be expected under large stress, strain and thermal excursions. A large part of the theoretical model work can be, and is being, pursued in the various fission reactor programs of the world.

The accurate knowledge of neutron interaction cross section around 13-15 MeV energies are of significant interest for fusion facilities. In D-T fusion almost 80% of the total energy is carried off by 14 MeV neutron [19]. In fusion reactor, the 14 MeV neutrons produced in the plasma are slowed down in the first wall and in the blanket. A typical spectrum of the neutrons entering the blanket extends down to keV energies, with the bulk of the neutrons centered in the MeV region and a strong component of 14 MeV neutrons. For neutronic calculations therefore all neutron cross sections of the fusion reactor materials have to be known from keV energies to about 15 MeV, with an emphasis on partial reactions such as (n,p), (n,np), (n,α), (n,nα), (n,2n) etc. and on energy and angular distribution of secondary particles (neutrons and charged particles) emitted in these reactions.

The (n,xn), (x $\geq$2) and (n,f) reactions can be used to enhance the neutron flux through neutron multiplication. In normal D-T fusion reactors, materials with high (n,2n) cross sections are used as main or additional materials in the first wall. They can lead to a significant multiplication of the neutrons impinging on the blanket. These neutrons enhance tritium breeding. Because of the Coulomb barrier, the emission of neutrons is more likely than that of charged particles.

Neutrons captured in (n,p), (n,α), as well as (n,γ), (n,d), (n,t) and (n,^{3}He) reactions with lower cross sections are not available for tritium breeding. Major parasitic neutron absorbers are the structural materials used in the first wall and in the blanket through (n,p) and (n,α) reactions.

14 MeV neutrons have a rather singular threefold importance:

(1) They represent about the upper energy limit of neutrons occurring in nuclear fission reactors.

(2) The D-T reaction in which 14 MeV neutrons are generated represents the basis for all contemporary fusion reactor designs based on magnetic plasma confinement.

(3) The D-T reaction used in neutron generators allows the measurements of 14 MeV neutron cross sections.

Now a days, neutron production from plasma is a reality, which makes the nuclear data specially useful in monitoring plasma temperature and assessing D-T fuel "burn" rates during the containment intervals. For blanket design purpose, tritium breeding cross sections and neutron multiplier cross sections for energies around 14 MeV and below are important. Radiation damage by energetic neutrons and long-lived activation of fusion reactor structure are also important. These are the effects which will influence the longevity and service of reactor facilities.

Since 14 MeV neutrons dominate the neutron field around D-T plasma, the accuracy of the cross section data at 14 MeV neutrons are important for the prediction of reactor parameters such as tritium breeding, nuclear heating, radiation damage, radioactive waste estimation, calculation of the activation in materials to be used in fusion reactors and so on. Hence nuclear data have a vital role to play in nuclear science and technology. To date there has been enormous advancement in the field of nuclear data measurement, evaluation and nuclear reaction theory as well as applications. The want of nuclear data, particularly nuclear cross sections have been increased during the last three decades. Measurement, calculation and evaluation of these cross sections have

been extensively undertaken during these days. Herein are described some fundamentals pertaining to the present investigation.

1.1 Basic Properties of Nuclear Reactions

A nuclear reaction refers to a transformation of a target nucleus by bombarding it with an incident particle. The interaction of this incident particle and target is conveniently described in terms of the cross section. This quantity essentially gives a measure of the probability for a reaction to occur and might be determined if the nature of the interaction between the particles is known.

In every nuclear reaction, the total energy, being the sum of the rest mass energies and kinetic energies of reactants and resulting products, must be conserved. The conservation of energy can describe the Q value of a reaction. Q value can be derived from the difference in the nuclidic masses and signals whether a reaction is energetically possible. However a definite amount of minimum energy is necessary in initiating a nuclear reaction and is called the threshold energy, E_{thres}. It takes into account the energy which is required to conserve the momentum in the reaction and can be represented as

$$E_{thres} = -Q\left(1+\frac{m}{M}\right) \qquad \text{.....(1)}$$

Where m and M are the mass of the projectile and target nucleus, respectively. However a particle has also to surmount the Coulomb barrier, not only on entering but also on leaving the nucleus.

The cross section for the reaction A(x,y)B is denoted by $\sigma_{x,y}$ and is defined as the number of reactions of the type shown (x,y) that take place per cm^2 per second under conditions of unit density of target nuclei and unit flux of the incident particles. The cross section has the dimension of area, is measured in units of barns ($1b=10^{-28}\ m^2$) and

is known as an integral cross section when integrated over all angles. The variation of the cross section with incident energy is called the excitation function.

1.2 The Nuclear Activation Process

The first and one of the most successful conception of the nuclear transformation process is the compound nucleus[20] which is a many body system of strongly interacting particles and is formed by the amalgamation of an incident particle with a target nucleus. Very often the projectile and target lose their identity and the entrance channel is forgotten. The incident particle captured by the nucleus gives up its energy to few nucleons and the new nucleus thus formed is in an excited state. If E_i is the kinetic energy of the incident particle of mass m, the excitation energy of the compound nucleus is given by[21]

$$E^* = \frac{E_i M}{m+M} + E_B \qquad \text{.....(2)}$$

Where M is the mass of the target nucleus and E_B the binding energy of the particle in the compound nucleus. A compound nucleus once formed, can decay in a number of different ways, each with its own probability. Due to the similarity of this process with the escape of molecules from a drop of hot liquid it is also known as the evaporation process. The spectrum for this process is symmetric to 90^0 and eventually isotropic. The interaction time is 10^{-14} to 10^{-18} seconds. Another way of interacting an incident particle with the nucleus without forming an intermediate state is the direct reaction. The direct reaction region is depicted at the high energy end of a nucleon emission spectrum. The angular distribution in this process is anisotropic and forward peaked. The interaction time is in the order of 10^{-22} seconds.

Whenever a product nucleus is in an excited state, it usually deexcites to the ground state in a time of the order of 10^{-13} seconds or less. In some cases, the time may be long enough to be measurable, ~0.1 seconds or longer. Such a nucleus is said to be in

a metastable and is distinguished from its ground state by an asterisk, B*. The nuclei B of the same mass number and atomic number which differ in this way in their state of energy, are called isomers. The isomeric state decays either by γ-ray emission to the ground state or by electron capture, β or α particle emission to another nuclide. The process of reversion to the ground state by emission of γ-ray is called isomeric transition (IT). Weizsacker[22] suggested that, if a relatively small energy difference between the excited state and the ground state of a nucleus was associated with a large spin difference between the nucleus in the one state and in the other, the transition would be forbidden, that is, the probability of the transition would be reduced. Thus the nucleus in the metastable state would have a measurable life time.

1.3 Neutron Induced Reactions

Neutron, a subatomic particle without electrical charge is composed of three tiny objects called quarks, bound or "glued" together in the neutron by massless particles known as "gluons"[23]. The mechanism of neutron induced reactions can be studied using the available data and it is observed that for nuclei with $40<A<100$ some form of statistical or evaporation model can explain the reaction, while for $A>100$ the reaction is less likely to proceed through a compound nucleus but rather by a direct reaction[24]. These reactions are somewhat helpful in explaining the degree of clustering of nucleons near the nuclear surface and the importance of shell effects. Hence the basic research on fast neutron induced reactions is of considerable significance in testing nuclear models.

1.4 Neutron Sources

Recently, much progress has been made in the production of intense neutron sources. The availability of neutron sources with well defined characteristics is essential for a detailed study of neutron induced reactions. The neutron sources are categorized as monoenergetic and continuous (white neutron sources) sources. There are three principal methods for producing neutrons. These are:

i) interaction of alpha or gamma radiation from radioactive substances with light elements like Be

ii) reaction of accelerated charged particles from accelerators with light nuclei

iii) fission reactor.

The first and third methods produce neutrons of continuous energy. The production of monoenergetic neutrons is achieved by the second method.

Different types of neutron generator producing monoenergetic neutrons through D-D and D-T reactions are used in many laboratories around the world with a view to facilitating research on nuclear reactor technology. A SAMDES J-25 AID (France) Neutron Generator was installed at the Institute of Nuclear Science & Technology(INST), Atomic Energy Research Establishment (AERE), Savar, under the coordinated research program with the International Atomic Energy Agency (IAEA) for the measurements of nuclear data. In J-25 neutron generator, 14 MeV monoenergetic neutrons are produced via $^{3}H(d,n)^{4}He$ reaction. The large positive Q-value[25] (17.6 MeV) and low atomic number makes it possible to produce 14 MeV neutrons even at low deuteron incident energies, e.g., E_d=100-200 keV. This intense neutron source is, therefore, used for the investigation of the interaction of fast neutrons with structural materials of nuclear reactors which are important for design, development, safe operation of fission and fusion nuclear reactors. In activation measurements, monoenergetic neutron sources are needed since the determination of cross section is energy dependent. Therefore in this work, only neutrons produced from the reactions of accelerated charged particles are discussed further in the latter section.

1.5 Present Status of Neutron Cross Section Data for Zn, Ge, Sc and Zr

A detailed survey of literature shows that ample cross section data of the (n,2n), (n,p) and (n,α) reactions on the isotopes of zinc, germanium, scandium and zirconium in the energy range of 13-15 MeV are not that available. S.M. Qaim et al.[26]measured the excitation functions for (n,p) reaction on ^{67}Zn, ^{70}Ge, ^{73}Ge, ^{74}Ge isotopes and (n,α) reaction on ^{68}Zn isotope in the neutron energy range of 6.2 to 12.4 MeV. R.U.

Miah[27]measured the cross sections of (n,2n) reactions on ^{45}Sc, ^{64}Zn, ^{70}Zn, ^{70}Ge, ^{76}Ge, ^{90}Zr isotopes and (n,p) reaction on ^{64}Zn and (n,α) reaction on ^{74}Ge isotopes in the energy range of 13.64-14.71 MeV. R.U. Miah also performed the theoretical calculation of cross sections of $^{64}Zn(n,2n)^{63}Zn$, $^{64}Zn(n,p)^{64}Cu$ and $^{76}Ge(n,2n)^{75m+g}Ge$ reactions using statistical code EXIFON[28]. Wenrong et al.[29] reported both the measured and evaluated cross section data for (n,2n) reaction on ^{45}Sc, ^{70}Zn and ^{90}Zr isotopes in the energy range of 13 to 15 MeV. Recently, Belgaid et al.[30] measured the cross section of $^{64}Zn(n,p)^{64}Cu$ reaction at 14.5 MeV neutron energy. Cullen et al.[31], Bychkov et al.[32], Ikeda et al.[33] and G. Erdtman[34] reported neutron activation cross section on the selected reactions. In most cases, it has been shown a significant deviation in cross section data measured / evaluated by different authors for the same reaction. The main sources of the discrepancy in the experimental data arise from the difference of the experimental conditions, neutron source characterization, radiation measuring technique, neutron monitoring method, standard cross section data and nuclear data (gamma-ray, half life, natural abundance) used to deduce the final data. Although extensive data for (n,2n), (n,p) and (n,α) reactions on various nuclides at 13-15 MeV neutron energy are found in the literature, many of them appear to contain relatively large systematic errors and needs further evaluation.

1.6 Aim and Scope

Semiconductor electronic components are sometimes needed to be used in intense fast neutron fields for nuclear measurements. There are many semiconductors available, but very few of them have practical application in electronics. Germanium has become the model substance among the semiconductors because it can be purified relatively well and crystallized easily. Therefore, the investigation of fast neutron interactions with atomic nuclei of this semi-conductor material would yield important information to the study of nuclear structure and reaction mechanism and provide a good way of testing the application of nuclear models. From the view point of semi-conductor technology, neutron activation cross section data around 14 MeV have also become important specially for calculations on nuclear transmutation rate, induced activity,

radiation damage and so on. Such data are also needed for further improvement of semi-conductor technology. The cross sections of the neutron induced reactions for Ge isotopes are of some interest, both from the fundamental point of view and for estimating radiation damage in semi-conductor materials.

Extensive measurements of fast neutron induced reactions cross sections on structural materials of fission and fusion reactors have been carried out during the last years at several laboratories over the neutron energy range from threshold up to 15.0 MeV. There is high demand of precision cross section data for engineering requirements as well as for validation support of nuclear model calculations.

The prediction of atomic displacement rates and helium production rates requires a knowledge of the cross sections of the nuclear reactions on the isotopes of structural materials. In addition nuclear power engineering needs, based on fission reactors, many other regions of science and technology have very large needs in nuclear cross section data.

New regions of nuclear data applications appeared for example such as nuclear safety, alternative reactors, space reactors, industrial applications, decommissioning of long time operated fission reactors, high energy neutron dosimetry which widen the needs for nuclear data both in energy range and number of reactions. To meet these needs the experimental and theoretical investigations are made of radiation interactions with nuclei in many countries and during long period of time.

The results of intensive activity of nuclear scientists allowed to meet many requirements, but nevertheless the present and future requirements put new tasks both in increasing nuclear cross section data amount and improving reliability and accuracy of evaluated data. It can be mentioned that the uncertainties in nuclear data lead to uncertainties in the prediction of reactor parameters. Large uncertainties in turn lead to the large and expensive margins in design.

In view of these consideration, we intend to carry out a piece of research work on the measurement of excitation functions of the reactions $^{64}Zn(n,2n)^{63}Zn$, $^{64}Zn(n,p)^{64}Cu$, $^{70}Zn(n,2n)^{69m}Zn$, $^{70}Ge(n,2n)^{69}Ge$, $^{74}Ge(n,\alpha)^{71m}Zn$, $^{76}Ge(n,2n)^{75m+g}Ge$, $^{45}Sc(n,2n)^{44m}Sc$ and $^{90}Zr(n,2n)^{89}Zr$ in the energy range of 13.82 to 14.71 MeV in the same experimental configuration. The cross sections of these reactions in this energy region are under taken to determine theoretically by using statistical code SINCROS-II[35] to validate the experimental data.

Activation cross section data in the neutron energy range 13 - 15 MeV, as mentioned earlier, are needed primarily for the engineering design of fusion reactors, especially for the calculations of tritium breeding, radiation damage, radiation shielding, induced activity, nuclear heating and so on. But there are other important applications of 14 MeV cross section data. These are investigation of nuclear theories and nuclear structures, testing of nuclear models, neutron dosimetry, isotope production, mineral exploration, fast neutron activation analysis and so on.

Scandium, Zirconium and Zinc are the most important constituents of the fusion structural materials[37]. Germanium is the important semiconducting material. A critical survey of the available literature reveals that some information of the cross sections of the selected reactions have been existed. However, for more information and better understanding on the field, extensive research work are still inevitable. The present measurement aims at adding some newer data points to the existing literature

$$D + T \longrightarrow \alpha\ (3.5\ MeV) + n\ (14.1\ MeV)$$

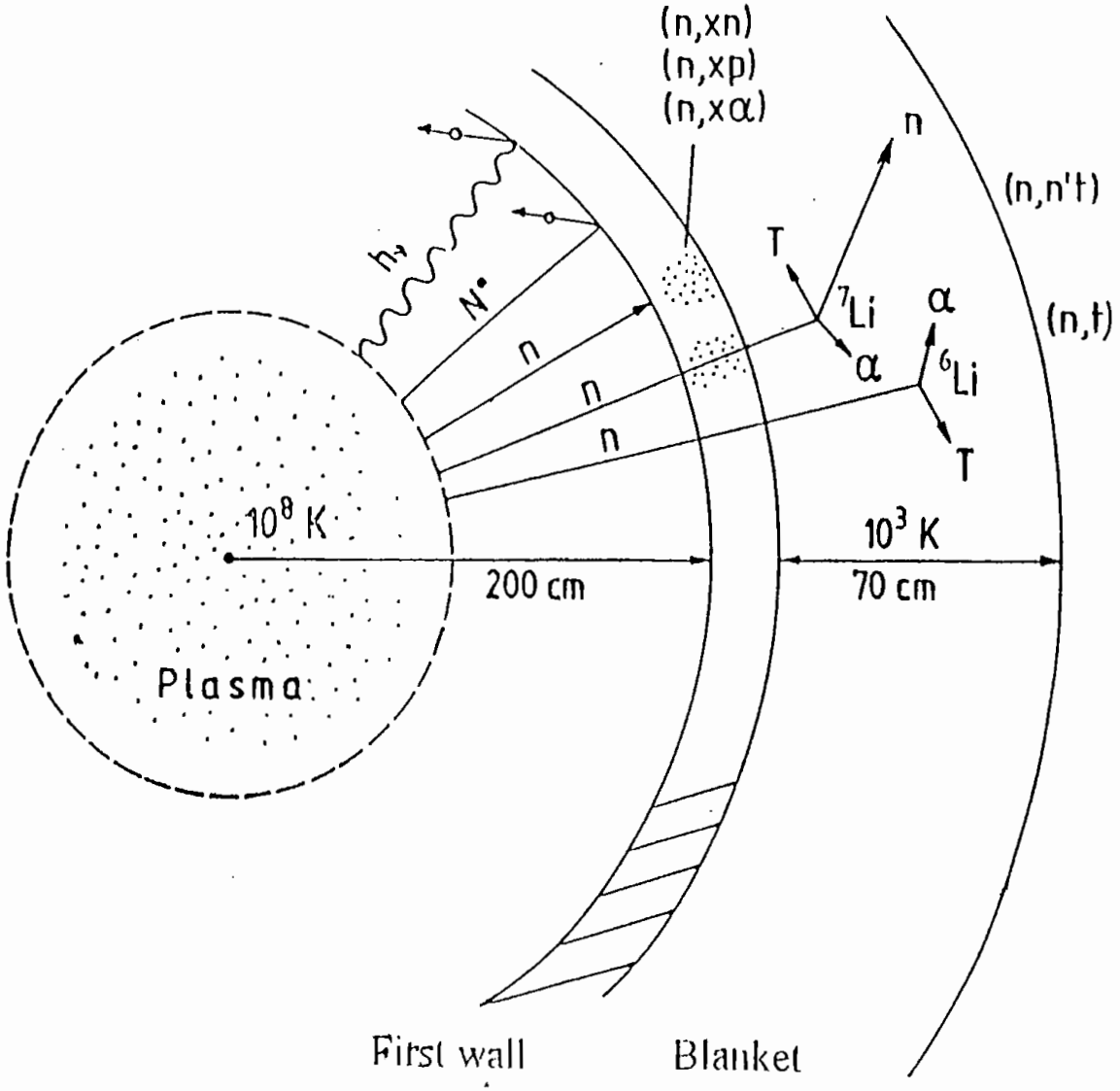

Fig. 1.1 Scheme of a possible tokamak-type fusion reactor. Major reactions occurring in the first wall and blanket are shown.

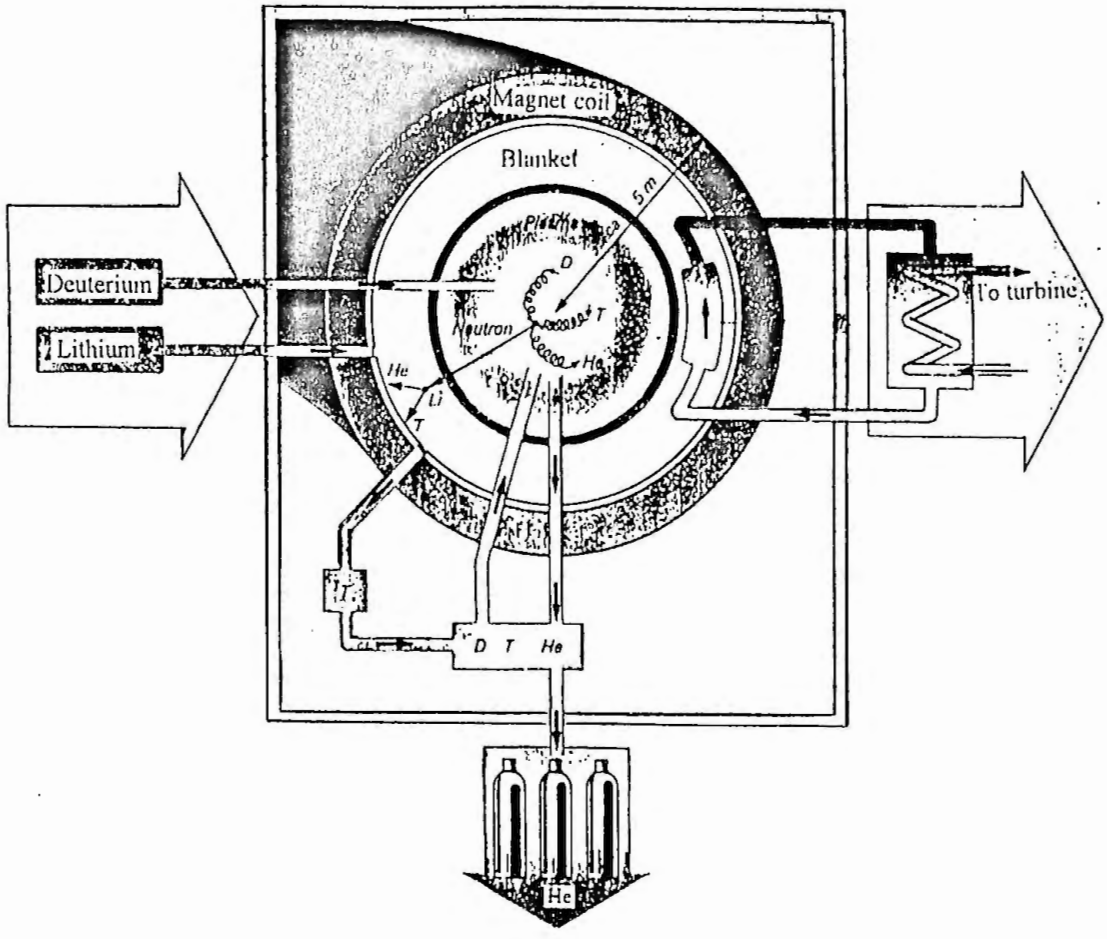

Fig.1.2 Complete design of a possible fusion reactor.

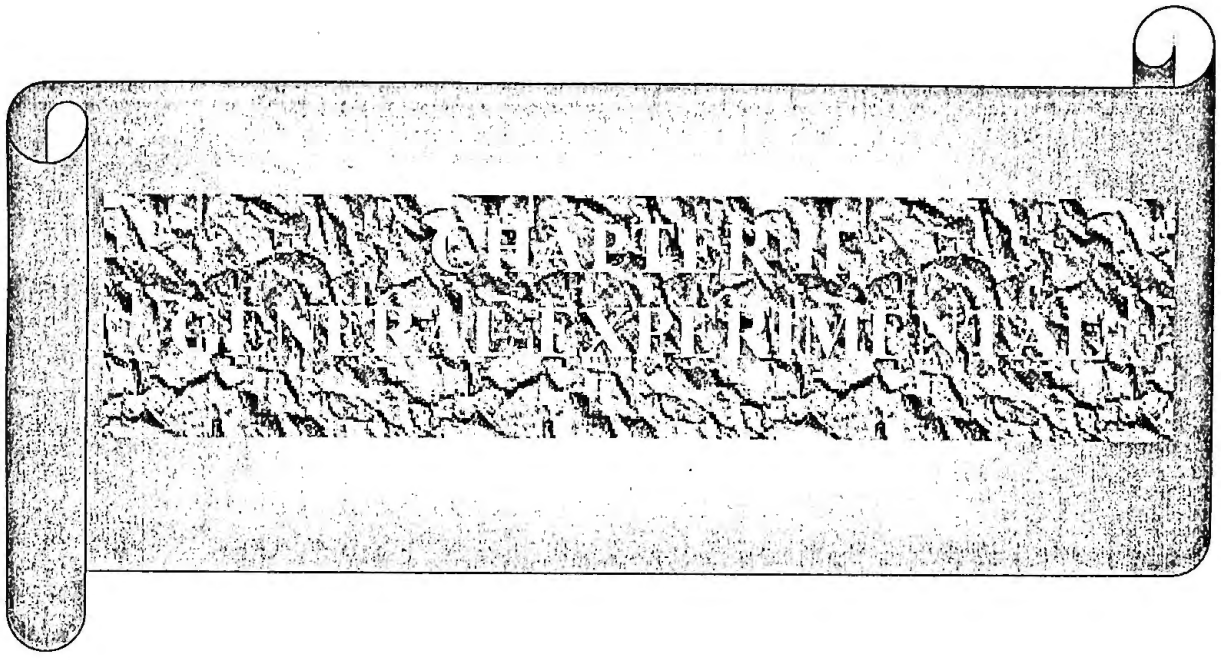
CHAPTER V
SCIENTIFIC INSTRUMENTS

CHAPTER II

GENERAL EXPERIMENTAL

2.1 General Consideration of Neutron Activation

The method of activation depends upon the formation of radionuclides from elements in the sample when they are subjected to bombardment with energetic particles, such as neutrons, photons, deuterons, α particles etc. Thus the process in which the sample is subjected to nuclear bombardment and then analyzed for its radioactive contents, is known as activation analysis. Thermal neutrons are particularly suitable, because many elements have high thermal neutron absorption cross sections, but 14 MeV neutrons have grown in importance, because the ease with which they can be produced by low voltage accelerators and their effectiveness in the detection of trace elements such as N, O, Si, P, Ti and Pb, which are difficult or impossible to detect with thermal neutrons. Neutrons with selected energies between thermal and 14 MeV are also helpful for emphasizing some elements in the presence of others which perhaps are present in greater concentration[41]. Based on highly characteristic and well defined nuclear properties of the elements, this technique is close to an ideal non-destructive analytical method, capable of handling samples in liquid, solid or powder form.

Neutron activation is a nuclear reaction phenomenon. When a neutron interacts with a target nucleus, a compound nucleus is formed. De-excitation of the compound nucleus can occur in different ways that are independent of the way the compound nucleus is formed. Each of these processes (shown below) has a certain probability, depending on the nuclear cross section of each mode, which is related to the excitation energy of the compound nucleus[42].

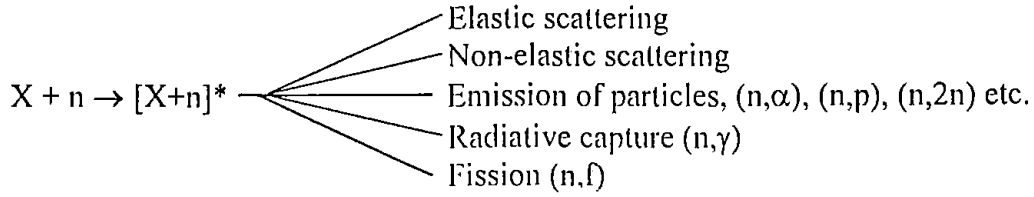

In elastic scattering the resulting nucleus is identical with the target, whereas in non-elastic scattering a radioactive isomer may be formed. In the emission of particles the resulting nuclide is usually radioactive and differs from the target nuclide in atom or mass number or both. In radiative capture (n,γ) the excited nucleus passes to a lower energy state by the emission of one or more γ-rays. The resulting nuclide is usually radioactive. In fission the excited nucleus splits into two nuclei accompanied by the emission of the neutrons and γ-rays. The fission process is limited to only a few elements with atomic high numbers ($Z > 90$), thus its significance in neutron activation is very limited.

A radioactive nuclide has a characteristic half-life ($t_{1/2}$), mode of decay and energy of emitted radiation during the decay process. Depending on the energy considerations (Q value), a radionuclide can decay to a daughter product (usually stable) by various ways, as shown below.

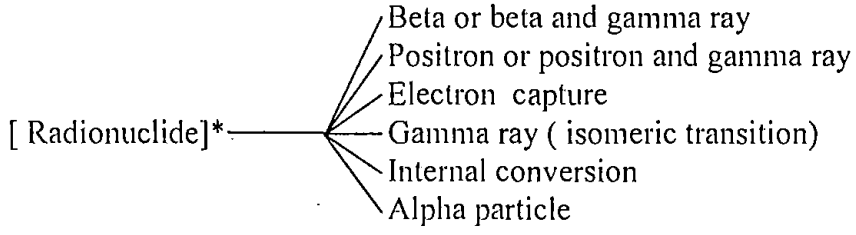

In neutron activation, neutrons are used to activate target nucleus. The neutron may be regarded as to be captured by atomic nucleus to give a large nucleus with the same positive charge, which is, therefore, an isotope of the element nuclei, which have been excited or activated by neutron capture, give characteristic gamma rays by which it is possible to identify the nuclei. The half life periods of various isotopes formed in this

manner from various elements will be widely different and this constant i.e., half life period may be made use in the identification of active isotopes along with other pertinent information in many instances. In activation analysis, activation and spectrometry take place separately.

Most of the radio-nuclides that undergo decay by alpha, beta or positron emission and by electron capture also emit gamma rays as a result of readjustment of energy content in the radio-nuclides during their transition from excited states to more stable states. Gamma-ray measurements have, in general, much wider applications in neutron activation because gamma-rays emitted from the most radio-nuclides have a wider range of energies (10-3000keV) and have large penetrating range and thus are subject to minimal loss by absorption in a sample matrix during their measurements. This property coupled with the developments in high resolution and high efficiency semiconductors such as High Purity Germanium (HPGe) detectors and availability of high neutron flux reactors, neutron generator, etc., make gamma spectrometry a powerful technique in measuring activation cross section.

2.2 Instruments and Techniques for Production of Neutrons

2.2.1 Organization of Neutron Generator

Neutron generators are small accelerators consisting of vacuum, magnetic, electrical and mechanical components, radiation sources, cooling circuits and pneumatic transfer systems. There are various types of ion sources, beam accelerating and transport systems, targets, high voltage and other power supplies, neutron and tritium monitors and shielding arrangements. To determine excitation function, the neutron with energy range of 13.82 to 14.71 MeV were produced via J-25 Neutron Generator (AID, MEYLAN, FRANCE) at the Institute of Nuclear Science and Technology, Savar, Dhaka. It was supplied by the International Atomic Energy Agency (IAEA) under the technical co-operation program. The general characteristics of the neutron generator is given in Table 2.1 and a partial view of the J-25 neutron generator is shown in Fig. 2.1.

Table 2.1 General characteristics of J-25 neutron generator.

Maximum high voltage	150 kV
Maximum current	2.5mA
Power consumption	2 kVA
Beam diameter	5-30 nm
Neutron production	D-T Reaction
Neutron energy	13-15 MeV
Maximum neutron yield	2×10^{11} n $cm^{-2}sec^{-1}$

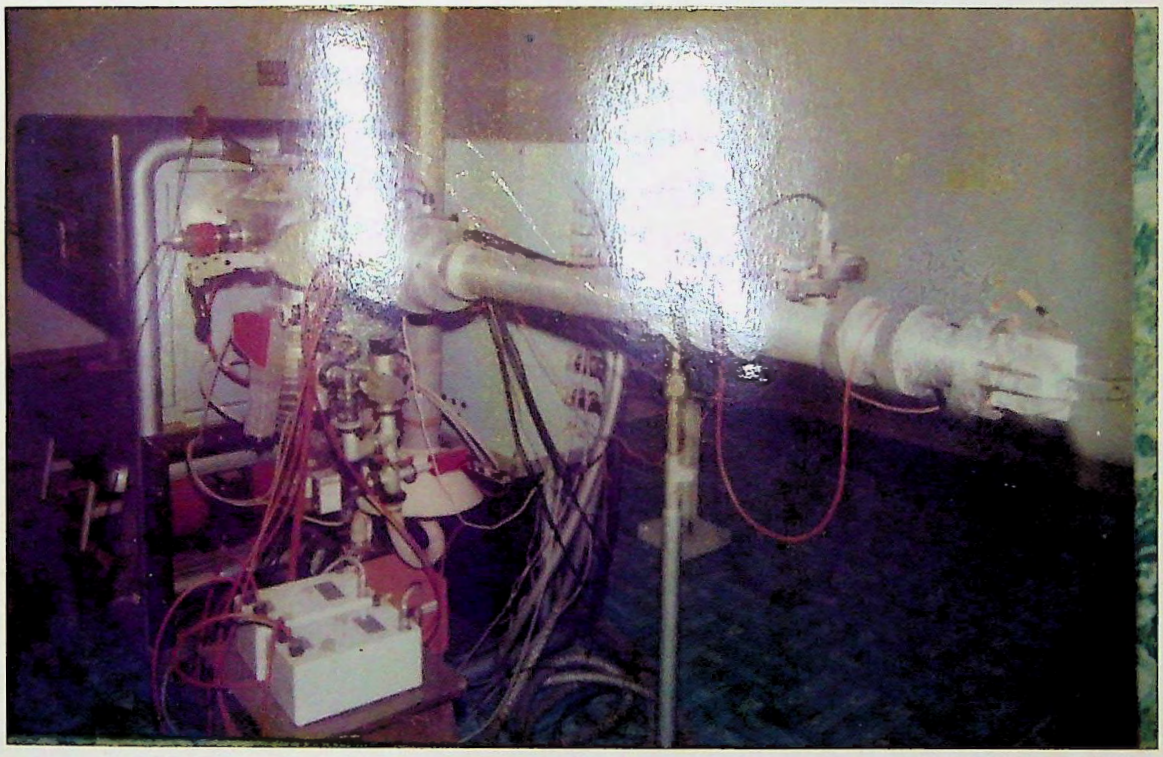

Fig. 2.1 Partial view of the J-25 neutron generator.

The major components of the neutron generator are briefly described below.

2.2.1.1 Positive ion source

The radio frequency (RF) type ion source is used to produce deuteron ion. The deuterium gas is fed at a controlled rate into the glass envelope via a gas leak. If an RF voltage is applied across the exciter rings, an electrical field is generated between the two ring electrodes located outside and in contact with the glass envelope. Since glass is an insulator, the electric field lines traverse the glass and pass into the gas. The power supplied to the RF oscillator is adequate to create and maintain intense ionization of the gas. This gas discharge glows with a bright pink color. The plasma color (a bright pink) is also one of the principal guides to the performance of the source. If a DC potential is now applied across the bottle, ions can be directed toward the exit canal of the bottle. A gap or electrostatic focusing lens is used to prevent the divergence in exit canal and directs the ions into the accelerating section of the generator. The ions enter the field of the acceleration tube where they are accelerated through a potential of 110 kV.

2.2.1.2 Acceleration tube

The intense ion plasma produced inside the ion source is directed through the exit canal and into the focusing and accelerating sections of the neutron generator. Generally, these functions take place in a single tube composed of 10 electrodes and a hollow cylindrical insulators of ceramic. The insulators and the metal electrodes are bonded together with polyvinylalchohol (PVA) glue to form vacuum tight (joints). It has permitted the dual action of focusing and acceleration. An equal division of the high voltage (110 kV) is performed for the whole length of the tube. As a result the beam receives a kick of 11 kV in passing each electrode. The focusing electrodes carry a negative DC potential with respect to the terminal high voltage (110 kV) applied to the first accelerating stage. By utilizing a system of resistors a potential difference is maintained between each accelerating stage. This division of high voltage can be evenly distributed between the individual stages so that the ion beam receives a boost in energy equivalent to the potential drop at each stage. At the end of the accelerating tube the ions have acquired an energy equivalent to the total potential drop between the high-voltage

terminal and ground. The positive ion beam reaches the target with an energy equal to their charge multiplied by the potential difference through which they have fallen and thus a continuous deuteron beam of 110 kV energy is obtained.

2.2.1.3 Vacuum system

The aim of all vacuum systems for a neutron generator, as for a charged particle accelerator, is that the accelerated deuteron ions should reach the tritium target without collision with gas molecules. To do this, it is necessary to keep the pressure in the accelerating tube so low that the mean free path of air molecules should exceed the length of the accelerating tube. The vacuum system of the neutron generator consists of a dipstick pump of EDWARDS high vacuum, England. The pressures of different mean free path are shown in Table 2.2.

Table 2.2 Mean free path vs. pressure[43].

Pressure (mbar)	Mean free path (cm)
atmospheric	$6x10^{-6}$
1	$5x10^{-3}$
10^{-3}	$5x10^{0}$
10^{-6}	$5x10^{2}$
10^{-9}	$5x10^{6}$

2.2.1.4 Quadrupole lens

Electrostatic (or magnetic) quadrupole lenses are commonly used as post-acceleration ion beam lenses at almost all accelerators. Electrostatic quadrupole lenses are more simple, but they need power and high voltage feed through into the vacuum system. Furthermore a high vacuum is required in the system to avoid corona discharges. Quadrupole lens consists of four hyperbolically shaped pole faces or electrodes. The quadrupole lens focuses in one plane and defocuses in the perpendicular plane. Thus

several such lenses must normally be combined to make a useful lens system. Usually quadrupole doublets and triplets are in use at neutron generators. The biased quadrupole lens is powered asymmetrically, so that the particle beams are focussed and steered. The biased quadrupole lens requires split power supplies.

2.2.1.5 High voltage generator

High voltage generators are used in neutron generators for excitation, focusing acceleration, etc. of the deuteron ions. It has the following main components:

a) Rotor
b) Ionize electrodes
c) Inductors.

The rotor, which is a tube-like cylinder, made of insulating material. The rotor is driven by an electric motor and charges are deposited on the surface of the rotor. The rotating cylinder is the only moving part of this electrostatic generator.

The ionize electrodes, which are very thin metallic needles (blades) placed in close proximity to the rotating cylinder. The charging needles spray the electric charges by corona discharge onto the surface of the rotor while the discharging electrodes (needles) collect the charges by drawing them off the surface of the rotor.

The segments or inductors, which induce a strong electric field on the sharp edge of the ionizers. The inductor electrodes are placed behind a slightly conductive special glass cylinder. The excitation inductors lay the electric charges onto the surface of the rotor whilst the extracting inductor withdraws them. The charge collecting (ionizer) electrode and the inductor pair on the opposite side are called a pole of the machine. The inductor and the conductive glass cylinder are together called the stator. The stator, the rotor and the ionize electrodes are closed hermetically in a tank under pressure of compressed hydrogen.

2.2.1.6 Tritium targets

Tritium solid target is especially made on copper backing. Tritium is a radioactive nuclide which decays by emission of β^- with a half life of 12.3 years. Some specifications of tritium target [44] are given below.

1. Activity of fresh target : 370 GBq ±10%
2. Gross diameter of the target : 45 mm
3. Active diameter of the target : 30 mm
4. Thickness of the copper backing : 1 mm.

During irradiation the tritium target is cooled by a jet of cooled compressed air to reduce tritium evaporation from the hot target. Collimator diameter used was 10 mm. For the present experiment the tritium targets were imported from Radioisotope Center, POLATOM, Poland.

2.2.1.7 The control console

This component which is located outside accelerator room is used for the operation of the neutron generator. A partial view of the control console of the neutron generator is shown in Fig.2.3. It consists of the following parts.

1. Power control
2. Vacuum control
3. High voltage generator
4. Ion source and beam control
5. Quadrupole lens.

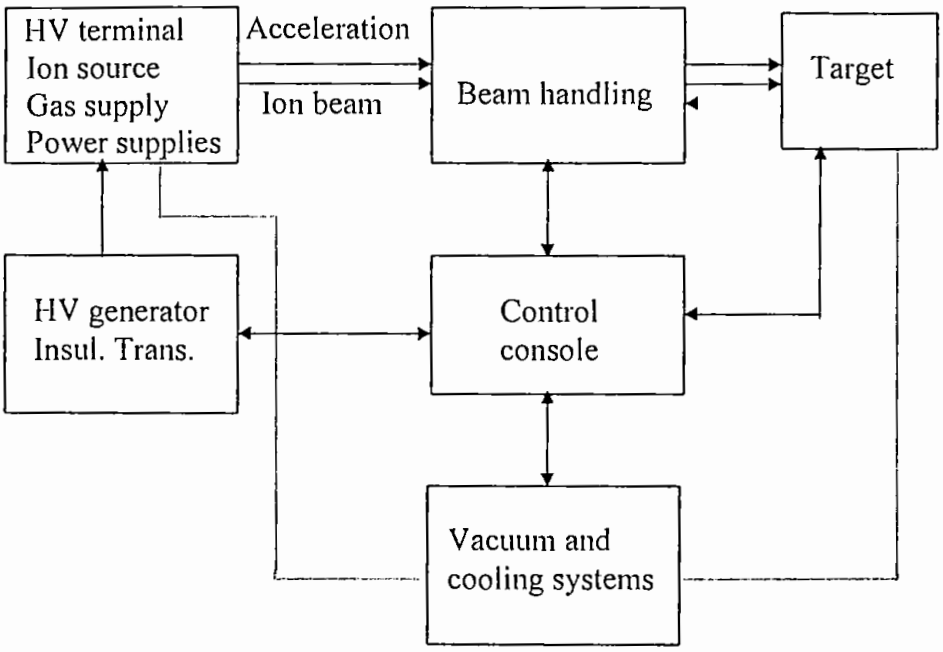

Fig.2.2 Block diagram of neutron generator.

Fig.2.3 Partial view of the remote control console of the neutron generator.

2.2.1.8 Neutron monitor

The inherently low detection efficiency for fast neutrons of any slow neutron detector can be somewhat improved by surrounding the detector with a few centimeters of hydrogen-containing moderating material. The incident fast neutron can then lose a fraction of its initial kinetic energy in the moderator before reaching the detector as a lower-energy neutron, for which the detector efficiency is generally higher[45]. A BF_3 long counter was used inside the neutron generator room for the detection of neutrons. Paraffin was used as the moderating material. As long counter detects the neutrons by the

$$n + {}^{10}B = {}^{7}Li + \alpha$$

reaction (after thermalization), the pulses from the gamma rays associated with the neutron field can be well separated. For monitoring the neutron flux, a multichannel analyzer was used in the multiscaler mode.

2.2.2 Production of Fast Neutron by J-25 Neutron Generator

The two nuclear reactions used for the production of fast neutrons by low-voltage accelerators can be expressed as follows:

1. ${}^{2}H + {}^{2}H \rightarrow [{}^{4}He]^* \rightarrow {}^{3}He + {}^{1}n + 3.266\ MeV$

2. ${}^{2}H + {}^{3}H \rightarrow [{}^{5}He]^* \rightarrow {}^{4}He + {}^{1}n + 17.586\ MeV$

At acceleration voltages normally used in neutron generator of about 150 to 200 keV, the cross section for the D-D reaction is about 3×10^{-26} cm^2/atom. Whereas, for thin targets, the D-T cross section at about 150 keV incident deuteron energy is about 4.55×10^{-24} cm^2/atom and the maximum value 5 barns are shown at 110 keV incident deuteron bombarding energy [46]. From cross section considerations, it would be expected that at 150 keV incident deuteron energy, the output from the D-T reaction would be about 300

times greater than that from the D-D reaction. Therefore, the contribution of the D-D background neutrons to those emitted in the D-T reaction can be neglected. Experimentally, it has been observed that this improvement is indeed approximated for thick target neutron production. The prolific yield from the D-T reaction makes it particularly useful for analytical applications requiring a high degree of sensitivity; however, the D-D reaction is sometimes preferred in special cases because of minimization of the number of interferences. Neutron sources based on the light particle reactions have played an important role in experimental fast neutron research[47,48]. Henceforth 14 MeV neutrons from neutron generator were used in the present investigation although various kinds of neutron sources with different energy ranges and intensities are available[49]. Using low-energy accelerators, monoenergetic neutrons are generally produced by the " big-4" reactions shown in Table 2.3.

Table 2.3 Data of the "big-4" neutron source reactions.

Reaction	Q-value (MeV)	Break up reaction	Break up threshold (MeV)	Monoenergetic neutron energy range (MeV)
$^{3}H(d,n)^{4}He$	+17.590	T(d,np)T $T(d,2n)^{3}He$	3.71	11.75 - 20.5
$^{2}H(d,n)^{3}He$	+3.270	D(d,np)D	4.45	1.65 -7.75
$^{3}H(p,n)^{3}He$	-0.763	T(p,np)D	8.35	0.3-7.6
$^{7}Li(p,n)^{7}Be$	-1.644	$^{7}Li(p,n)^{7}Be^{*}$	2.37	0.12-0.6

The production of neutrons by bombarding suitable targets with the isotopes of hydrogen is particularly attractive since the net energy gain by the reaction system is quite large. For instance, a proton entering a nucleus adds about 8 MeV of energy to the system. In the case of an α-particle, the net gain is not quite as much since the difference

between approximately 28 MeV of binding energy required to break up an α-particle into two neutrons and two protons and the 32 MeV gained by the reaction system from the addition of four extra nucleons, is only 4 MeV. When compared with the entry of a deuteron, however, even the energies brought in by protons and α-particles are considered small. The deuteron requires only 2 MeV to split into a neutron and a proton but adds 16 MeV into the reaction system, a net gain of 14 MeV.

In the present experiment, reaction (2) was used to produce monoenergetic fast neutron. To take place this reaction (2), the J-25 neutron generator was so designed that deuterium molecules are ionized in the ion source bottle, accelerated in an electrostatic field of 110 keV at a beam current of 200 μA and focused on a tritium target. The deuteron interacts with tritium in the target to form a compound nucleus $[^5He]^*$ at a highly excited state which later breaks down into a ^4He nucleus and a neutron with the release of 17.6 MeV energy.

The reaction $T(d,n)^4He$ has a positive Q-value of 17.6 MeV. Q-value means the energy released or absorbed in a reaction. An amount of energy equal to the Q-value of the reaction plus kinetic energy of the incident particle ($_1H^2$) is shared by the outgoing particle (^1n) and residual nucleus (^4He). The fraction of the energy which each of them receives can be determined by applying the principle of conservation of energy and momentum. However, the lighter particle always takes the greater portion of the available energy. A neutron emitted in the forward direction carries away about 14.1 MeV of the energy. The remaining 3.5 MeV appears as the kinetic energy of the alpha-particle. The alpha particles are absorbed in the target holder but the neutrons being very penetrating, escape into the room.

For 110 keV deuteron, the D-T source properties were studied earlier[27] at the J-25 neutron generator facility, INST, AERE, Svar, Dhaka. The energy of the neutrons in the center of mass system is 14.1 MeV. In the laboratory system the neutron energy varies from 14.71 MeV at 0° to 13.55 MeV at 180°.

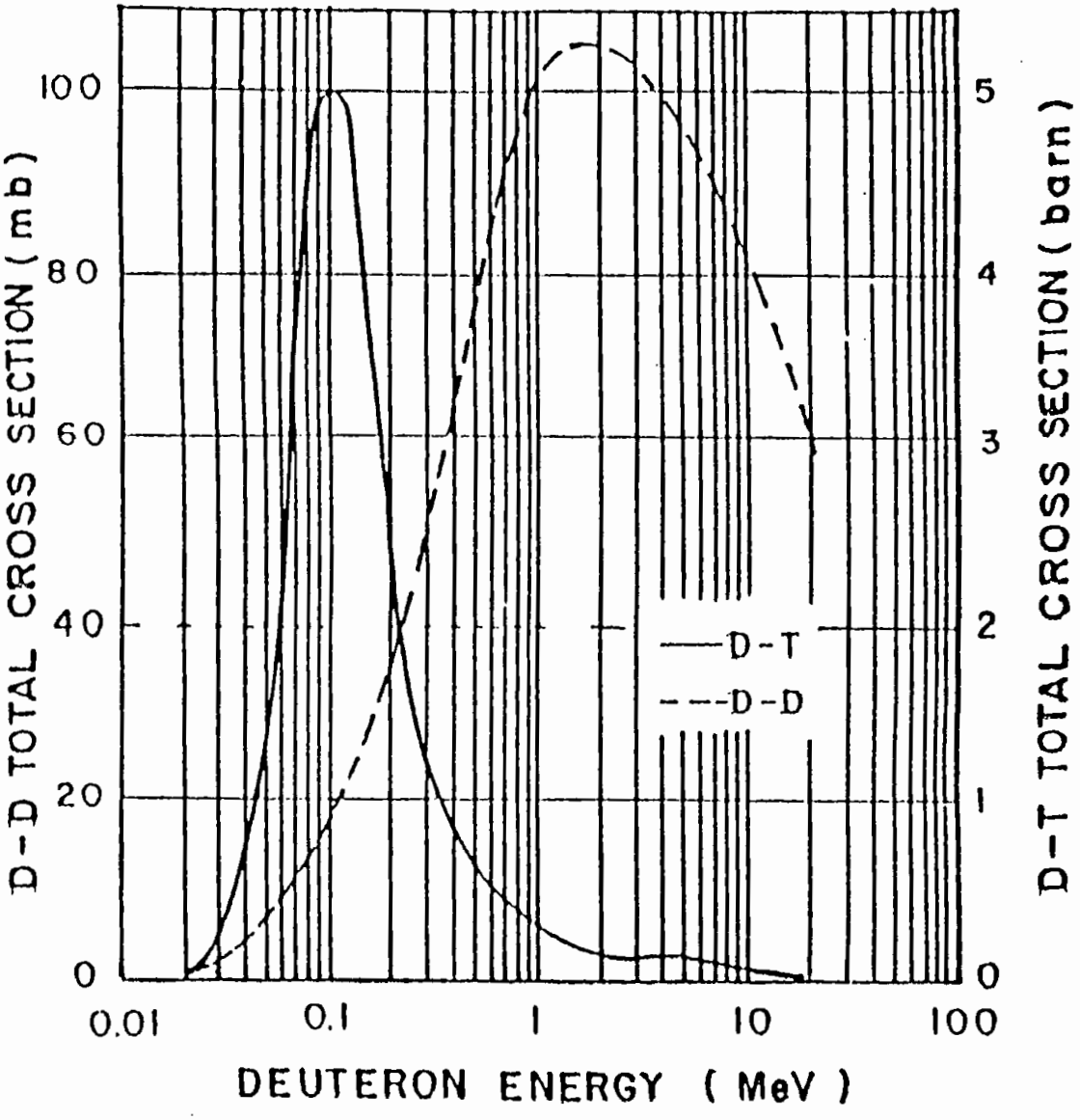

Fig. 2.4 Cross section of D-D and D-T reactions as a function of deuteron Energy[48].

2.3 Gamma-ray Spectrometry

2.3.1 Interaction of Gamma rays with Matter

The interaction process of gamma rays with matter are complex. The γ photons may surpass an indefinite distance through matter without interacting i.e., without losing any energy. On the other hand, suddenly in a single encounter with atomic electron or in the nuclear field, it may lose all its energy by being captured or lose a fraction of its energy and get scattered as a photon of longer wave-length. In view of this unpredictable characteristic behavior, photons do not have a specific range in matter as the charged particles. In order to understand the detectors used for gamma-ray detection and to be able to select one for a particular measurement, it is necessary to review the ways in which gamma rays interact with matter. Although a large number of possible interaction modes are known for gamma rays with matter, only three major types play important roles in the radiation measurements are as follows.

1. Photoelectric effect
2. Compton scattering and
3. Pair production.

2.3.1.1 Photoelectric effect

The photoelectric emission is the principal mode of interaction of low energy photons (10-100 keV) with matter. An incoming gamma-ray photon undergoes on interaction with an absorber atom in which the photon completely disappears in this process as shown in Fig. 2.5. The photon of energy E_γ is wholly absorbed by a single electron of the atom and this electron is ejected with an energy E_e given by the difference between E_γ and the energy E_b binding the electron in the atom.

$$E_c = E_\gamma - E_b$$

Obviously, for photoelectric emission to be possible, $E_\gamma > E_b$. As the initial photon is wholly absorbed (i.e., it vanishes), the photoelectric emission is not possible with a free electron. It has to be with an electron bound in an atom, such that the latter (now an ion) can recoil to conserve momentum.

If E_γ is sufficiently high to release K shell electrons, about 80% of the electrons will be from the K shell and the rest from the L shell. The hole created in the K or L shell will be filled by the successive jumps of outer electrons, emitting corresponding X-rays (the fluorescent radiation) or by Auger emission.

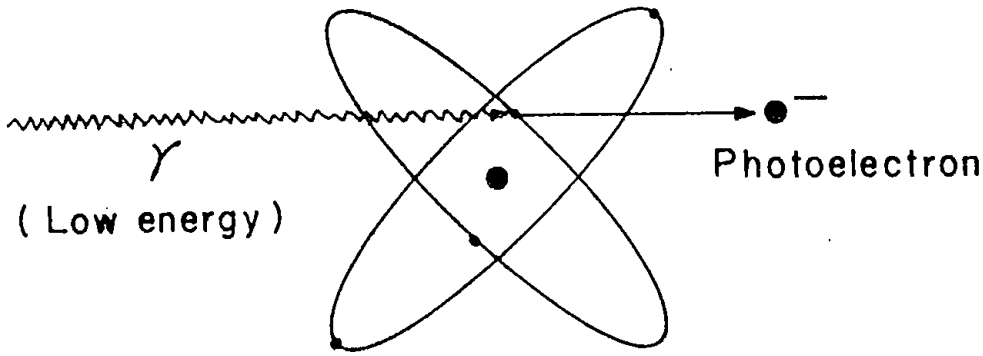

Fig. 2.5 Photoelectric effect

Absorption of a photon due to photoelectric effect decreases sharply with increase of photon energy, but increases rapidly with atomic number Z of the absorber material. The probability of photoelectric absorption (σ_{pe}) is shown below mathematically[50].

$$\sigma_{pe} \propto Z^5 / E_\gamma^{3.5}$$

Hence, it is the dominant mode of radiation absorption for low energy photons and in heavy elements. The photoelectric absorption falls smoothly with increasing photon energy but rises again sharply as the energy reaches the photoelectric edge E_K or E_L, i.e., the binding energy of K or L shell electrons.

2.3.1.2 Compton scattering

For intermediate energy photons over a wide range (0.1 to 10.0 MeV), the dominant interaction is by Compton scattering. Here the photon interacts with a free or loosely bound electron, transfers a part of its energy to it and itself gets scattered as a photon of correspondingly reduced energy. The energy E_γ and momentum E_γ/c of the incident photon are shared between the scattered photon and the recoil or Compton electron as shown in Fig.2.6.

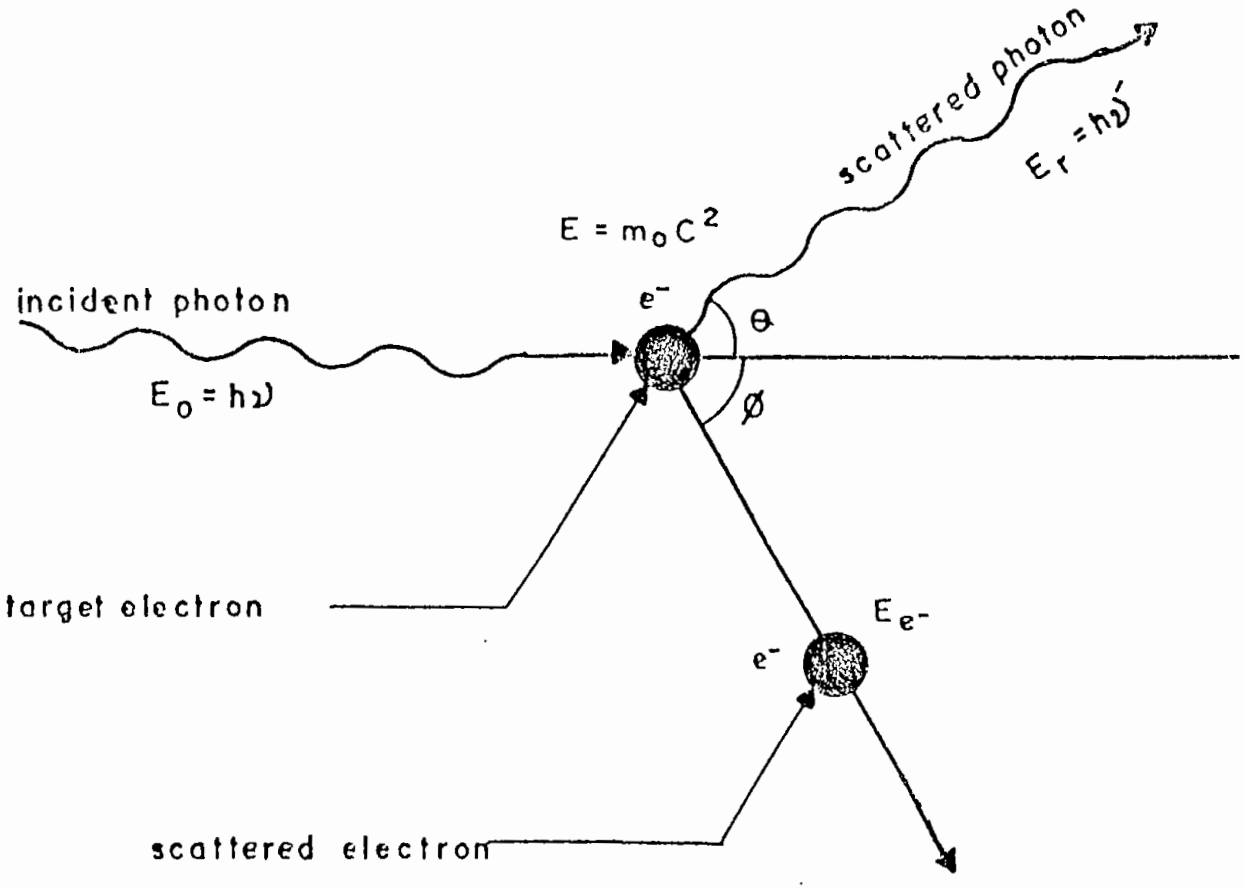

Fig.2.6 The mechanism of Compton scattering[51] process.

Here θ and ϕ are the angles of the scattered photon of energy E_γ and the Compton electron of energy E_e, respectively with the initial trajectory.

The Compton effect is a favored mode of interaction for γ-rays of medium energy interacting with absorbers of medium-to-low atomic number. As in the photoelectric effect, if an inner orbital electron is ejected, X-ray and Auger electron emission will result. The probability of Compton scattering per atom of the absorber depends on the number of electrons available as scattering targets and therefore increases linearly with Z. This probability falls off gradually with increasing energy.

2.3.1.3 Pair production

The third mechanism by which electromagnetic radiation can be absorbed is the production of electron-positron pair. The phenomenon of photon absorption leading to the creation of an electron-positron pair becomes important with photons of energies greater than 10 MeV. In pair production, the incident photon vanishes and a positron-electron pair is created in its place. Being an antiparticle, the positron has a short life $\sim 10^{-9}$s and it annihilates in its turn on meeting the first electron, available all around. The $e^+ - e^-$ annihilation is accompanied[52] by the creation of a pair of γ photons each of energy 0.512 MeV, proceeding in opposite directions as shown in Fig.2.7.

The pair production probability is given by

$$\sigma_{pp} \propto Z^2 \ln E_\gamma$$

For this to happen, the incident photon should have a minimum energy of $2\, m_e c^2$ (= 1.02 MeV).

$$\gamma \rightarrow e^+ + e^-$$

photon	positron	electron
1.02 MeV	0.51 MeV	0.51 MeV

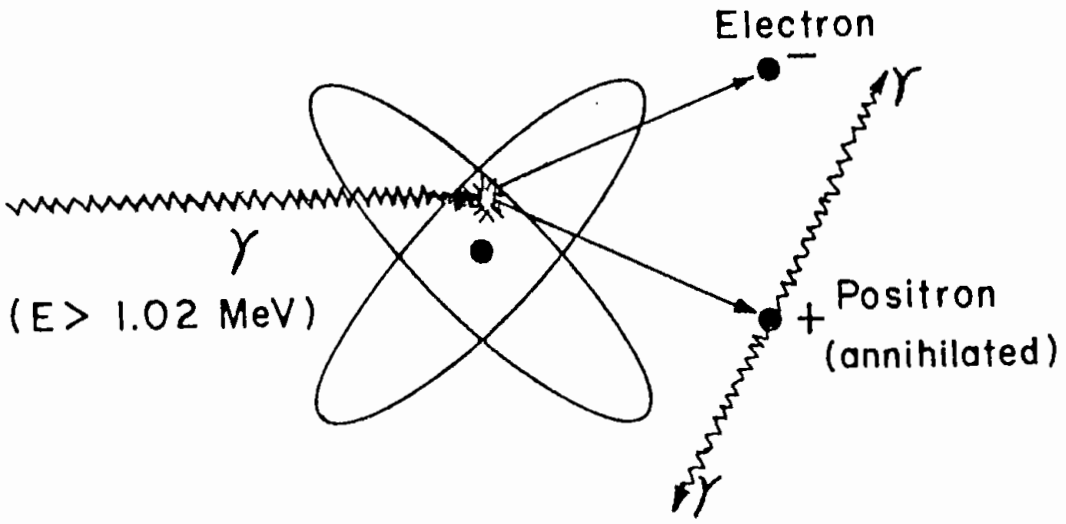

Fig. 2.7 Pair production

It was found that the possible values of the energy of a free electron are either greater than $+ m_e c^2$ or smaller than $- m_e c^2$ and that no possible energies for the electron exist between these two limits. This state of affairs is shown in Fig.2.8, where the shaded regions are those in which values of the energy exist[53]. Electrons in states of positive energy behave in the usual manner of electrons that are ordinarily observed, while electrons in states of negative energy should have properties which have no classical analogy. In terms of Dirac's theory, the production of a positron is interpreted as follows: A photon of energy greater than $2 m_e c^2$ can raise an electron from a state of negative energy to a state of positive energy. The disappearance of an electron from a negative energy state leaves a hole, which means the appearance of a positron; the appearance of an electron in a positive energy state means the appearance of an ordinary electron. Thus, a pair of particles is created.

Absorption coefficient

The probability of the interaction of γ-rays with matter can be expressed as an absorption coefficient. The resultant absorption coefficient, μ is the sum of mainly coefficients for photoelectric, Compton scattering and pair production process.

$$\mu = \mu_{pe} + \mu_{cs} + \mu_{pp}$$

Where, μ_{pe} = Absorption coefficient for photoelectric process

μ_{cs} = Absorption coefficient for Compton scattering

μ_{pp} = Absorption coefficient for pair production.

The variation of absorption coefficients by the different modes of γ interaction with germanium [54,55] is shown in Fig. 2.9. It has been seen that the curve for Compton effect coincides with the resultant over the region from about 0.3 to 2 MeV. The absorption of energy can be expressed per cm length of matter or per gram, atom or electron per cm^2 in the path of the beam. The absorption coefficient depends on the energy of the incident γ-rays as well as on the nature of the absorbing material.

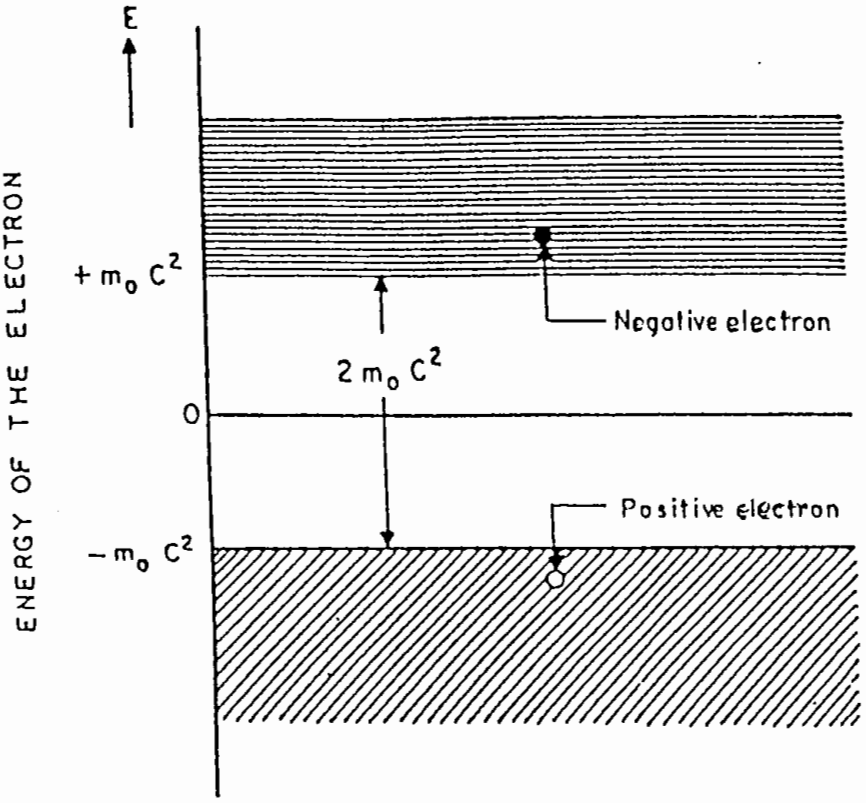

Fig. 2.8 Possible values of the energy of an electron according to Dirac theory.

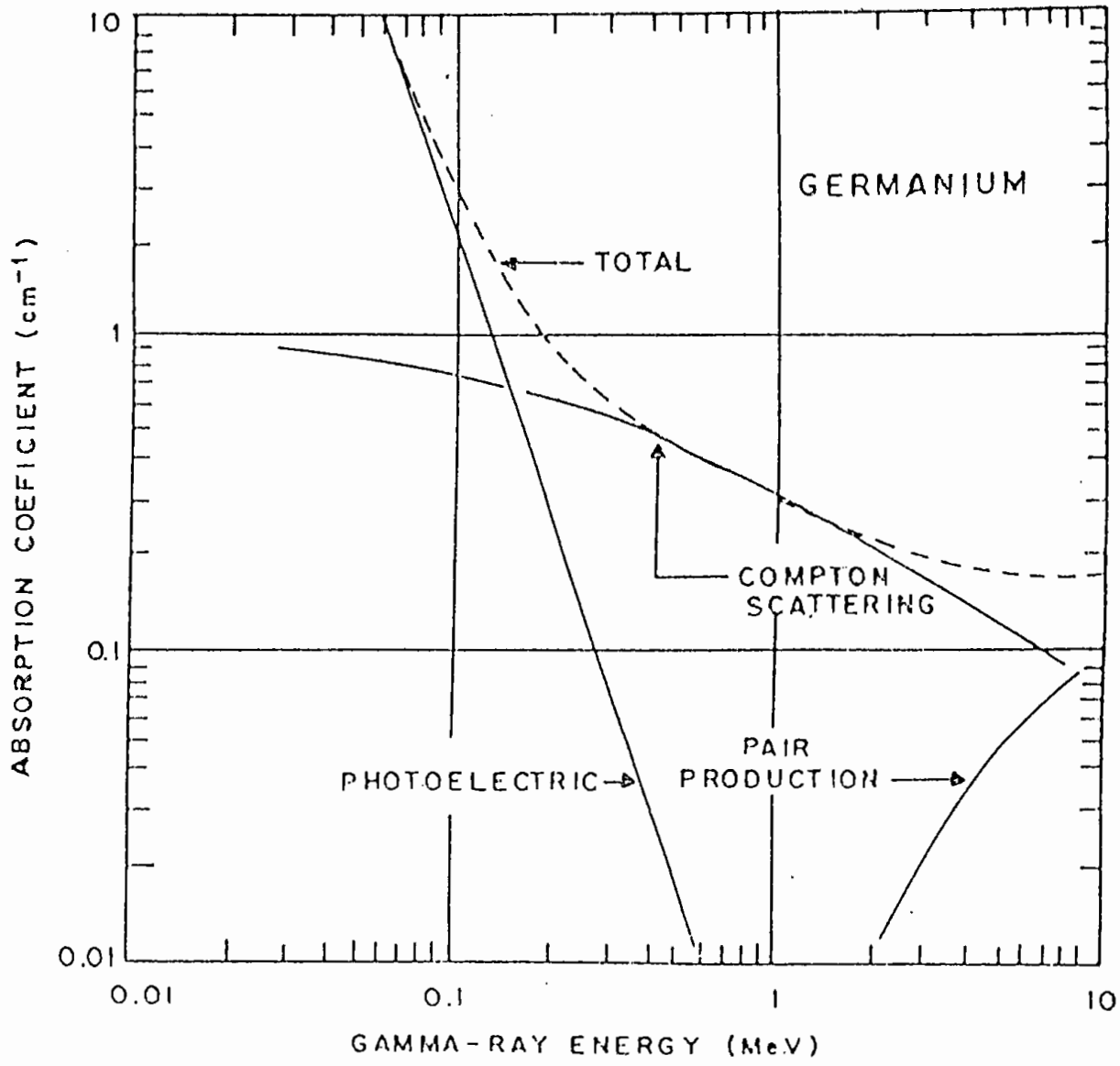

Fig. 2.9 Photon linear absorption coefficients vs photon energy for germanium.

2.3.2 Detection and Measurement of Gamma rays

This section provides information for the proper selection of detectors and electronics for detection and analysis of γ-ray. The choice of a particular detector type for an application depends upon the gamma energy range of interest and the application's resolution and efficiency requirements. In the present work, the detector with semiconductor material Ge has been selected. A semiconductor material is one whose electrical properties lie in between those of insulator and good conductor. Semiconductor which have almost empty conduction band and almost filled valence band with a narrow energy gap (of the order of 1 eV) separating the two. Germanium is the most frequently used semiconductor material. It is because the energy required to release an electron from their valence bands is very small[56]; being of 0.74 eV. In electronics the term solid state is often used interchangeably with semiconductor, but in the detector field the term can obviously be applied to solid scintillators. Therefore, semiconductor is the preferred term for those detectors which are fabricated from either element or compound single crystal materials having a band gap in the range of approximately 1 to 5 eV. Germanium is by far the most widely-used semiconductor. To perform the detection and counting of γ-ray, HPGe-detector associated with preamplifier, amplifier, analog-to-digital converter (ADC) and multichannel analyzer (MCA) has been used. The block diagram of the system is shown in Fig. 2.10.

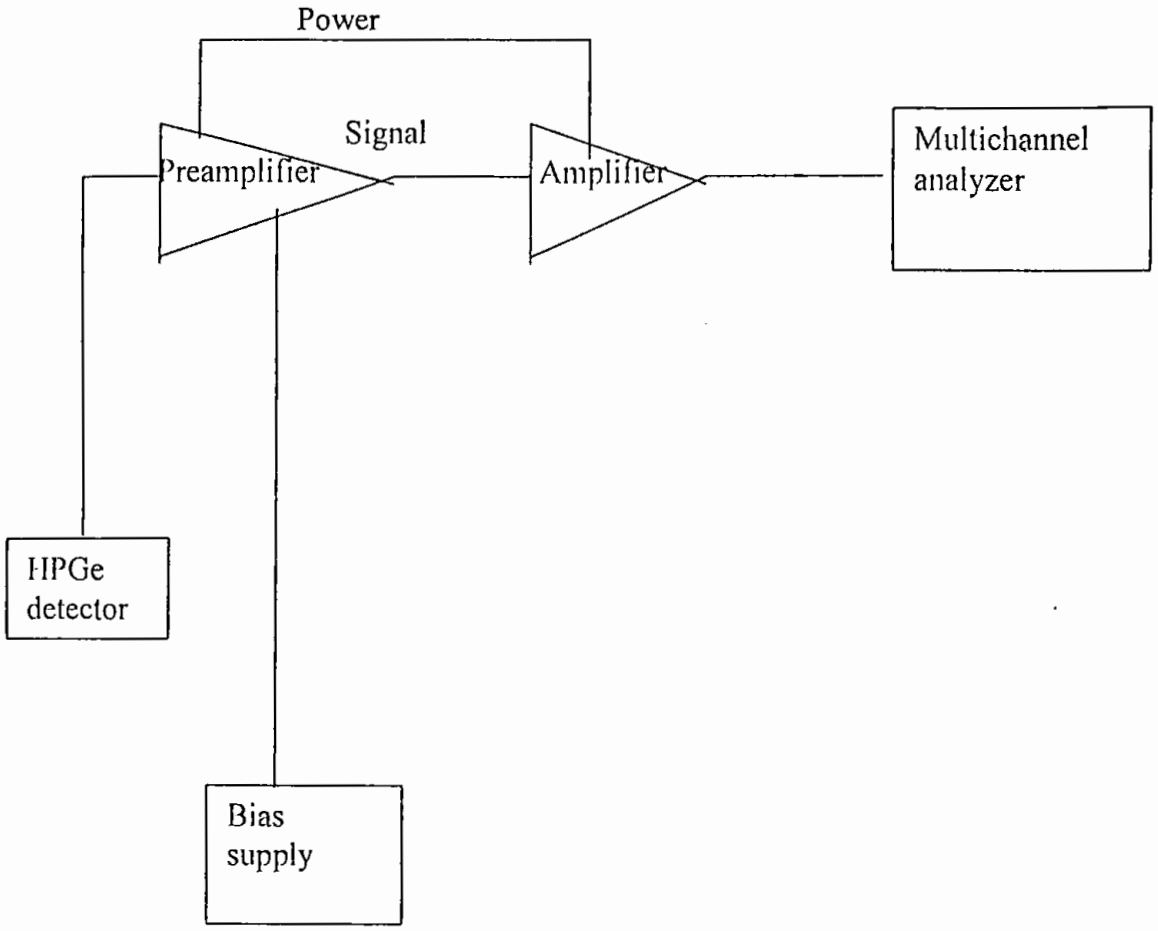

Fig.2.10 A schematic view of the electronic equipment associated with HPGe detector.

2.3.2.1 High purity germanium (HPGe) detector

The conventional coaxial germanium detector is often referred to as Pure Ge, HPGe, Intrinsic Ge or Hyperpure Ge. Regardless of the superlative used, the detector is basically a cylinder of germanium with n-type contact on the outer surface and a p-type contact on the surface of an axial well. The germanium has a net impurity level of around 10^{10} atoms/cm^3.

The n and p contacts, or electrodes, are typically diffused lithium. The reliable performance of the detector depends on its depletion depth which is inversely proportional to the net electrical impurity concentration in the detector material and on applied potential difference. The principle in brief is that semiconductor material contains impurities which can be of the donor or the acceptor type. A donor (n-type) gives electrons to the conduction band, where as an acceptor (p-type) takes electrons out of the valence band, thus creating a hole by forming a p-n junction. By applying a reverse biased voltage, i.e., a positive voltage to the n-type material and a negative voltage to the p-type material, electrons are " pulled farther away" from the junction and thus a depletion region is formed that is sensitive to γ-radiation. The greater the reverse bias the wider the depletion layer becomes. The depletion layers stops growing when its difference of potential equals the source voltage[57]. Thus, when a γ-ray interacts within the depletion region, it causes ionization and creates holes in the valence band and electrons in the conduction band[58,59]. The electrons migrate to the positive voltage on the n-side, while the holes migrate to the negative voltage on the p-side, thereby creating an electrical output signal which is directly proportional to the amount of incident γ -ray energy absorbed in the depletion region. In a Ge(Li) detector only 2.9 eV needed to obtain the equivalent of one ion pair. As a practical matter Ge detector must be cooled in order to prevent rediffusion of the Li and to reduce the thermal charge carrier generation (noise) to an acceptable level. The most common medium for detector cooling is liquid nitrogen. In liquid nitrogen (LN_2) cooled detectors, the detector element (and in some cases preamplifier components), are housed in a clean vacuum chamber which is attached to or inserted in a LN_2 Dewar. The detector is in thermal contact with the liquid

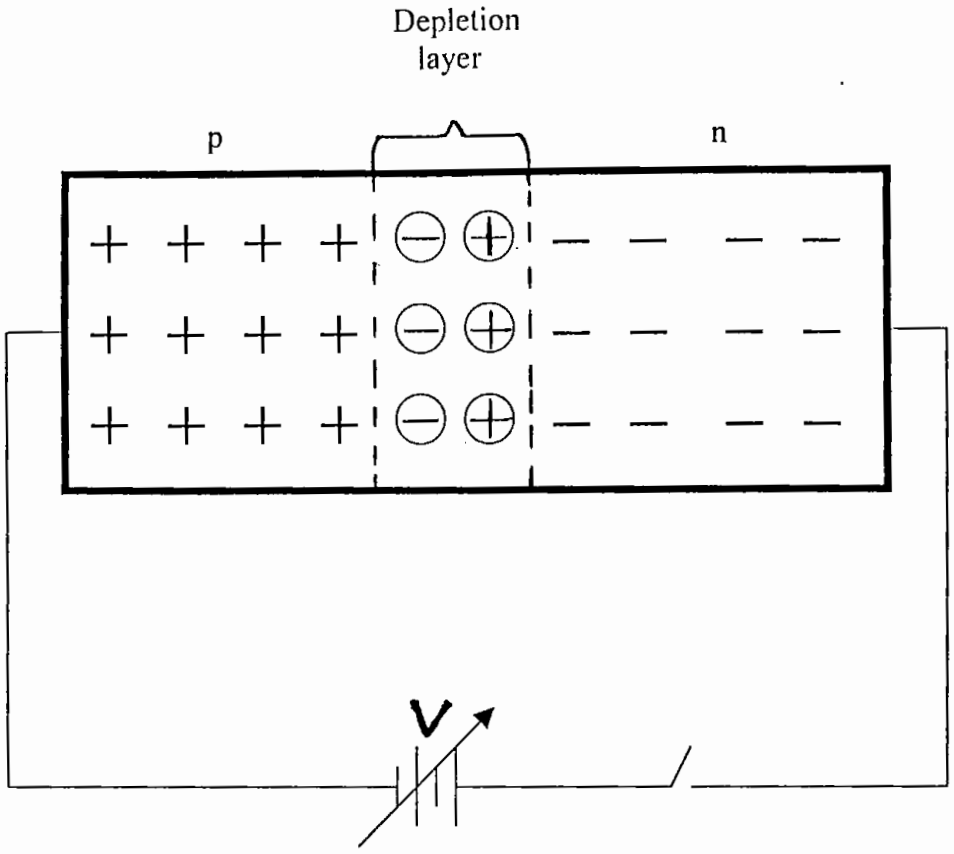

Fig. 2.11 Formation of depletion layer across a p-n junction.

nitrogen which cools it to around 77^0K or -196^0C. At these temperatures, reverse leakage currents are in the range of 10^{-9} to 10^{-12} amperes.

HPGe detector provide greatly improved energy resolution over other types of radiation detectors for many reasons. Fundamentally, the resolution advantage can be attributed to the small amount of energy required to produce a charge carrier and the consequent large output signal relative to other detector types for the same incident photon energy. A cross-sectional view of a coaxial germanium detector is shown in Fig.

2.12a. Some important dimensions of the closed end vertical dipstic detector are mentioned below.

Diameter	: 4.1cm
Length	: 5.5 cm
Active area facing the window	: 17.50 cm^2
Distance from the window	: 0.5 cm

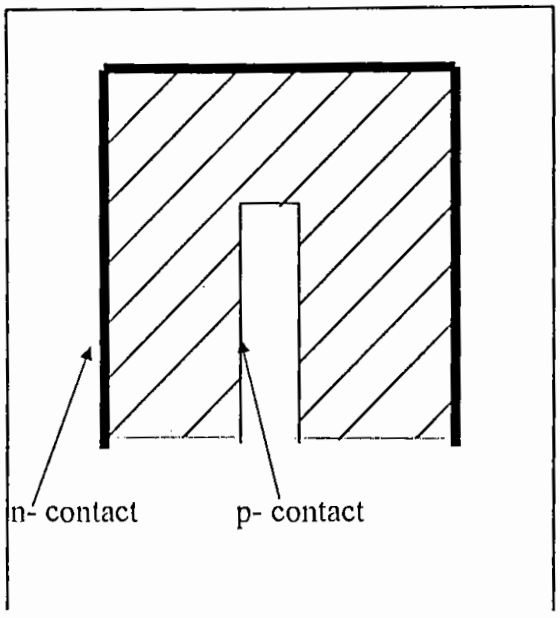

Fig.2.12a Coxial germanium detector cross section[60]. The hatched region indicates active volume for gamma ray interaction.

2.3.2.2 High voltage power supply

An external high voltage called "detector bias" is used for operation and optimum performance of radiation detectors. The high voltage module is a d.c converter where low voltage d.c output which is regulated, filtered and can be varied by the front

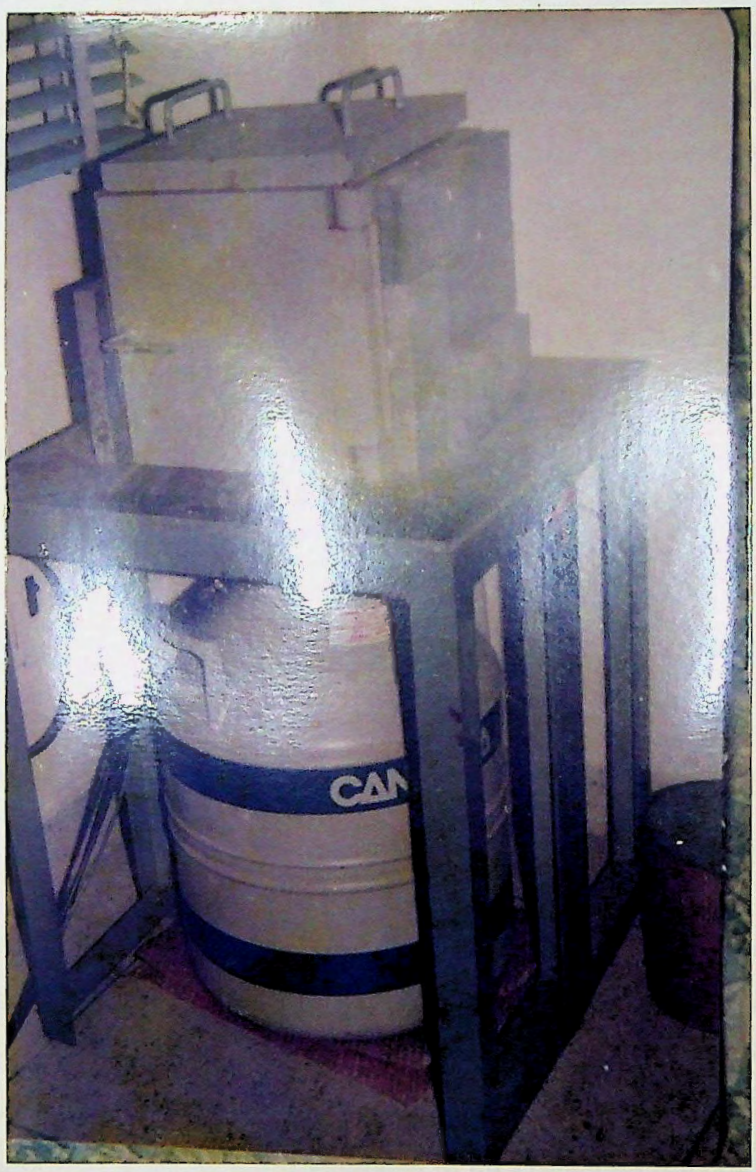

Fig.2.12b A partial view of HPGe-detector with shielding

panel controls. The unit is powered from a standard Nuclear Instrumentation Modules (NIM) bin power supply.

The Canberra model 3105 is suitable for use with high resolution detector systems. It is a NIM high voltage power supply, designed primarily for operation with semiconductor detectors and can accommodated all types of detectors requiring up to 5 KV bias with a current of 100μA. The applied bias voltage to the detector used in our experiment was 4000 volts. The 3105 Canberra power supply can withstand any overload or direct output short circuit for an infinite period of time and provide normal output when the ONN-OFF switch is reset. Output voltage can be continuously adjusted over the full range, 0 to ±5000 volts by means of five turn control.

2.3.2.3 Preamplifier

The preamplifier associated with radiation detectors performs four essential functions:

i) Conversion of charge to voltage pulse
ii) Signal amplification
iii) Pulse shaping
iv) Impedance matching

Most preamplifiers in used today are charge sensitive and provide an output pulse with an amplitude proportional to the integrated charge output from the detector. General purpose preamplifiers have a RC feedback network which results in a quasi-step function output. The preamplifier is isolated from the high voltage by a capacitor. The rise time of the preamplifier's output pulse is related to the collection time of the charge, while decay time of the preamplifier's output pulse is the RC time constant characteristic of the preamplifier itself. Rise times range from a few nanoseconds to a few microseconds, while decay times are usually set at about 50 microseconds. The RC preamplifier gives better performance at high total energy rates. It is, therefore, used exclusively on larger detectors which have greater stopping power for high energy photons.

To maximum performance, the preamplifier should be located at the detector to reduce capacitance of the leads, which can degrade the rise time as well as lower the effective signal size. Additionally, the preamplifier also serves to provide a match between the impedance of the detector and the low impedance of coaxial cables to the amplifier, which may be located at great distances from the preamplifier.

Canberra model 2001 is an advanced type of charge sensitive preamplifier which has been used in the present work. A few major characteristics of the preamplifier are as follows;

1. The pulse time is less than 40 n sec
2. The pulse decays exponentially with a time constant of 50 μ sec
3. The source capacity is 0 pF
4. The noise level is equivalent to less than 600 eV.

2.3.2.4 Amplifier

The major role of an amplifier is to convert the preamplifier output signal into a form most suitable for the measurement desired. Since the number of applications and signal characteristics are numerous, so there are many techniques for treating the signal to optimize each application. The amplifier serves to shape the pulse as well as further amplify it. The purpose of this additional amplification and shaping is two fold. First, further amplification improves the signal-to-cable noise ratio. Secondly, further shaping acts to prevent pulse overlap by clipping pulses. The spectroscopy amplifier provides a uni-polar output and include pole zero cancellation and rapid baseline restoration after the occurrence of a pulse. The important characteristics of the amplifier are the linearity, the output pulse shape, the gain stability and the noise level. Canberra model 2022 amplifier is used in this experiment. It offers the better resolution performance features and flexibility than any other nuclear pulse amplifier used commercially.

2.3.2.5 Pulse height analyzer and counting techniques

Pulse height analyzer may consist of a simple discriminator that can be set above noise level and which produces a standard logic pulse for use in a pulse counter or as gating signal. However, most data consists of a range of pulse heights of which only a small portion is of interest. One can employ either of the following:

1. Single channel analyzer and counter
2. Multichannel analyzer

The single channel analyzer (SCA) has a lower and an upper level discriminator and produces an output logic pulse whenever an input pulse falls between the discriminator levels. With this device, all voltage pulses in a specific range can be selected and counted. If additional voltage ranges are of interest, additional SCAs and counters (i.e., scalars) can be added as required, but the expense and complexity of multiple SCAs and counters usually make this configuration impractical.

If a voltage (i.e.,energy) spectrum is desired, the SCAs discriminators can be set to a narrow range (i.e.,window) and then stepped through a range of voltages. If the counters are recorded and plotted for each step, an energy spectrum will result. However, the preferred method of collecting a full energy spectrum is with a multichannel analyzer.

The multichannel analyzer (MCA), which can be considered as a series of SCAs with incrementing narrow windows, basically consists of an analog-to-digital converter (ADC), control logic, memory and display. The multichannel analyzer collects pulses in all voltage ranges at once and displays this information in real time, providing a major improvement over SCA spectrum analysis.

Figure 2.13 illustrates a typical MCA block diagram. An input energy pulse is checked to see if it is within the selected SCA range and then passed to the ADC which

is heart of MCA and converts the incoming analog amplifier signal to a group of standard shaped pulses. If the incoming pulse is 4 volts, the ADC might produce 400 standard pulse; or if the incoming pulse was 3 volts, 300 pulses would be produced. In this way, analog information (the signal height) is converted to digital information (the number of pulses). The ADC converts the pulse to a number proportional to the energy of the event. This number is taken to be the address (channel number) of a memory location and one count is added to the contents of that memory location. After collecting data for some period of time, the memory contains a list of numbers corresponding to the number of pulse at each discrete voltage. The display reads the memory contents vs. memory locations, which is equivalent to number of pulses vs. energy.

For the present experiment PC based system 100 MCA boards and software were used for data acquisition and display. The system 100 MCA has a full 16K channels of data memory, which can be configured as 4K (4096 channels), 8K (8192 channels), or the entire 16K (16384 channels).

Some features of S 100 MCA are

- Vertical axis in linear or log scale
- Built-in energy calibration function
- Built-in peak analysis function
- Built-in live time correction function
- Read out of dead time in percentage.

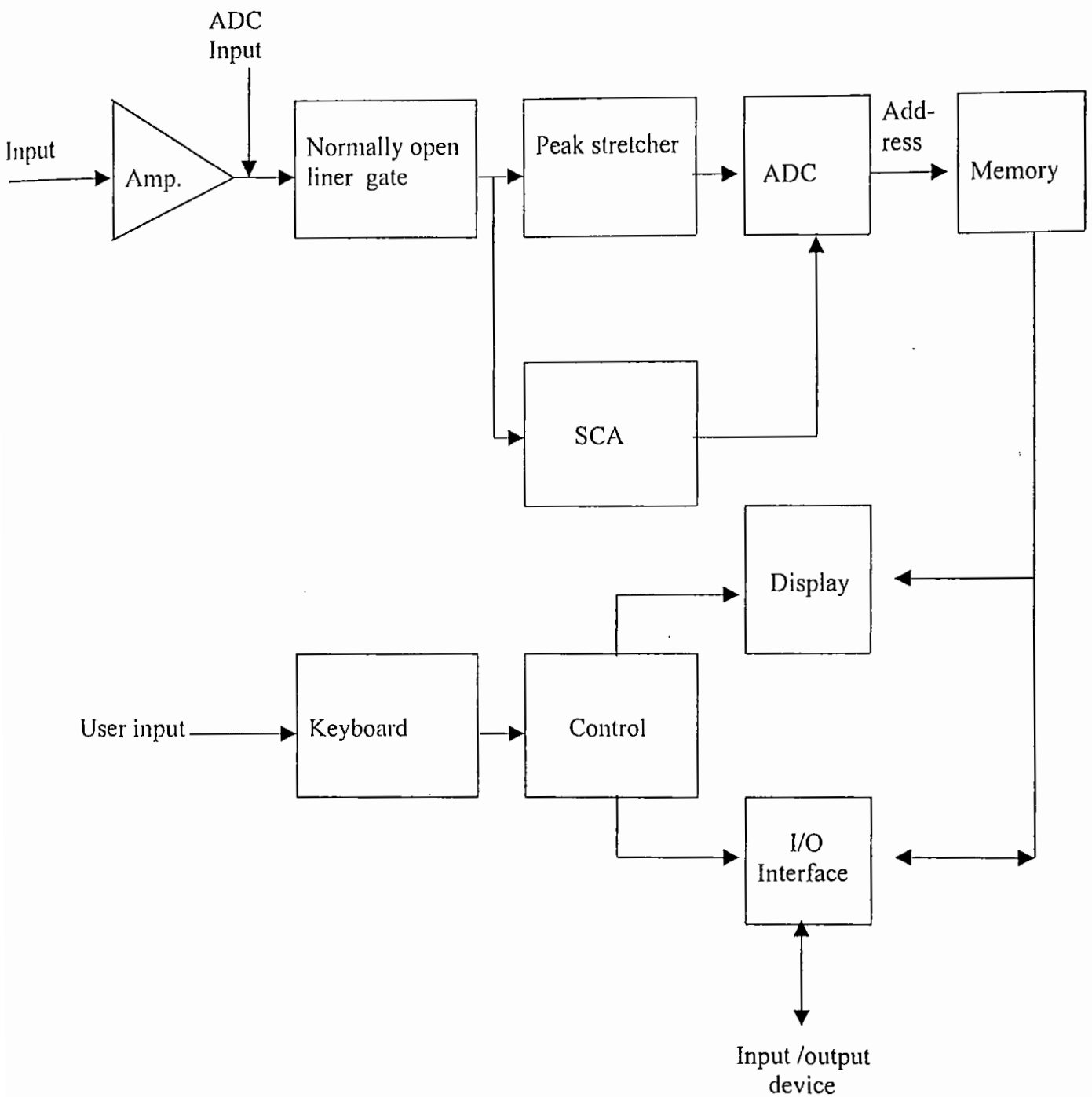

Fig. 2.13 Multichannel analyzer components.

2.3.3 Measurements of Detector Parameters

2.3.3.1 Energy resolution

Energy resolution is very important among the detector parameters. Energy resolution of a detector is defined as its ability to separate two adjacent peaks in gamma-ray spectrum. It is a measure of the width (full width half max, FWHM) of a single energy peak at a specific energy. Better (lower) resolution enables the system to more clearly separate the peaks within a spectrum. Thus the narrower the peak, the better the resolution capability. Resolution is a function of gamma-ray energy. Generally, the superior resolution of a HPGe-detector is sufficient enough to avoid the problem of peak convolution, (i.e., all peaks are separate and distinct). The sensitivity of a system improves as the resolution improves because higher resolution means that spectral line widths are smaller and fewer background counts are therefore involved in calculating peak integrals. To measure the resolution of the HPGe-detector, a gamma-ray spectrum was taken using standard ^{60}Co source for a counting time 600 sec. In the spectrum two adjacent gamma-ray peaks at the energies 1173.23 keV and 1332.51 keV as shown in Fig.2.14 was considered. The peaks are 159.28 keV apart. From the Fig.2.14 the full width at half maximum (FWHM) value was found to be 3.40 channels at 1332.51 keV peak. The resolution in keV can be determined using following equation.

$$\text{Resolution} = \text{FWHM (in channel)} \times \frac{159.28\,\text{keV}}{\text{No. of channels between the peaks}}$$

The detector resolution is found to be 2.04 keV at 1332.51 keV gamma-line of ^{60}Co source.

The dominant characteristics of germanium detectors is their excellent energy resolution, when applied to gamma-ray spectrometry. The great superiority of the germanium system in energy resolution allows the separation of many closely spaced

gamma-ray energies, which remain unresolved in the NaI (Tl) spectrum. A narrow peak includes fewer channels and fewer background counts. So, accuracy of measurement increases when high-resolution measuring system is used.

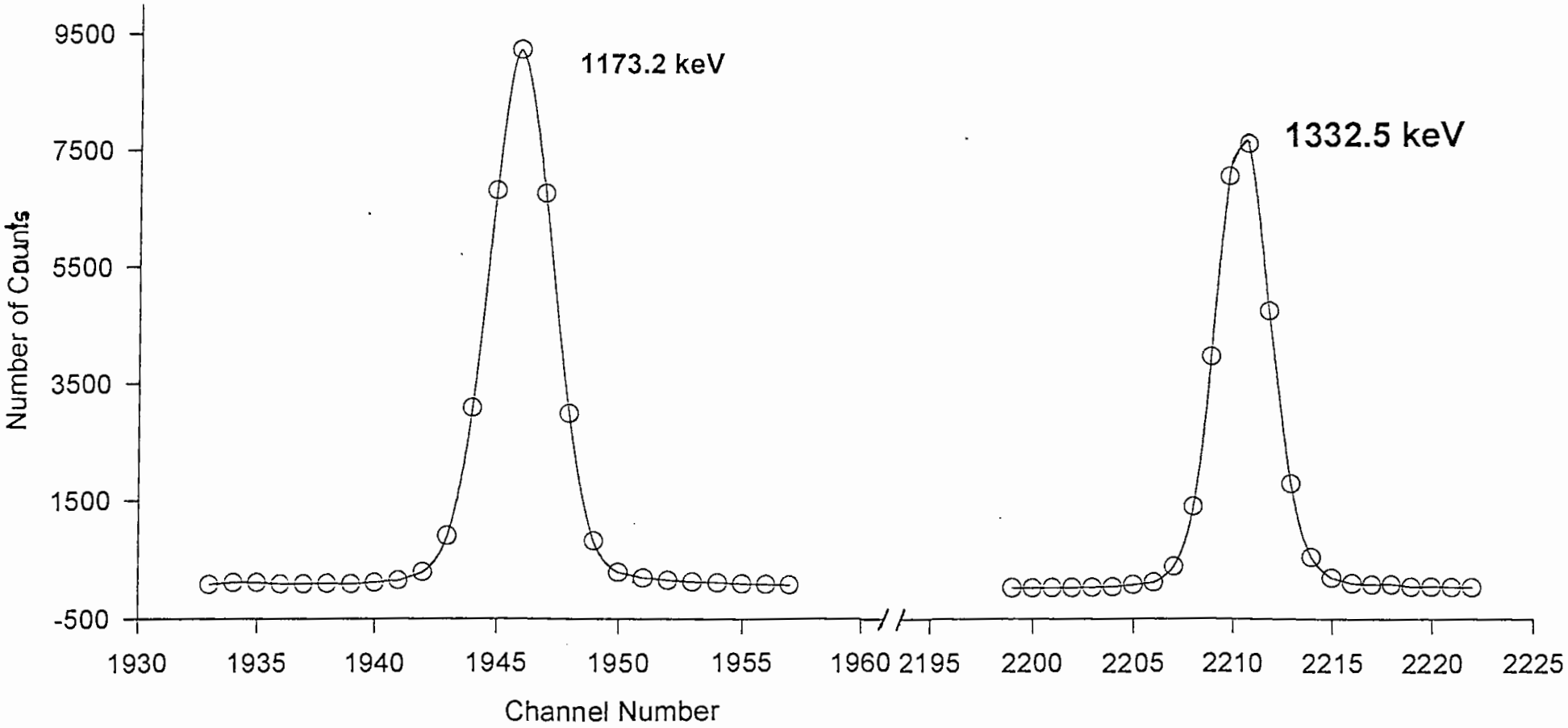

Fig.2.14 The ^{60}Co spectrum for energy calibration.

2.3.3.2 Efficiency calibration

The efficiency of detector is a measure of how many pulses occur for a given number of gamma rays emitted by the source. This parameter allows us to convert the count obtained from spectral analysis to unit of activity. With the physical change of counting system and the surrounding environment, efficiency changes. It means that the geometry of the counting system must remain unchanged throughout the experiment. Various kinds of efficiency definitions are in common use for gamma-ray detectors.

a. Absolute efficiency : Absolute efficiency is defined as the ratio of the number of counts produced by the detector to the number of gamma rays emitted by the source in all directions. It depends upon the distance between the source and the detector and the solid angle subtended by the detector. It takes into account, the full energy peak and all incomplete absorption represented by the continuum.

Absolute efficiency:

$$\varepsilon_{abs} = \frac{\text{No. of counts recorded by the detector}}{\text{No. of gamma rays emitted by the source}}$$

b. **Intrinsic efficiency** : The ratio of the number of pulses produced by the detector to the number of gamma rays striking the detector is called intrinsic efficiency.

Intrinsic efficiency:

$$\varepsilon_{ins} = \frac{\text{No. of pulses produced by the detector}}{\text{No. of gamma rays incident on the detector}}$$

c. Relative efficiency : Relative efficiency is the efficiency of one detector relative to another ; commonly that of a germanium detector relative to a 3 in. diameter by 3 in. long NaI crystal, each at 25 cm from a point source and specified at 1.33 MeV only.

Knowing the intensities and the peak areas, the relative efficiency for the full energy and escape peaks can be calculated by using the relation,

$$\text{Relative efficiency, } \varepsilon_{re} = \frac{\text{Peak area}}{\text{Relative intensity}}$$

d. Full-energy peak or (photo peak) efficiency : This is the efficiency for producing full-energy peak pulses only, rather than a pulse of any size for the gamma ray.

For the measurement of detector efficiency, the standard radioactive point sources of known strength such as ^{22}Na, ^{57}Co, ^{60}Co, ^{133}Ba and ^{137}Cs shown in Table 2.4 were used. Using standard calibrated sources, spectra were acquired at 8 cm above the surface of the detector for a counting time sufficient for peak area equal to or greater than 10,000. Counts were taken at a distance from the surface of the detector to avoid coincidence losses when a single source emits more than one gamma-ray energy. The standard source, ^{137}Cs has single energy, hence spectra for ^{137}Cs were obtained both at 8 cm and at the surface. The ratio of the counts at surface of the detector to the counts at 8 cm from the surface of the detector for ^{137}Cs with the same counting time is called normalizing factor. For other sources, the counts at the surface of the detector were obtained by the multiplication of normalizing factor with the counts at 8 cm.

Efficiency at the surface of the detector is determined from the following relationship.

$$\text{Efficiency, } \varepsilon = \frac{\text{Detected count /sec}}{\text{Present activity of the source, } A_t \times I_\gamma}$$

Where, I_γ is the gamma-ray intensity of the source.

The present activity of the source is given by

$$A_t = A_o \times e^{-\lambda t}$$

Where, A_t = Present activity of the source

A_o = Initial activity of the source

t_d = Decay time

λ = Decay constant

Clearly, to be useful, the detector must be capable of absorbing a large fraction of the gamma ray energy. This is accomplished by using a detector of suitable size or by choosing a detector material of suitable high atomic number. The efficiency also depends on source-detector distance and experimental geometry. The measured efficiencies of HPGe-detector are shown as a function of gamma-ray energy in Fig. 2.15.

Table 2.4 Source activity and efficiency at the surface of HPGe-detector.

Radioactive source	Gamma energy (keV)	Activity at 04.01.88 (μCi)	Gamma ray intensity Iγ	Half-life of radio-nuclide	Present activity (DPS)	CPS	Efficiency (%)
^{133}Ba	80.99	0.945	0.354	10.54 y	16030.47	417.22	7.35
^{57}Co	122.06	1.150	0.855	271.76 d	0.71	.01	22.12
^{133}Ba	276.40	0.945	0.073	10.54 y	16030.47	59.78	5.11
	302.85		0.184			143.36	4.86
	356.01		0.619			418.45	4.22
	383.85		0.089			57.15	4.00
^{22}Na	511.00	1.123	1.811	2.60 y	1781.58	96.86	3.00
^{137}Cs	661.64	0.903	0.860	30.14 y	25462.41	534.02	2.44
^{60}Co	1173.23	1.007	0.998	5.27 y	7877.75	123.24	1.56
^{22}Na	1274.55	1.123	0.999	2.60 y	1781.58	27.28	1.53
^{60}Co	1332.51	1.007	1.000	5.27 y	7877.75	109.49	1.39

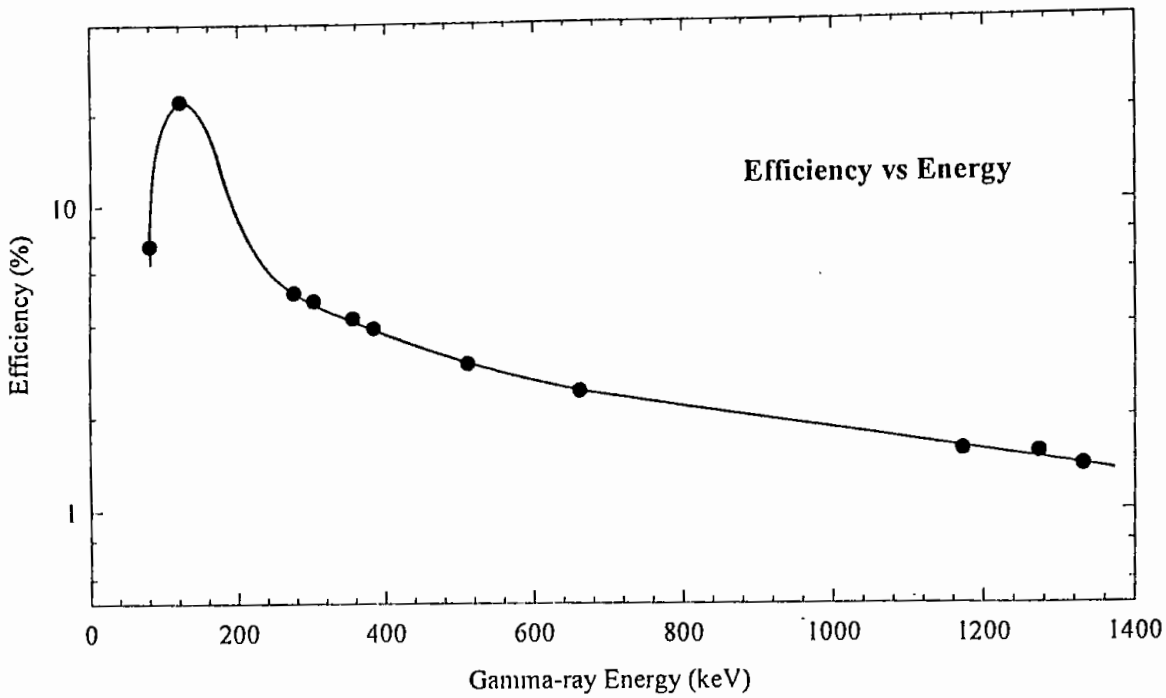

Fig.2.15 Detector efficiency as a function of gamma-ray energy.

2.3.4 Background Radiation

For the present work, the background effect is very important in detecting gamma rays by high purity germanium(HPGe) detector. Some counts in the detector were observed due to background radiation during the experiment. These counts are mainly produced by the cosmic radiation because of its interaction with earth's atmosphere and it determines the minimum detectable radiation level. The background counts depend upon the size and type of the detector and also upon the shielding around it. The sources of background radiation are as follows:

1. Radioactivity in the air surrounding the detector.
2. Radioactivity from the earth's surface (the terrestrial radiation), walls of the laboratory or other far away structures.

3. Natural radioactivity of the constituent materials of the detector itself.
4. Some fission products activities.
5. Activity of cosmic ray that continuously interacts with earth's atmosphere.

2.3.5 Shielding Arrangement of the Detector

For the protection of background of the detector, shielding arrangement is very essential. The shielding not only reduces the background resulting from cosmic radiation and from natural radioactive traces in the building materials or in the surface of the earth, but also from nearly nuclear facilities and other radiation sources like air, which presumably contains trace of radioactive gases, Radon (Rn) and Thorium (Th 220) etc. Mathematically the shielding effectiveness is expressed as

$$I = I_0 e^{-\mu t}$$

Where, I_0 is the initial beam intensity, I is the beam intensity after penetrating a thickness, t of the material and μ is the linear absorption coefficient of the material of the shield.

In our experiment, lead is used as shielding material across the HPGe detector. The important advantages of lead are high density (11.4 g/cc), large atomic number (Z= 82) and comparatively low cost. A brief description of the shielding used in the experiment is summarized in the Table 2.5.

Table 2.5 Summary of shielding arrangement around the HPGe detector.

Low background shielding	Material	Lead
	Length	12 inch
	Height	12 inch
	Thickness	4 inch
	Form	Square

2.3.6 Composite Decay Curve

A radioactive nuclide may be characterized by the rate at which it disintegrates and any one of three quantities, the disintegration constant, the half life or the mean life, may be used for this purpose. It often happens that two or more radioactive species are mixed together, in which case the observed activity is the sum of separate activities. If the activities are independent, i.e., one component of the mixture does not give rise to another, the various activities can sometimes be distinguished and the separate half-lives determined. When the total activity is plotted against the decay time, a curve like solid one is obtained. The curve is concave upward because the shorter-lived components. After a sufficiently long time, only the longest-lived activity will remain and the value of its half-life can be read from the portion of the decay curve, which will be a straight line. If this straight line portion is extrapolated back to $t_d = 0$ and if the values of the activity given by the line are subtracted from the total activity, the curve that remains will represent the decay of all the components of the mixture except the longest-lived. The curve for the total activity is the sum of the two straight lines which represent the individual activity.

The use of the decay curve is one in which two elements give photopeaks of the same energy and thus discrimination of the elements must be made on the basis of difference in half-lives. Two decay curves (cps vs. t_d) for the radionuclides of germanium and zinc isotopes were made. With the help of these curve, the activities of ^{69}Ge, ^{71m}Zn, ^{64}Cu and ^{63}Zn were corrected using the γ-ray energies, 511 keV and 511.5keV. The composite decay curve only for ^{64}Cu and ^{63}Zn radionuclides are shown in Fig. 2.16.

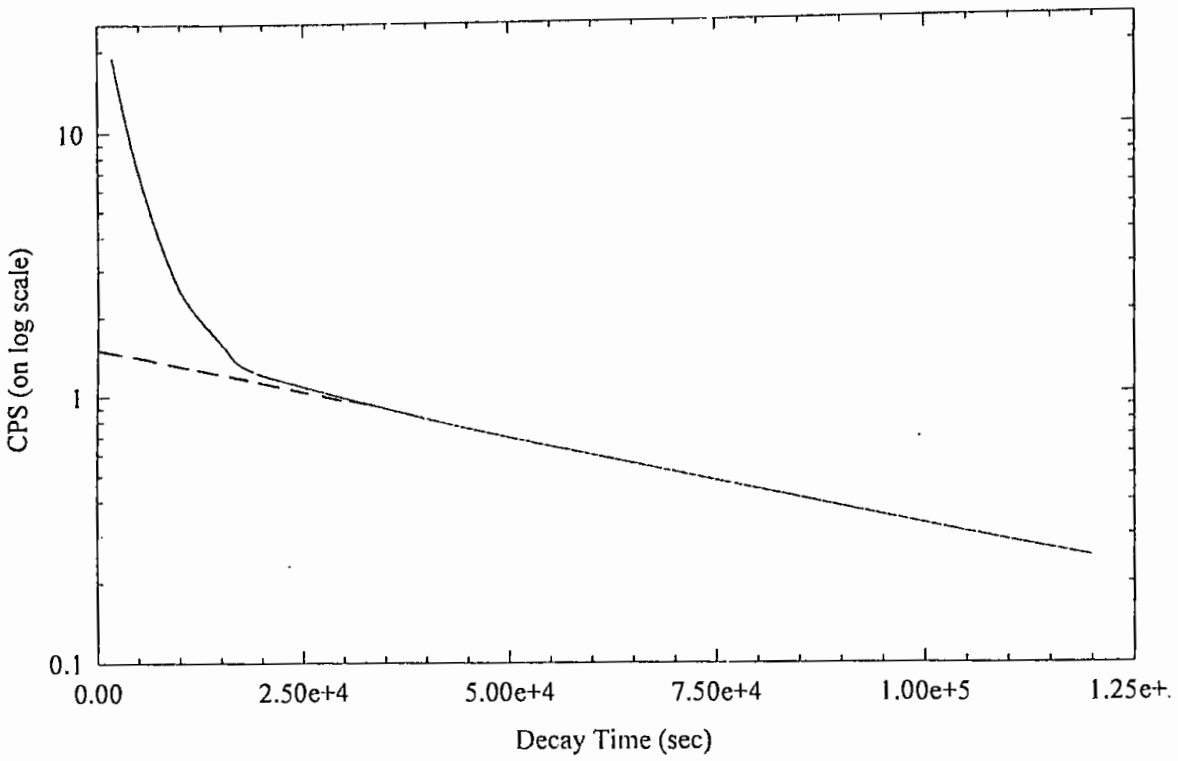

Fig. 2.16 Composite decay curve for the radionuclides ^{64}Cu and ^{63}Zn.

2.3.7 Measurements of Radioactivity and its Calculation

The induced activities of ^{24}Na from the irradiated monitor foils and the activities of the reaction products of interest from the irradiated samples were determined non-destructively using HPGe-detector gamma ray spectroscopy. The samples and foils were placed directly on the surface of the detector. Counting of the samples and the flux monitor foils were performed under the same geometry as was used at the time of efficiency measurement of the detector. Peak area analysis was done in a Canberra S-100 Multi Channel Analyzer (MCA) master board package based personal computer with the associated electronics. The detector was shielded with lead and iron to reduce the background radiation. The γ-ray energies which were used to characterize the activation product are shown in Table 2.6. The back ground counts of 511 keV gamma-energy due to pair annihilation and interfering reaction were subtracted from the total counts to give

accurate count of desired radionuclides. The background count was also corrected for 909.10 keV gamma-ray energy. Using the measured count rates, efficiency of the detector and other decay data, the activities (disintegration per second, DPS) after the irradiation were determined by the following equation.

$$DPS = \frac{CPS}{\varepsilon \times I_\gamma} \times e^{\lambda t_d}$$

The cross section values of the desired reactions were calculated using the following standard activation equation

$$\sigma = \frac{DPS}{N\varphi(1 - e^{-\lambda t_i})}$$

Where, CPS = Net area under a photo-peak / counting time

I_γ = Gamma-ray intensity of the source.

t_d = Decay time

ε = Efficiency of the detector

N = Total number of target nuclei

$$= \frac{W \times F \times N_A}{M}$$

M = Atomic weight

F = Isotopic abundance of target nuclei

W = Weight of sample in gram

N_A = Avogadro's number (6.023×10^{23} atoms/mole)

φ = Neutron flux ($n\ cm^{-2}sec^{-1}$)

t_i = Irradiation time (sec)

σ = Cross section (mb)

DPS= Disintegration per second

λ = Decay constant $=0.693/T_{1/2}$

$T_{1/2}$ = Half-lives of the product radionuclide.

Table 2.6 Nuclear and other related data concerned in this work[34,61,62].

Nuclear reaction	Isotopic abundance of the target nucleus (%)	Q-value (MeV)	Half-life of the product nuclei	Decay mode	Gamma ray energy (keV)	Gamma ray intensity Iγ (%)
$^{64}Zn(n,2n)^{63}Zn$	48.90	-11.86	38.50 m	β^+	669.6	8.5
$^{64}Zn(n,p)^{64}Cu$	48.90	0.20	12.74 hr	EC, β^+, β^-	511.00	37.00
$^{70}Zn(n,2n)^{69m}Zn$	0.62	-9.65	13.9 hr	β^-	438.90	100.00
$^{70}Ge(n,2n)^{69}Ge$	20.70	-11.54	39.2 hr	β^+	511.00	68.00
$^{74}Ge(n,\alpha)^{71m}Zn$	36.40	-0.61	3.97 hr	β^-	511.50	28.40
$^{76}Ge(n,2n)^{75m+g}Ge$	7.70	-9.43	82.8 m	β^-	264.80	12.00
$^{45}Sc(n,2n)^{44m}Sc$	100	-11.60	58.60hr	β^+	271.40	86.00
$^{90}Zr(n,2n)^{89}Zr$	51.40	-11.97	3.271 d	β^+	909.10	99.00

2.3.8 Neutron Flux Measurement

The effective neutron flux density during the irradiation at the each sample position was determined via the monitor reaction $^{27}Al(n,\alpha)^{24}Na$ ($T_{1/2}$= 15.02 hr, E_γ= 1369 keV, Iγ= 100%). The cross section data for the monitor reaction were taken from the work of H. Vonach[63]. For determining the average flux density effective on each

sample, the two Al foils from the front and back of the irradiated sample were detached and placed together on the HPGe-detector surface for γ-ray counting. For the sample irradiation angles of interest, the measured neutron flux densities are given in Table 2.7-2.9. To determine neutron flux, the following equation was used.

$$\varphi = \frac{DPS}{N\sigma(1-e^{-\lambda t_i})}$$

The description of the notations used in above equation are mentioned in previous section.

Table 2.7 Neutron energy and flux at different angular positions for zinc samples.

Sample	Sample position	Corresponding Neutron energy (MeV)	Cross section of $^{27}Al(n,\alpha)^{24}Na$ reaction (mb)	Neutron flux ($ncm^{-2}s^{-1}$) (measured)
Zn-1	0°	14.71±0.11	113.10	1.85×10^{6}
Zn-2	30°	14.63±0.11	114.53	1.77×10^{6}
Zn-3	60°	14.41±0.08	117.54	1.70×10^{6}
Zn-4	90°	14.10±0.04	121.91	1.57×10^{6}
Zn-5	120°	13.82±0.06	122.72	1.47×10^{6}

Table 2.8 Neutron energy and flux at different angular positions for germanium samples.

Sample	Sample position	Corresponding Neutron energy (MeV)	Cross section of $^{27}Al(n,\alpha)^{24}Na$ reaction (mb)	Neutron flux ($n\ cm^{-2}s^{-1}$) (measured)
Ge-1	10^{o}	14.70±0.11	113.10	9.13×10^{5}
Ge-2	50^{o}	14.51±0.09	116.04	8.81×10^{5}
Ge-3	70^{o}	14.31±0.07	119.97	7.75×10^{5}
Ge-4	90^{o}	14.10±0.04	121.91	7.36×10^{5}
Ge-5	110^{o}	13.90±0.04	123.02	7.80×10^{5}

Table 2.9 Neutron energy and flux at different angular positions for scandium and zirconium samples.

Sample	Sample position	Corresponding neutron energy (MeV)	Cross section of $^{27}Al(n,\alpha)^{24}Na$ reaction (mb)	Neutron flux (n $cm^{-2}s^{-1}$) (measured)
Zr-1	0^0	14.71±0.11	113.10	9.45×10^5
Sc-1	10^0	14.70±0.11	113.10	9.06×10^5
Sc-2	30^0	14.63±0.11	114.53	9.76×10^5
Zr-2	50^0	14.51±0.09	116.04	8.64×10^5
Zr-3	70^0	14.31±0.07	119.97	8.41×10^5
Sc-3	80^0	14.21±0.06	121.99	8.72×10^5
Zr-4	100^0	14.00±0.03	122.24	7.38×10^5
Sc-4	110^0	13.90±0.04	123.02	7.97×10^5

2.3.9 Q-value Determination

In a manner analogous to that used with chemical reactions, a nuclear reaction can be written to indicate the energy Q released or consumed, as

$$X + a \rightarrow Y + b + Q$$

The Q value for a particular reaction can be calculated using the Einstein equation

$$E = m c^2$$

Where, E is the energy associated with the mass, m and c is the velocity of light. Hence it can be shown that 1 g of matter is equivalent to an energy, $E = 1 \times (3 \times 10^{10})^2$ or 9×10^{20} ergs. The nuclear interaction energy Q is that associated with the difference between the mass of the products and reactants. Thus if m_y and m_b represent the individual masses of the products and m_a and m_x the masses of the reactants, the difference Δm is given by

$$\Delta m = (m_a + m_x) - (m_y + m_b)$$

and

$$Q = \Delta m\, c^2$$

If Q is positive, the reaction is termed exoergic (energy releasing) ; if negative, the reaction is endoergic (energy consuming). In nuclear reactions masses are expressed in atomic mass units (amu) and a conversion is necessary to express the energy in MeV units. The energy associated with nuclear mass is $E = mc^2 = 1.66 \times 10^{-24} \times 9 \times 10^{20}$ or 1.49×10^{-3} erg. The electronic charge of an electron is 1.6×10^{-19} C and the work W corresponding to 1 eV is $W = q \times V = 1.6 \times 10^{-19}$ C $\times 1$ V or 1.6×10^{-19} J or 1.6×10^{-12} erg. Therefore, 1 amu has an energy equivalent of $1.49 \times 10^{-3} / 1.6 \times 10^{-12}$ or 0.931×10^{9} eV or 931 MeV. Hence the equation of Q –value determination can be expressed as

$$Q = [(\text{mass of reactant}) - (\text{mass of product})] \times 931 \text{ MeV}$$

To determine Q-value of our investigated reactions, the mass of reactant and product were taken from the work of G.Friedlander[62].

Table 2.10 Principal sources of uncertainty and their magnitudes.

Source of uncertainty	Magnitude (%)
Error in flux determination	1.0-3.0
Neutron flux variation with time	0.5-1.5
Statistic of counting	0.5-8.0
Efficiency of the detector	1.5-3.0
Neutron absorption and scattering within the sample	0.5
Self absorption of gamma-ray in sample	0.5
Irradiation geometry	0.5-1.5
Sample weight	≤1
Decay data	0.3-1.0
Gamma-ray emission probability	0.3-1.0
Error in peak area analysis	0.5-1.0

2.3.10 Health Precaution

One can only protect oneself and others from injury if one is aware of the danger, observes the safety regulations and takes appropriate precautions. This is particularly true when handling ionizing radiation.

During the decay of radioactive substance, ionizing radiation is emitted (α-, β-, γ-radiation). In the case of external irradiation, α-rays present no danger, since they do not penetrate the upper layer of the skin which is insensitive to radiation and it can be shielded by just a sheet of paper. On the other hand, α-emitters are particularly dangerous if they are incorporated, e.g. by respiratory air, food or open wounds (incorporation).

β-radiation consists of fast electrons emitted at the decay of most atomic nuclei. The penetrating power of β-radiation depends on its energy and it can be shielded by 1-2 cm of Plexiglas. In the case of external β-radiation, the external sections of the skin are particularly endangered. From the point of view of radiation protection, positrons behave similarly to β-radiation.

γ-radiation is almost always emitted simultaneously with α- or β-radiation during the decay of radioactive substances. γ-radiation is very penetrating. Heavy materials, such as lead or iron, are particularly suitable for shielding purposes.

Neutrons are very penetrating. They are effectively shielded by substances of light atomic weight (water, concrete). Neutrons can be captured by substances with stable atomic nuclei thus resulting in radioactive substances.

Various types of radiation (α-radiation, γ-radiation, neutrons) cause different degrees of injury at the same absorbed dose. A new dose concept has therefore been introduced for the purposes of radiation protection, the equivalent. This is a uniform measure of possible injury for all types of radiation. In the case of neutrons or α-radiation, the severity of injury is greater than with γ- radiation at the same dose.

Injury may arise years or even decades after irradiation with high dose. In contrast to acute injury, the late somatic radiation injury is not characterized by a special syndrome. These are rather illnesses which can also result without irradiation. The most serious and most frequent late somatic injury is the formation of malignant tumors (cancer). Genetic radiation injury is the damage to the genes embedded in the gametes[65]. The aim of radiation protection is to prevent acute radiation injury and to keep the amount of late somatic injury and genetic injury as low as possible. Therefore, the following rules were always observed in handling the radioactive substances:

1. The quantity of radioactive material handled at any one time was kept as small as possible.

2. The distance from the radiation source was kept as large as possible.
3. The prescribed protective clothing was worn (smock, overall, overshoes, lead apron, gloves or also a respirator).
4. Due to the increased danger of incorporation it was forbidden to eat, drink, smoke or apply make-up in the controlled area.
5. Radioactive and contaminated waste was only be placed into the containers provided for this purpose after it had been properly sorted.
6. Radiation was shielded as far as possible.

i) Neutron shielding

All the walls surrounding the neutron generator and the roof of the neutron generator room is made of 5 ft concrete for neutron shielding. Nevertheless neutron is monitored in the adjacent control room at the operating hours. In neutron induced reactions, gamma rays are usually emitted by radioactive reaction products. Therefore, the concrete walls are also necessary for the shielding of gamma rays.

ii) γ-radiation shielding

In spite of very penetrating, γ-radiation is attenuated in matter. Materials with a high atomic number or of great thickness considerably attenuate γ-radiation. In the present investigation lead, iron and concrete containing scrap iron were used as shielding materials. Shielding made of these materials was correspondingly thicker.

2.3.11 Radioactive Waste Disposal

The atomic nuclei of radioactive substances decay spontaneously and emit α-, β-, γ-radiation. After counting of radioactive samples and contaminated waste were stored in a container that was made of lead, iron or concrete etc. Every radioactive substance decays with a half-life characteristic to the emitted concerned. This is the time in which half of the radioactive atoms present are decayed. After two half-lives, the

number of these atoms has been reduced to ¼ and after 10 half-lives to 1/1000 of those originally present. There are radioactive substances with half-lives of a fraction of a second and also those with half-lives of many years. Storage of radioactive waste is a very useful procedure when dealing with nuclides of relatively short half-life (e.g. up to a few months). Hold-up of the waste for a period of up to few years may reduce the activity to a sufficiently low level to permit release. The principle being applied is the delay and decay[66].

It is important to note that radioactivity decreases very greatly with time but never completely disappears. It will decay eventually, but in view of the very long half-life of many radionuclides, it is not always practicable to await the decay of radioactive material. After storing sufficient time, the waste was transferred to health physics division for disposal.

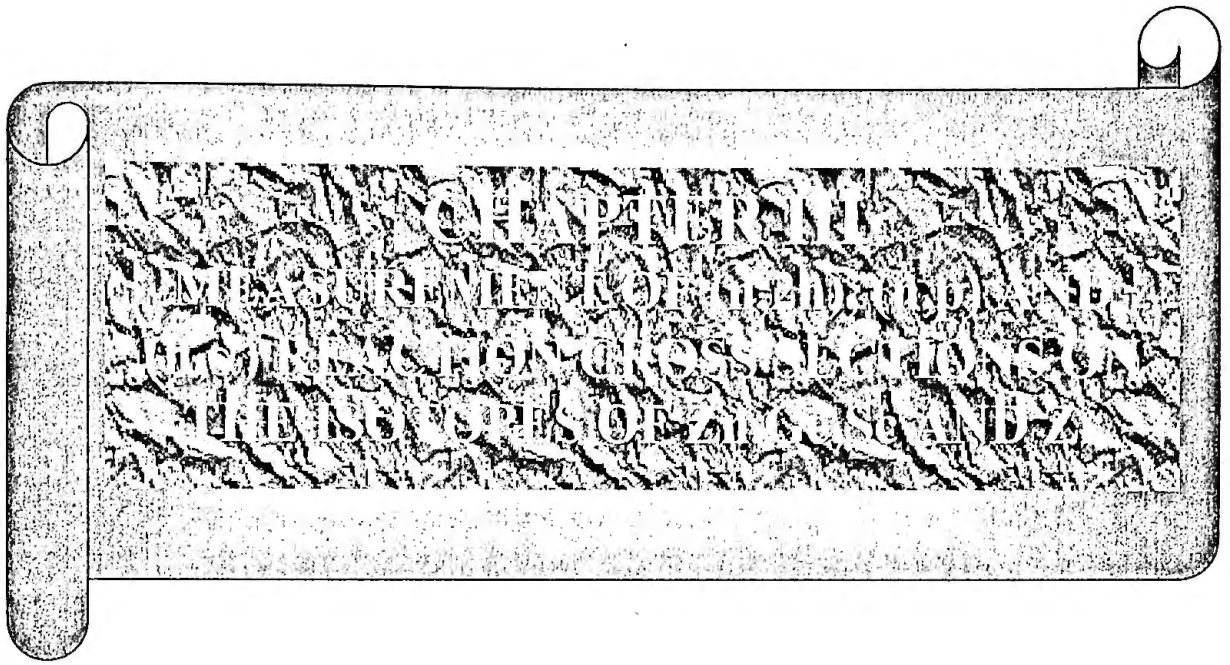

CHAPTER III

MEASUREMENT OF (n,2n), (n,p) AND (n,α) REACTION CROSS SECTIONS ON THE ISOTOPES OF Zn, Ge, Sc AND Zr

In cross section data measurements for the reactions $^{64}Zn(n,2n)^{63}Zn$, $^{64}Zn(n,p)^{64}Cu$, $^{70}Zn(n,2n)^{69m}Zn$, $^{70}Ge(n,2n)^{69}Ge$, $^{74}Ge(n,\alpha)^{71m}Zn$, $^{76}Ge(n,2n)^{75m+g}Ge$, $^{45}Sc(n,2n)^{44m}Sc$ and $^{90}Zr(n,2n)^{89}Zr$ in the neutron energy range of 13.82 to 14.71 MeV, we have followed activation technique in combination with high resolution HPGe-detector gamma-ray spectrometry.

3.1 Measurement of Activation Cross Sections of (n,2n) and (n,p) Reactions on the Isotopes of Zinc.

3.1.1 Materials

i) ZnO
ii) Al-foil
iii) Acetone
iv) Polyethylene bag
v) Cellulose tape

3.1.2 Experimental Procedure

High purity sample of Zn like ZnO (purity 99.99%) from E. MERCK, Germany, in powder form was used. Five zinc samples were prepared in the form of pellets by applying a pressure of 5 tons per cm^2 using a hydraulic press. Each pellet weighed between 0.7216 and 0.7835 g and had the dimension of 1.2 cm diameter and ~0.2 cm thickness. The samples used for non-destructive measurements were sealed in very thin

polyethylene bags. Aluminium (purity 99 %) of the same diameter as the sample were then attached at front and back of each samples. Mass of the each foil was between 0.1226 and 0.2072 g. Aluminium foils were used to measure the neutron flux at the scattering–free ring geometry arrangement shown in Fig.3.1 and was used for the irradiation of the samples and the flux monitor foils at 6.6 cm from the D-T source. The samples and the monitor foils were fastened to the ring which was accurately graduated for the indication of angular positions. The angular positions of the samples with respect to direction of deuteron beam were 0°, 30°, 60°, 90° and 120°. The irradiation of sample and aluminium foil by neutron was carried out at J-25, AID, FRANCE Neutron Generator facilities of the Institute of Nuclear Science and Technology (INST), Atomic Energy Research Establishment, Savar, Dhaka. For the present experiment, the main operational parameters of the neutron generator are as follows.

Beam current : 200μA
Beam diameter : ~1 cm
Deuteron energy : 110 keV
Irradiation time : 3 hours

During the irradiation, the target was cooled by a jet of cold air. The neutron production rate was monitored by BF_3 long counter which was placed at a 2 meter from the tritium target and at 45° with respect to the deuteron beam direction. During irradiation, the relative changes of the neutron production as a function of time were monitored by means of a BF_3 long counter calibrated earlier with ^{252}Cf neutron source.

The activities of the radioactive products from the desired reactions and monitor reaction were measured separately by counting γ-ray of the interested energy using HPGe-detector in combination with S-100 MCA. From the activities, the neutron flux and cross sections were determined using known standard formula that are shown earlier. Partial decay scheme[61] of the product nuclei and the origin of the gamma rays are shown in Fig. 3.2-3.4.

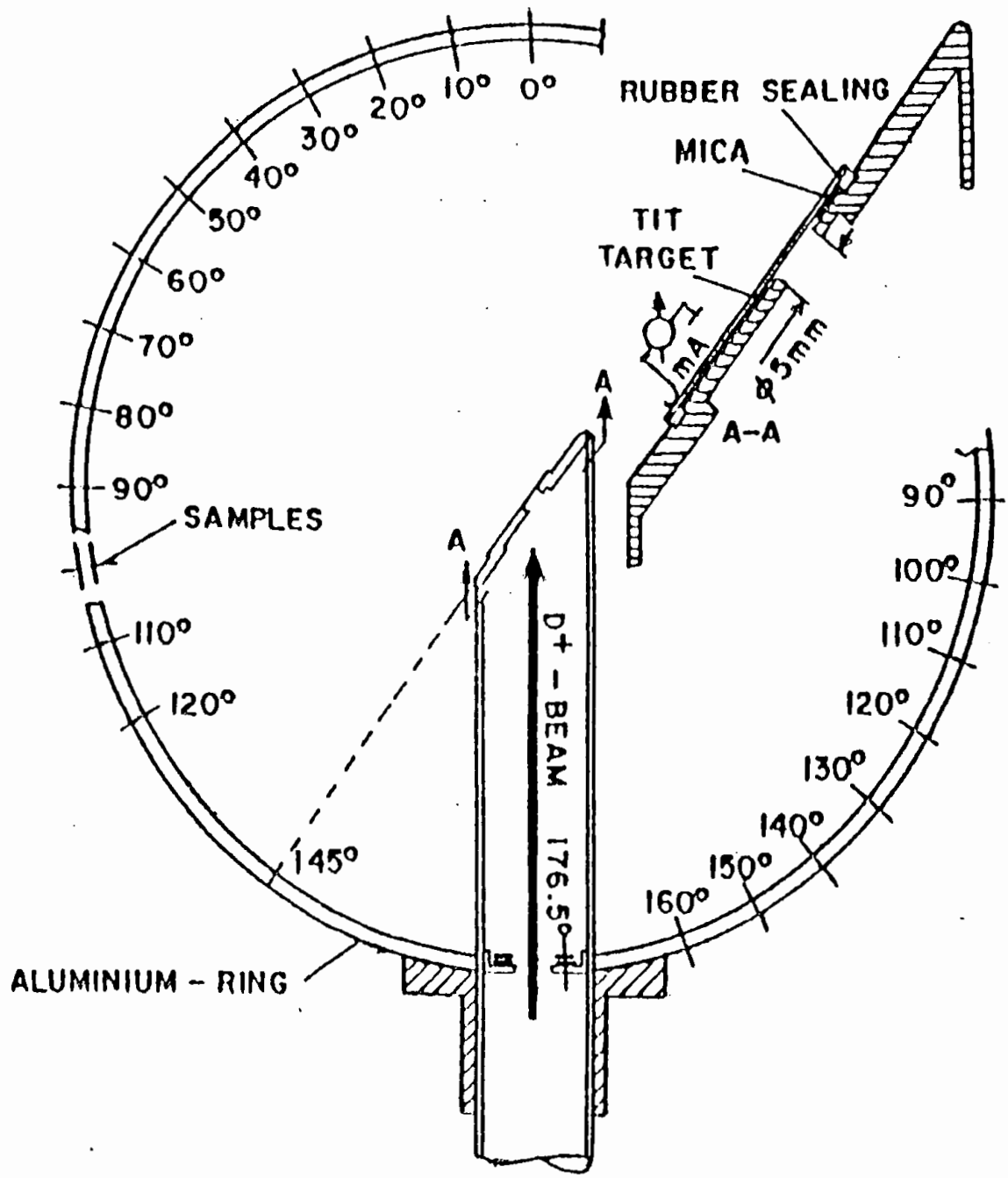

Fig.3.1 A sketch of the scattering-free ring geometry arrangement for the irradiation of samples

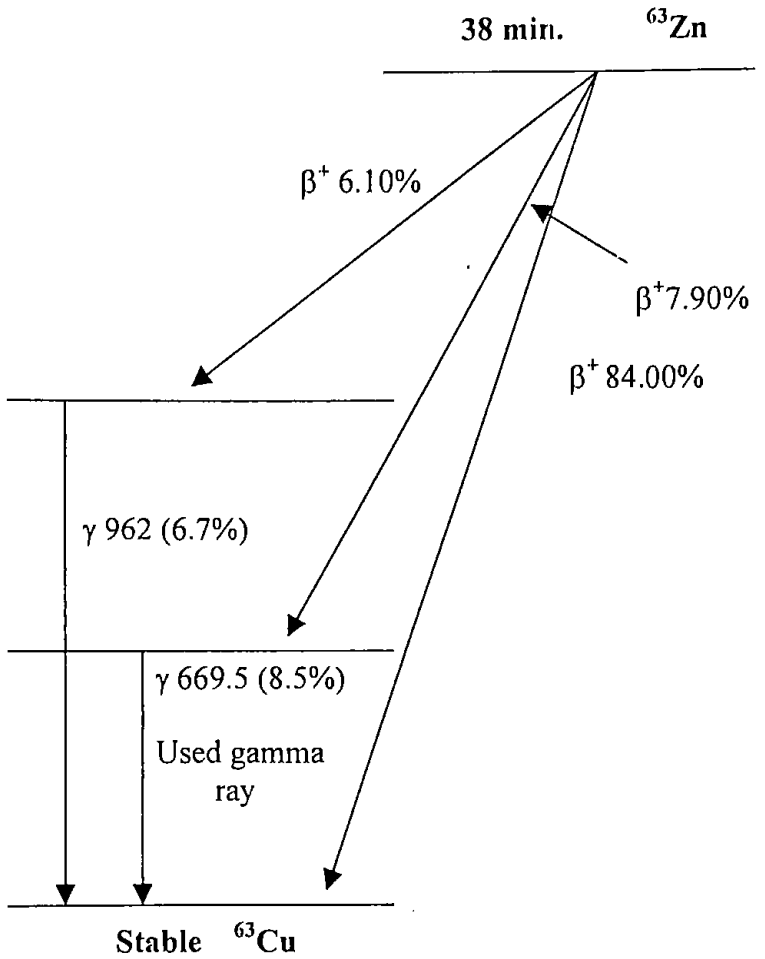

Fig.3.2 Partial decay scheme of the product nucleus of ^{64}Zn(n,2n)^{63}Zn reaction.

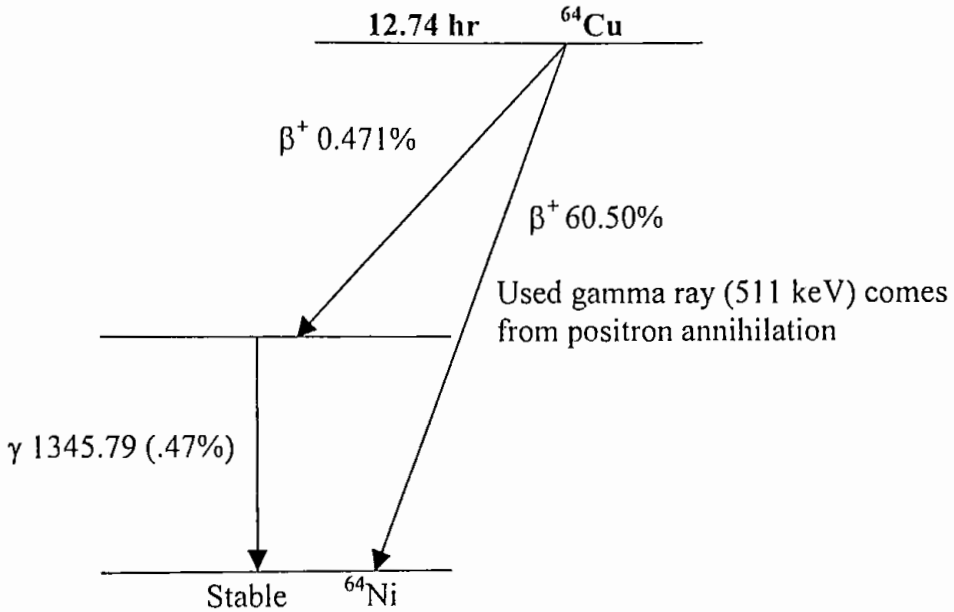

Fig.3.3 Partial decay scheme of the product nucleus of ^{64}Zn(n,p)^{64}Cu reaction.

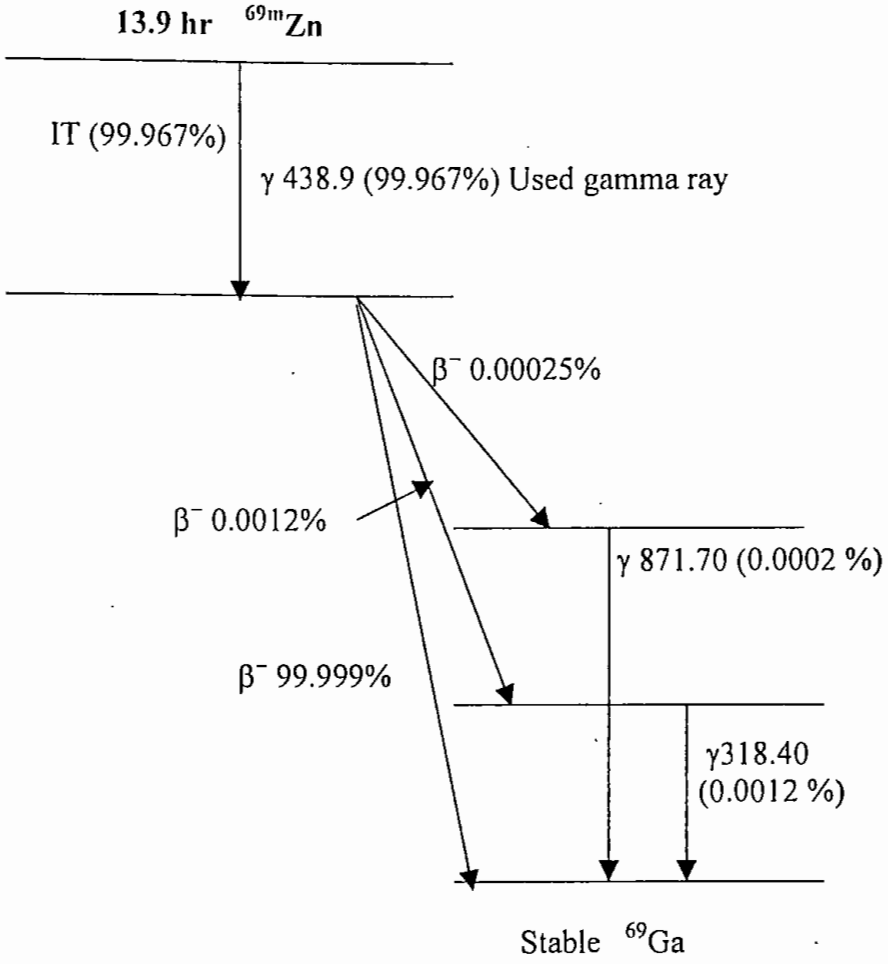

Fig.3.4 Partial decay scheme of the product nucleus of ^{70}Zn(n,2n)^{69m}Zn reaction.

3.1.3 Results and Discussion

The measured cross sections including errors at different energies in the range of 13.82 to 14.71 MeV are given in Table 3.1. The quoted uncertainty in the cross section values include both systematic and statistical errors. The deviation in the neutron energy does not give an error; it describes the energy spread due to the angle of emission of neutron, the finite size of the sample and deuteron energy loss in gas. The cross section values in this work, literature data and the values obtained by nuclear model calculations using the statistical codes SINCROS-II and EXIFON are shown in Fig. 3.5-3.7 as a function of neutron energy. The results of the three reactions of zinc isotopes are discussed in the subsequent sections.

^{64}Zn(n,2n)^{63}Zn Reaction

On the measurement of cross section for the reaction ^{64}Zn(n,2n)^{63}Zn, extremely few published data are available. More experiments are needed to give precision cross section data of this reaction. Our measured data and the literature data are shown in Fig.3.5 as a function of neutron energy. The measured data are lower than those of evaluated data of Bychkov et al.[32] and the data reported in the Hand Book[67] on Activation Cross Sections but these data are relatively older. The data of our experimental work are also lower than that of R.U.Miah[27] and coverage in the middle of theoretical calculations using SINCROS-II and EXIFON. The present experiment introduces some newer data points to the existing literature and theoretical calculations.

$^{64}Zn(n,p)^{64}Cu$ Reaction

The results of the nuclear model calculation are also shown as a curve along with the measured values. The quoted uncertainty in each cross section value includes both statistical and systematic errors. The estimated total uncertainties in the cross section values lie between 7 to 9 % (cf. Appendix 3).

The present results agree well with both the experimental value reported by Belgaid et al.[30] and the evaluated data of Cullen et al.[31] and the Hand book[67]. The results of the work of R.U.Miah[27] at different energies are consistently larger than the trend of the present work. From the Fig. 3.6 it is observed that the cross sections of the present work at the energies 14.10, 14.41, 14.63, 14.71 MeV are closer with the line of theoretical value obtained by using the code EXIFON and the values at 13.82, 14.10 MeV energies are larger. The present values at the last four energies are below the values obtained via for SINCROS-II but near. It may be mentioned that the present experimental data shown in figure 3.6 agree well with the results obtained from the nuclear model calculation using both the computer codes EXIFON and SINCROS-II. With the increasing neutron energy, the corresponding experimental result decreases that is similar with the result of model calculations. In general, the agreement between experimental and theory is fairly well.

$^{70}Zn\ (n,2n)^{69m}Zn$ Reaction

The cross section values as a function of neutron energy obtained from the present investigation along with literature data for $^{70}Zn(n,2n)^{69m}Zn$ reaction have been plotted as a function of neutron energy which is shown in Fig. 3.7. Experimentally determined shape of excitation function is very important because an unknown cross section can predicted from it by extrapolation. Fig. 3.7 shows that the cross section for the reaction $^{70}Zn(n,2n)^{69m}Zn$ increases with the increase

of incident neutron energies. From the Fig. 3.7, it is observed that the measured cross section value at 14.10 MeV neutron energy have deviated from the trend of other selected energy. The measured value at 13.82 MeV is larger than that of the literature and theoretical calculation but nearer. The cross section data of this work at 14.41, 14.63 and 14.71 MeV neutron energies may be defined as the average cross section values of corresponding neutron energy obtained from R.U.Miah[27], Wenrong et al.[29], Hand book[67] and SINCROS-II calculation. However, the measured data obtained from the present work agree well with the literature data and SINCROS-II calculation. It may be mentioned that a large number of values of cross section over a wide range of neutron energies covering both ends of the curve would be necessary to draw a definite conclusion about the shape of the curve.

Table 3.1 Activation cross sections of (n,2n) and (n,p) reactions on some isotopes of zinc.

Nuclear reaction	Neutron energy (MeV)	Measured reaction cross section (mb)
$^{64}Zn(n,2n)^{63}Zn$	14.71±0.11	121.01±11.57
	14.63±0.11	100.49±10.05
	14.41±0.08	91.29±9.36
	14.10±0.04	96.53±10.62
	13.82±0.06	86.49±10.40
$^{64}Zn(n,p)^{64}Cu$	14.71±0.11	162.49±12.00
	14.63±0.11	168.95±14.81
	14.41±0.08	180.90±14.58
	14.10±0.04	184.28±13.79
	13.82±0.06	172.36±13.62
$^{70}Zn(n,2n)^{69m}Zn$	14.71±0.11	692.22±55.94
	14.63±0.11	677.28±56.21
	14.41±0.08	664.24±54.52
	14.10±0.04	687.10±59.14
	13.82±0.06	643.62±53.17

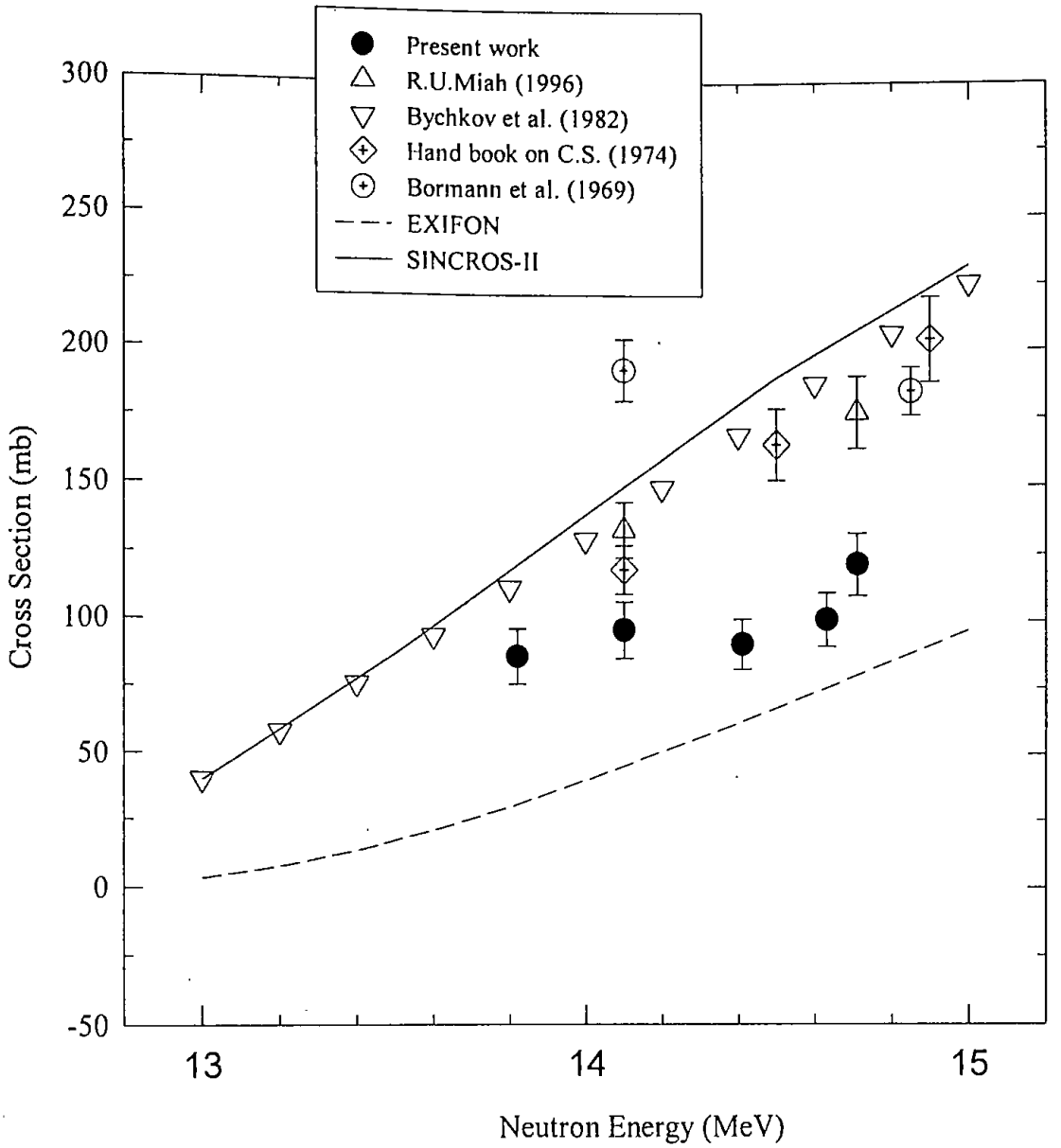

Fig. 3.5 The excitation function of $^{64}Zn(n,2n)^{63}Zn$ reaction.

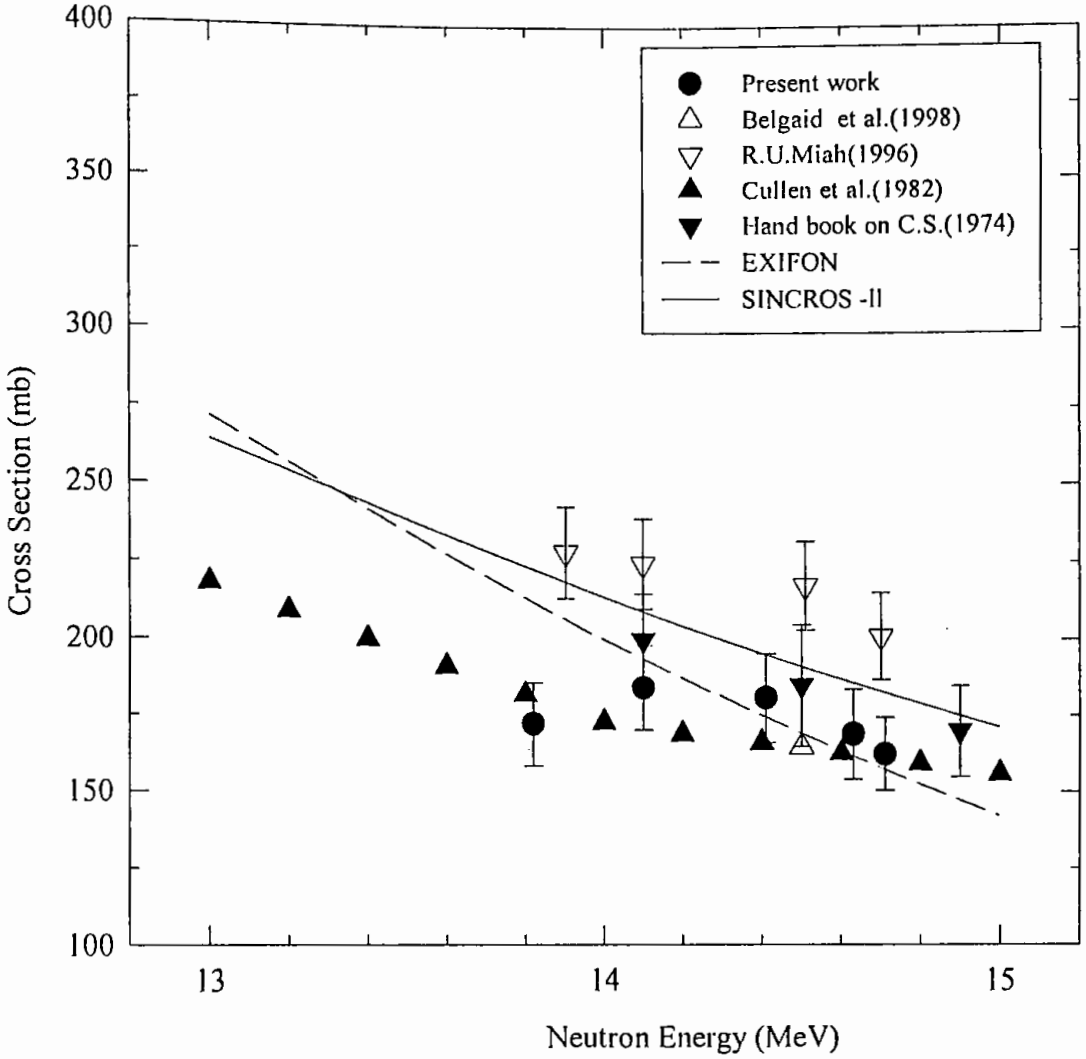

Fig. 3.6 The excitation function of $^{64}Zn(n,p)^{64}Cu$ reaction.

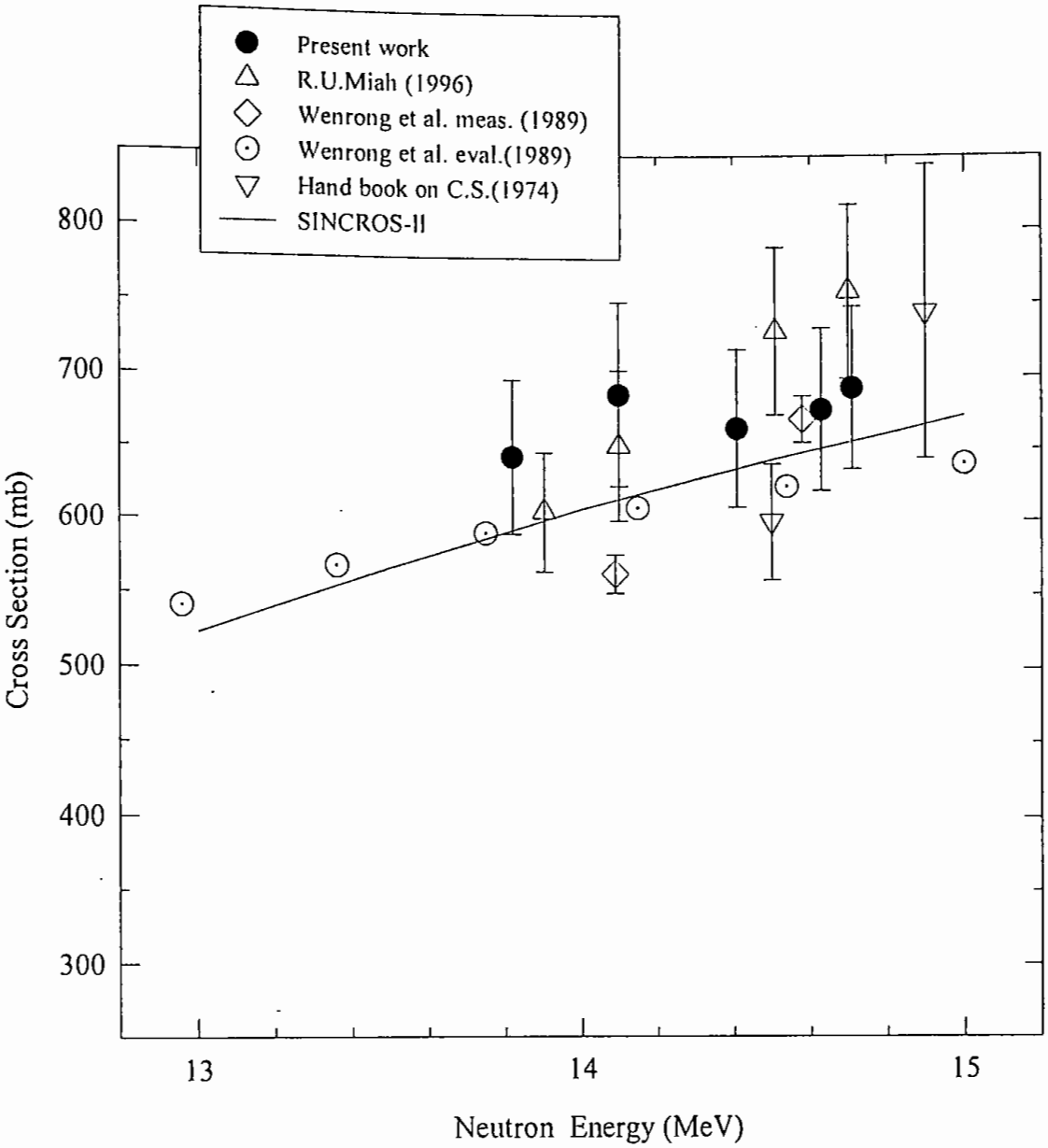

Fig. 3.7 The excitation function of ^{70}Zn (n,2n) ^{69m}Zn reaction.

3.2 Measurement of Activation Cross Sections of (n,2n) and (n,α) Reactions on the Isotopes of Germanium.

3.2.1 Materials

i) Ge-metal powder
ii) Al-foil
iii) Acetone
iv) Polyethylene bag
v) Cellulose tape

3.2.2 Experimental Procedure

In the present experiment, high purity target materials of germanium metal powder of natural isotopic abundance was used. Five germanium samples were prepared in the form of pellets. Each pellet has the diameter 1.2 cm and thickness ~0.15 cm. Mass of each pellet was between 0.4961 and 0.7047g. The germanium pellets were then sealed in thin polyethylene bags and sandwiched between aluminium flux monitor foils of same diameter as it. Mass of the each aluminium foil was between 0.1916 and 0.2035 g. The samples sandwiched between flux monitor foils were irradiated by neutrons at 10°, 50°, 70°, 90° and 110° with respect to the deuteron beam direction in a ring geometry arrangements described in previous section. The neutron generator operation data are as follows.

Beam current : 100μA
Beam diameter : ~1 cm
Deuteron energy : 110 keV
Irradiation time : 1 hour and 7 minutes

By measuring the activities of reaction products with the help of γ-ray counting system that are described earlier, the neutron flux and cross section were determined using the

known activation formula shown in section 2.3.7. Partial decay schemes[61] of product nuclei for germanium are shown in Fig.3.8-3.10.

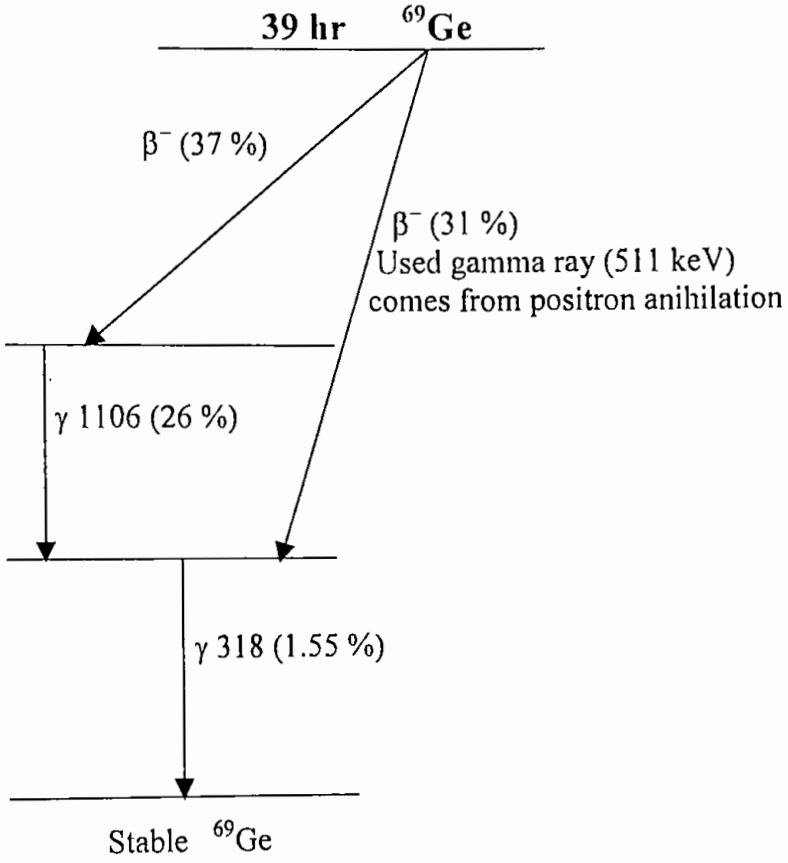

Fig.3.8 Partial decay scheme of the product nucleus of ^{70}Ge(n,2n)^{69}Ge reaction.

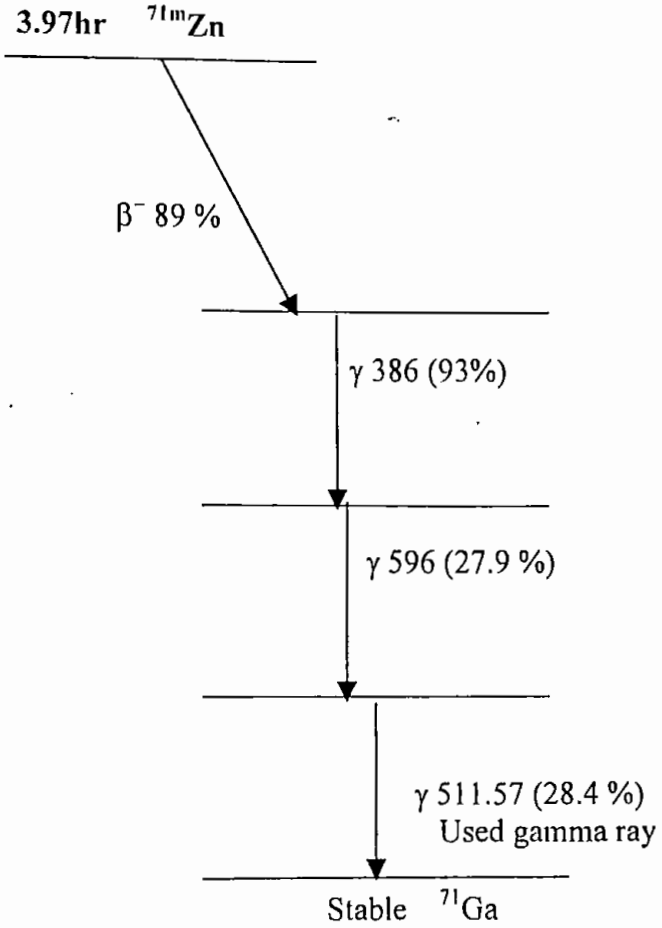

Fig. 3.9 Partial decay scheme of the product nucleus of ^{74}Ge(n,α)^{71m}Zn reaction.

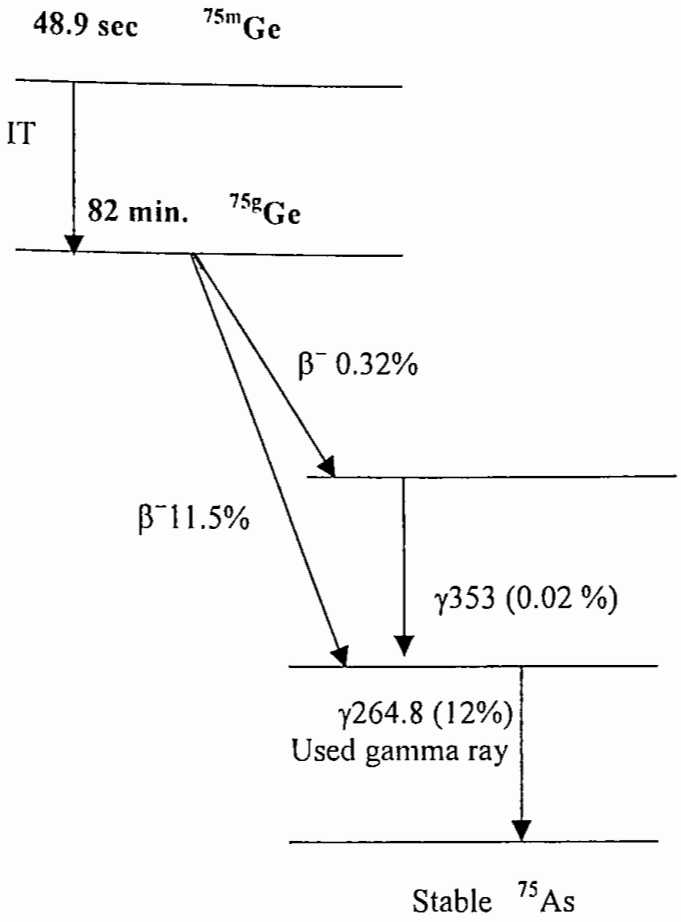

Fig.3.10 Partial decay scheme of the product nucleus of ^{76}Ge(n,2n)$^{75m+g}$Ge reaction.

3.2.3 Results and Discussion

The measured cross sections with error limit of the interested reactions for germanium isotopes are given in Table 3.2. The results of these reactions are discussed separately in different sections.

^{70}Ge(n,2n)^{69}Ge Reaction

The cross section values as a function of neutron energy obtained from the present investigation along with literature data for the ^{70}Ge(n,2n)^{69}Ge reaction are shown

in Fig.3.11. Results of the nuclear model calculations are also shown as a curve along with the measured values. The quoted uncertainty in each cross section value includes both statistical and systematic errors. The total uncertainties in the cross section values are in the range 8 - 9%.

From the figure it is observed that the values of cross section of the present work at the energies 14.51 and 14.70 MeV fall on the line of the theoretical value obtained by using the code SINCROS-II. The measured values at 13.90, 14.10, 14.31 MeV energies are slightly deviated from that of SINCROS-II. The present values are above the values obtained via EXIFON. Large discrepancy in the nuclear model calculations using SINCROS-II and EXIFON codes is observed for the investigated reaction in the energy range 13-15 MeV. The model consists of a pure multistep approach with the fixed global parameter set. It contains both statistical multistep direct (SMD) and statistical multistep compound (SMC) processes. The probable reason of large discrepancy in the cross section estimations via these codes is that the compound nucleus formation cross section is underestimated in SINCROS-II whereas direct reaction is overestimated. The results due to.Miah[27], Bychkove et al. and the values at 14.5 and 14.9 MeV energies obtained from the Hand Book[67] are clearly larger than the present result. The measured cross section at 14.10 MeV in our work is close to that of Bychkove et al.[69]. The literature values for this reaction in the energy range 13-15 MeV show to have large discrepancy. So there was a strong need to remeasure the cross sections of this reaction in this energy range. The difference in cross sections of this reaction between our experiment and literature are due to the different techniques, poor counting statistics and decay data. It may be mentioned that the measured data of present work are in excellent agreement

with the results obtained from the nuclear model calculations using the latest computer code SINCROS-II. The present experiment introduces some newer data points to the existing literature and theoretical calculations.

$^{74}Ge(n,\alpha)^{71m}Zn$ Reaction

Over the energy range investigated in this work, a very few cross section data exist in the literature and there is large discrepancies among them. These informations are not sufficient for many applications that need further experiment for $^{74}Ge(n,\alpha)^{71m}Zn$ reaction. The measured data along with literature values are shown in Fig. 3.12. The values of cross section of the present work at the energies 13.90, 14.10, 14.31, 14.51 MeV are well supported by the literature values. The measured value at 14.70 MeV is higher than literature values. But all the experimental values are larger than that of theoretical values obtained using statistical code SINCROS-II. However, measured data may be considered as more reliable.

$^{76}Ge(n,2n)^{75m+g}Ge$ Reaction

Extremely few published experimental cross section data of $^{76}Ge(n,2n)^{75m+g}Ge$ reaction are available and there exist large discrepancies among them that demand more experiment to give reliable data. The measured data with literature are shown in Fig.3.13 as a function of neutron energy. The results of the nuclear model calculation using statistical code EXIFON performed earlier in our laboratory[27] are also shown in Fig.3.13. All the measured values give the cumulative cross section for the formation of the ground state. Since the metastable state could not be measured due to its short half life of 48.9 seconds, a correction for its contribution to the cumulative cross section could not be estimated. We therefore calculated cross sections for the independent formation of the two isomeric states and obtained the cumulative cross section for ^{75}Ge. The present data are lower than those of R.U.Miah. Our measured data are well supported by S.Okumura[70] and G.Erdtman[34]. Our measured data give 3-8 % lower values than the data

evaluated by Bychkov et al. and ~ 4 % higher than those of theoretical calculation. There appears to be a good agreement between the experimental results and the theory.

Table 3.2 Activation cross sections of (n,2n) and (n,α) reactions on some isotopes of germanium.

Nuclear reaction	Neutron energy (MeV)	Measured reaction cross section (mb)
$^{70}Ge(n,2n)^{69}Ge$	14.70±0.11	455.13±36.78
	14.51±0.09	436.24±36.20
	14.31±0.07	402.16±33.01
	14.10±0.04	415.08±35.72
	13.90±0.04	408.34±33.74
$^{74}Ge(n,\alpha)^{71m}Zn$	14.70±0.11	4.29±0.25
	14.51±0.09	3.67±0.21
	14.31±0.07	3.41±0.22
	14.10±0.04	3.11±0.20
	13.90±0.04	2.51±0.16
$^{76}Ge(n,2n)^{75\,m+g}Ge$	14.70±0.11	1076.50±95.16
	14.51±0.09	1068.71±90.34
	14.31±0.07	1065.09±90.20
	14.10±0.04	1055.16±89.29
	13.90±0.04	1053.24±89.12

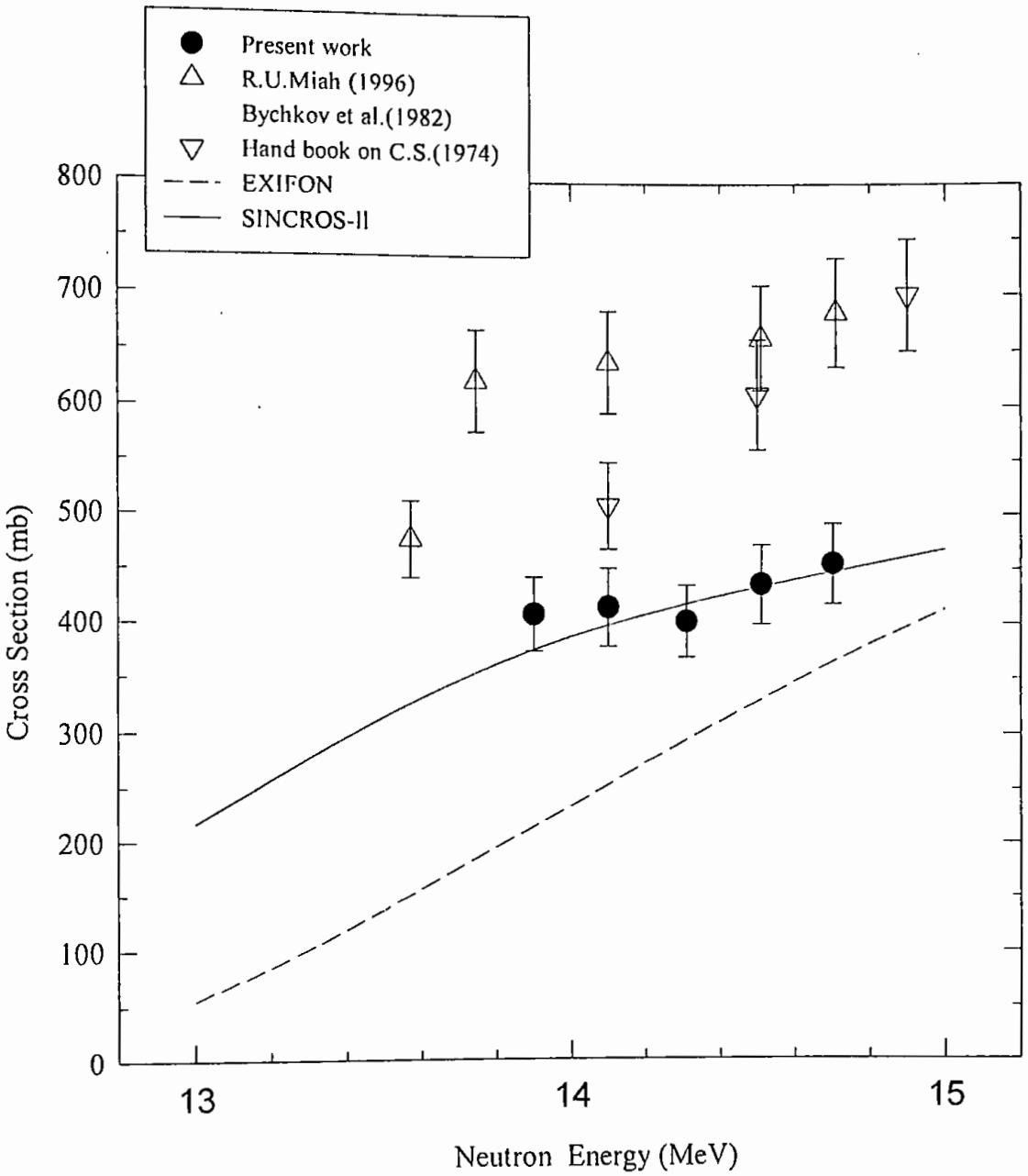

Fig.3.11 The excitation function of $^{70}Ge(n,2n)^{69}Ge$ reaction.

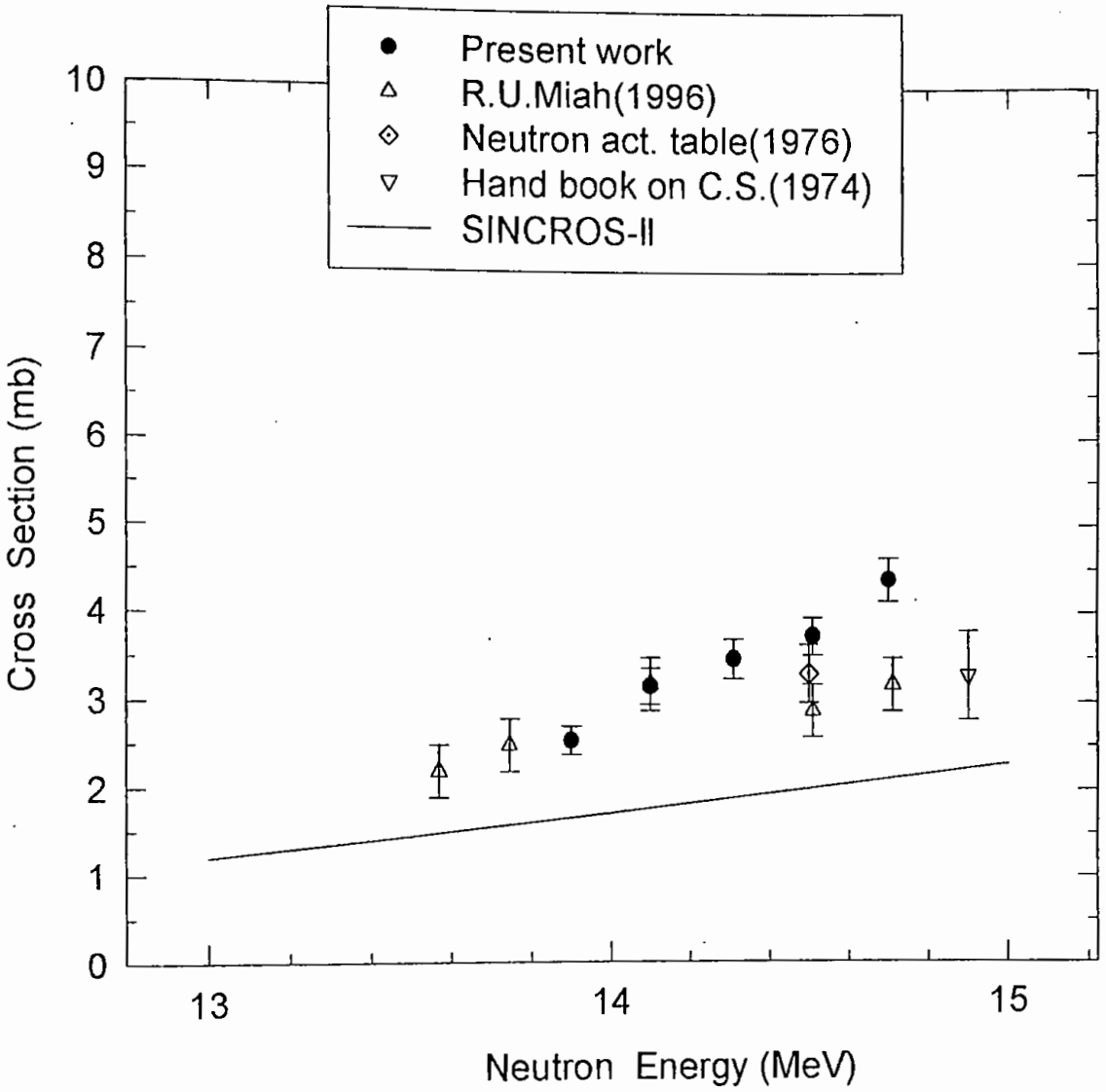

Fig.3.12 The excitation function of $^{74}Ge(n,\alpha)^{71m}Zn$ reaction.

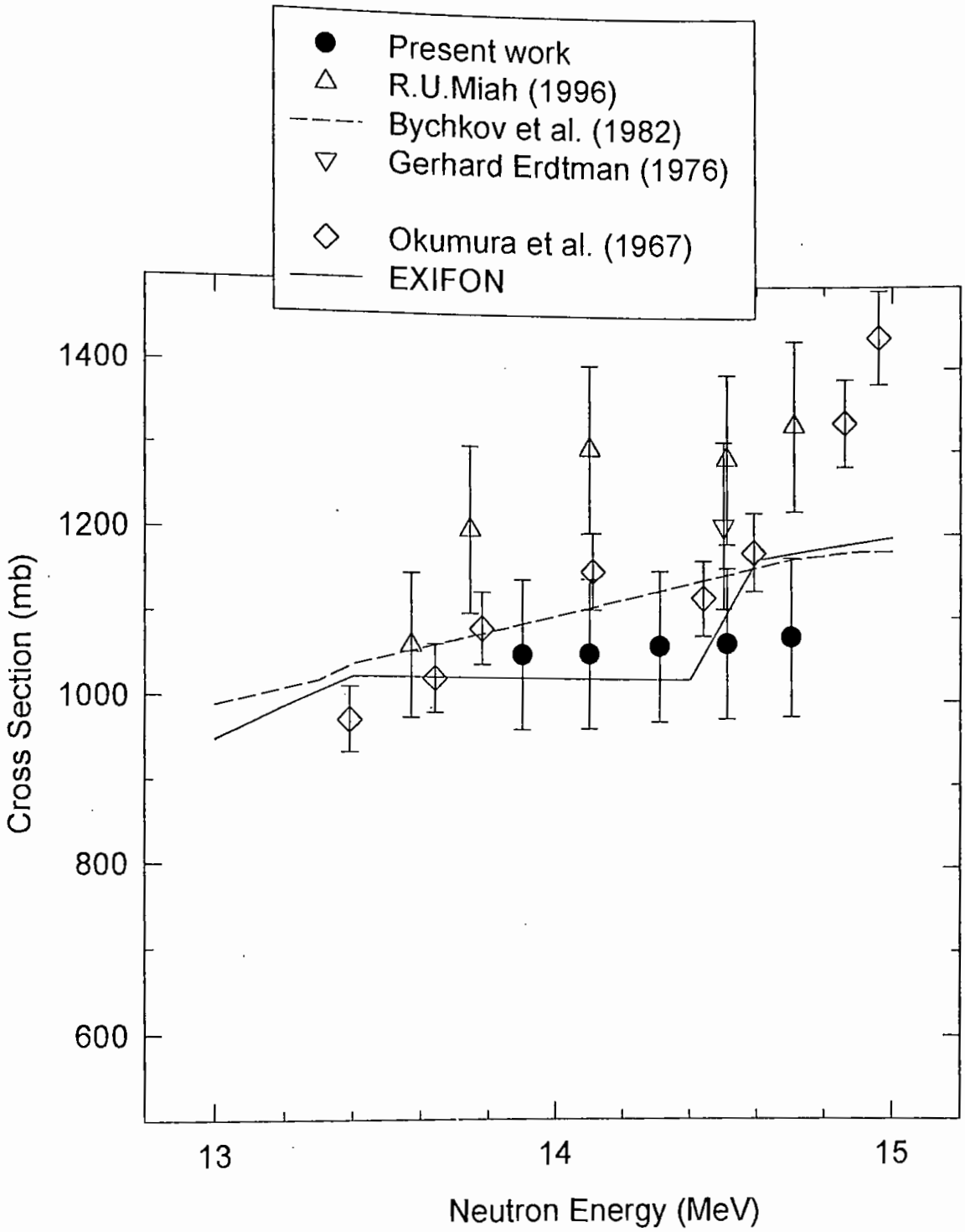

Fig.3.13 The excitation function of $^{76}Ge(n,2n)^{75m+g}$ reaction.

3.3 Measurement of Activation Cross Sections of (n,2n) Reaction on the Isotope of Scandium.

3.3.1 Materials

i) Sc_2O_3

ii) Al-foil

iii) Acetone

iv) Polyethylene bag

v) Cellulosic tape

3.3.2 Experimental Procedure

Scandium oxide (Sc_2O_3) from E. MERCK, Germany in powder form was pressed with the pressure of 5 tons per cm^2 using a hydraulic press to obtain pellet of 1.2 cm diameter and ~0.15 cm thickness. Four pellets were made. The each pellet was weighed between 0.2250 and 0.2756 g. The pellets were sealed separately in polyethylene bags and then sandwiched between aluminium foils of same diameter as sample. Mass of the each aluminium foil was between 0.0931 and 0.1000 g. The samples sandwiched Al-foils were placed to the ring geometry arrangement. The angular positions of the samples with respect to the deuteron beam were 10°, 30°, 80° and 110° for scandium. The samples with aluminium foils were irradiated by neutrons using the neutron generator facility. In this irradiation, the main neutron generator operation data are as follows.

Beam current : ~100μA

Beam diameter : ~1 cm

Deuteron energy : 110 keV

Irradiation time : 3 hours

After irradiation, the activities, neutron flux and cross sections were determined using same procedure as zinc sample that are cited in earlier. A partial decay scheme of ^{44m}Sc is shown in Fig.3.14.

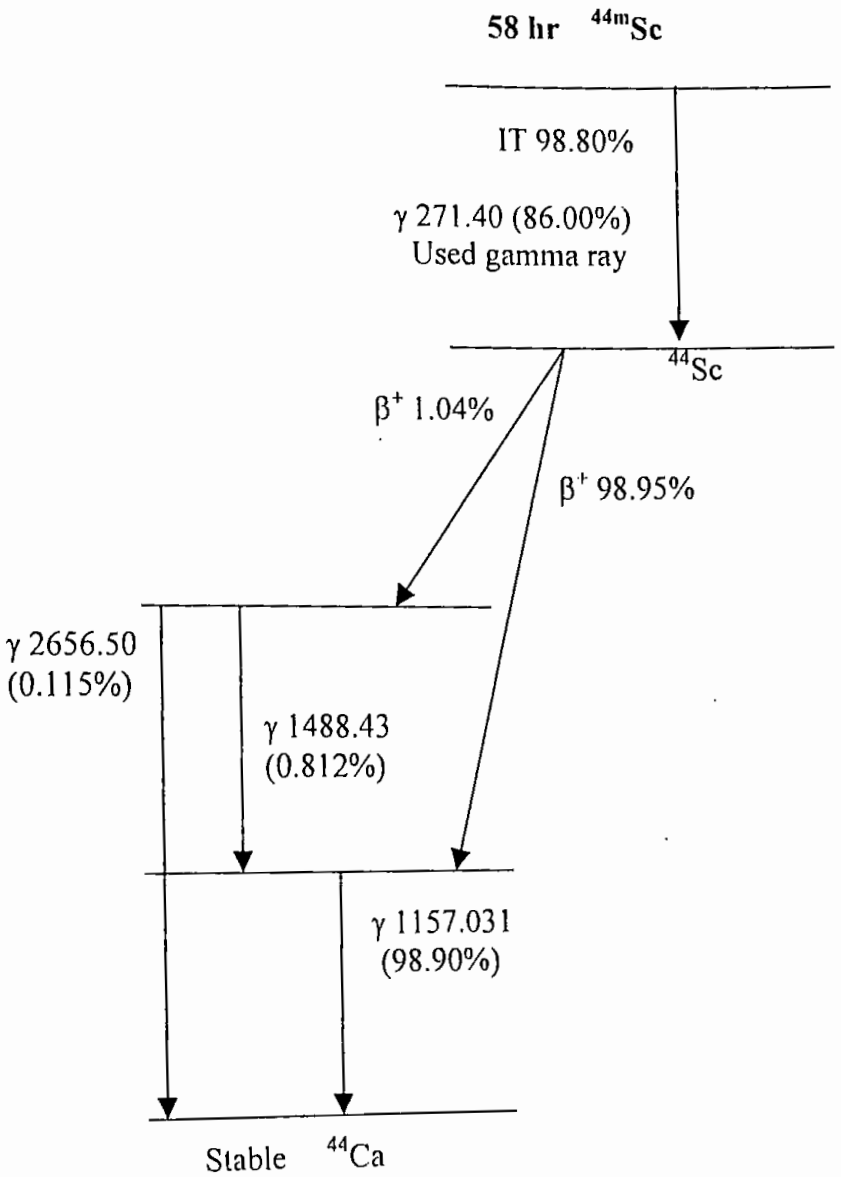

Fig.3.14 Partial decay scheme of the product nucleus of $^{45}Sc(n,2n)^{44m}Sc$ reaction.

3.3.3 Results and Discussion

$^{45}Sc(n,2n)^{44m}Sc$ Reaction

The results of this study along with the other literature data are shown as a function of neutron energy in Fig.3.15. Although activation cross sections data of $^{45}Sc(n,2n)^{44m}Sc$ reaction are abundant in literature, the discrepancies of some reported cross section data need further investigation. The measured data in the energy range of 13.90 to 14.63 MeV are well supported with the data reported in the Hand Book[67] on Activation Cross sections and by R.U.Miah. The cross section value of the present experiment at 14.70 MeV gives good agreement with Arnold et al.[72]. The other literature values for this reaction show some discrepancies than the measured data. However, the increasing tendency of the present data with increasing energy is similar to the literature data. The results of the model calculation using SINCROS-II are reproduced as a curve which is appreciably higher than the measured and all of literature data. The curve could possibly be fitted to experimental data by adjusting some input parameters.

Table 3.3 Activation cross sections of (n,2n) reaction on the isotope of scandium.

Nuclear reaction	Neutron energy (MeV)	Measured reaction cross section (mb)
$^{45}Sc(n,2n)^{44m}Sc$	14.70±0.11	164.70±13.75
	14.63±0.11	150.94±12.01
	14.21±0.06	133.89±10.65
	13.90±0.04	115.37±9.44

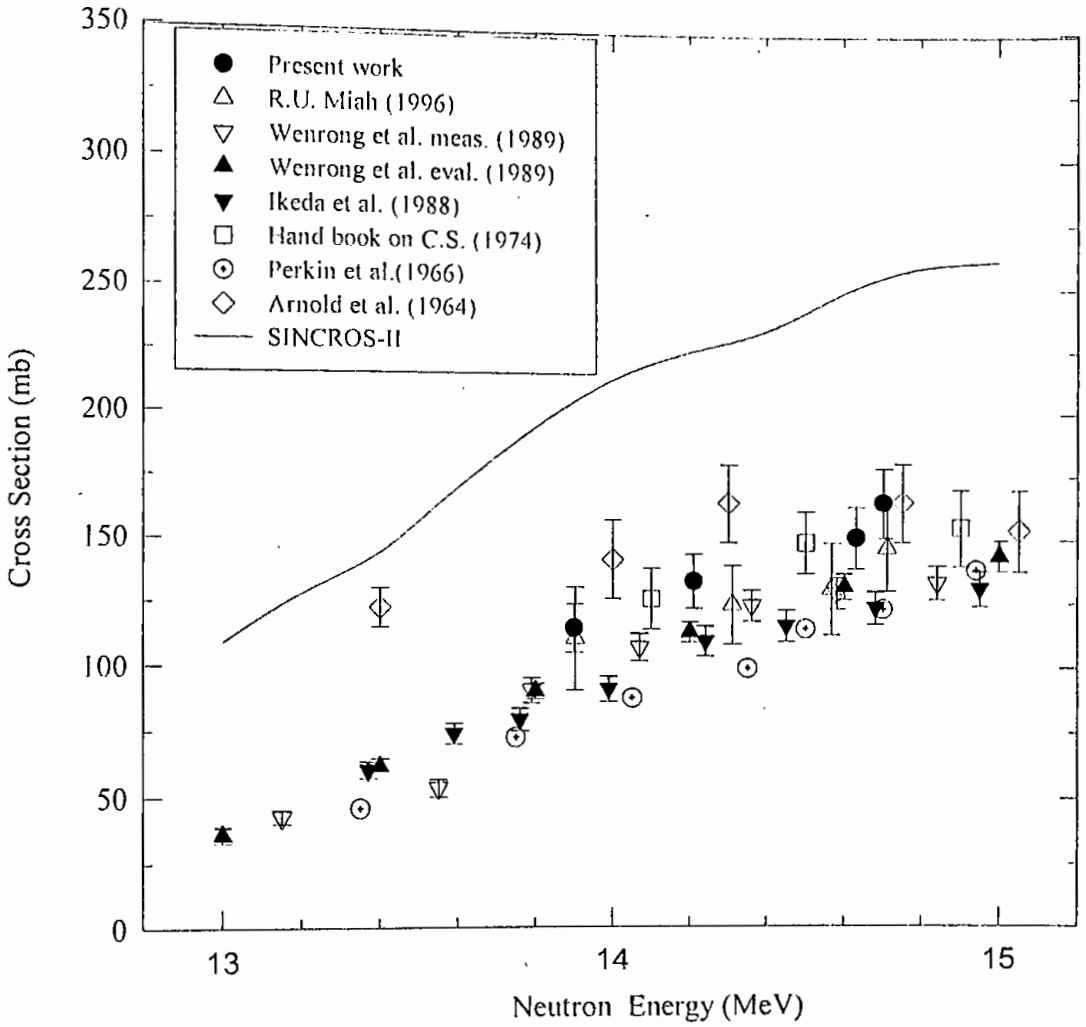

Fig.3.15 The excitation function of $^{45}Sc(n,2n)^{44m}$ reaction

3.4 Measurement of Activation Cross Sections of (n,2n) Reaction on the Isotope of Zirconium.

3.4.1 Materials

i) Zr-foil

ii) Al-foil

iii) Acetone

iv) Cellulose tape

3.4.2 Experimental Procedure

Four zirconium (purity > 99.5 %) foils were made squire shaped and cleaned well by acetone. Mass of the each foil was between 0.1358 and 0.1539 g. Each zirconium cleaned foil was sandwiched between two layers of aluminium foils. Mass of the each Al-foils was between 0.1943 and 0.2035 g. The samples together with Al-foils were irradiated at 0^{o}, 50^{o}, 70^{o} and 100^{o} positions with respect to deuteron beam direction by neutrons. During the irradiation, the neutron generator operation data are as follows.

Beam current : ~100μA

Beam diameter : ~1 cm

Deuteron energy : 110 keV

Irradiation time : 3 hours

After five minutes from the end of irradiation, the zirconium foils were detached from Al-foils. Each irradiated sample was placed on detector surface to identify and measure the activities of the reaction product. Using same procedure, the activity of the monitor foil was determined and it was used to determine the neutron flux of the sample positions. The detection/counting system was described details in section 2.3.2. The count rates for the investigated reaction were converted to decay rates after correction of dead time loss, coincidence effects detection efficiency and gamma transition intensities. From the decay rates thus obtained, the cross sections were

determined using the well-known activation equation cited in section 2.3.7. The partial decay scheme of ^{89}Zr is shown in Fig.3.16.

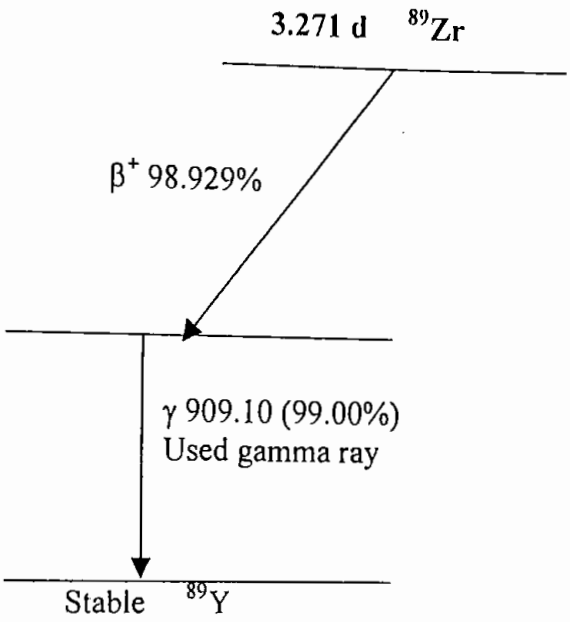

Fig.3.16 Partial decay scheme of the product nucleus of $^{90}Zr(n,2n)^{89}Zr$ reaction.

3.4.3 Results and Discussion

$^{90}Zr(n,2n)^{89}Zr$ Reaction

Many cross section measurements for $^{90}Zr(n,2n)^{89}Zr$ reaction have already been performed that are shown in Fig. 3.17 along with measured data. The measured data are slightly larger than all of literature values[27, 29, 33, 34, 73] but closer to them. The present measured data match well with the common trend of the literature data. The results of theoretical calculation shown in Fig.3.17 are lower than the measured and literature values. The present measured data give 4 -14% higher values than that of literature. The good agreement of the measured data with literature confirms the reliability of technique used in our laboratory.

Table 3.4 Activation cross sections of (n,2n) reaction on the isotope of zirconium.

Nuclear reaction	Neutron energy (MeV)	Measured reaction cross section (mb)
$^{90}Zr(n,2n)^{89}Zr$	14.71±0.11	898.994±71.91
	14.51±0.09	796.27±54.86
	14.31±0.07	758.44±51.95
	14.00±0.03	646.19±44.58

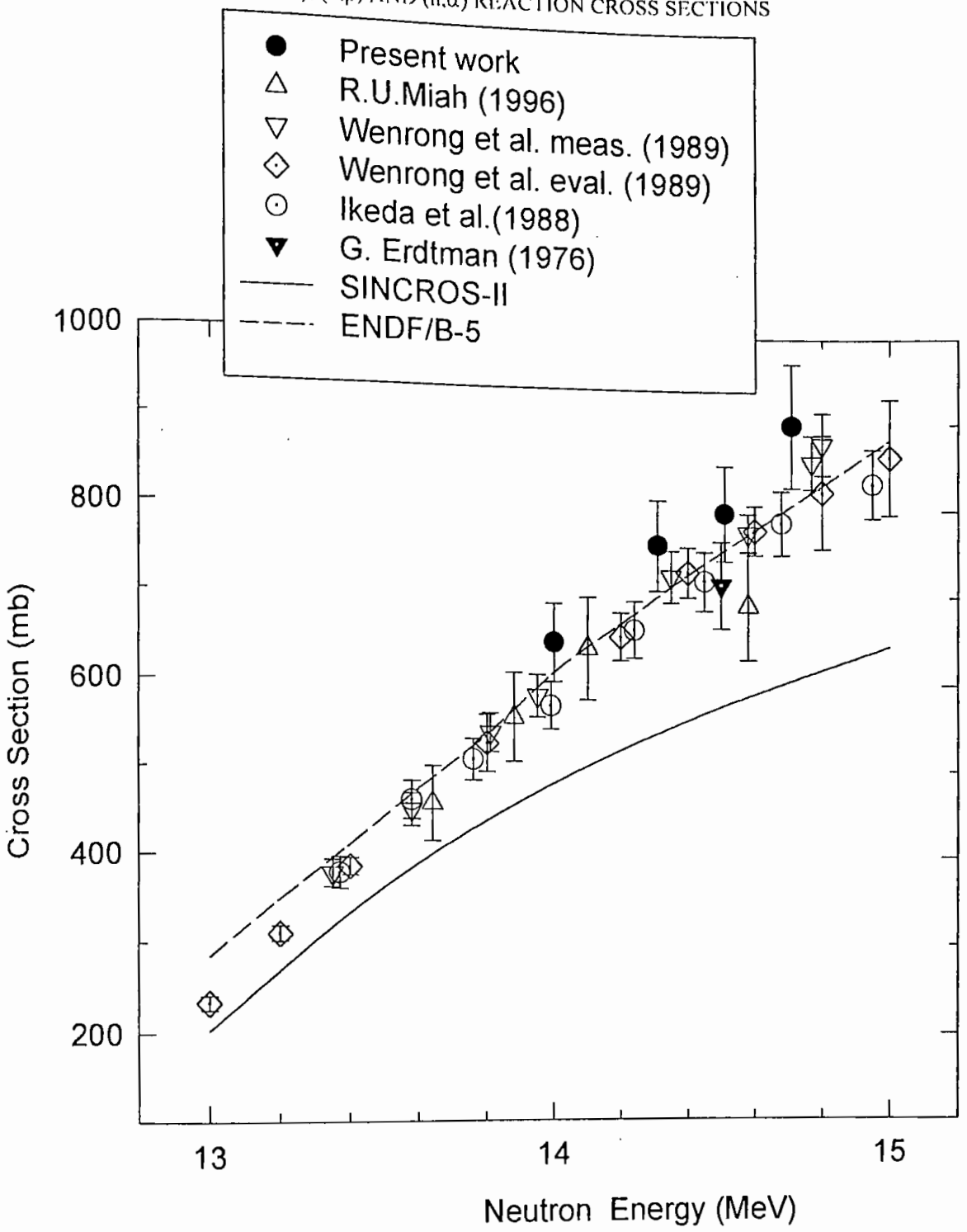

Fig.3.17 The excitation function of $^{90}Zr(n,2n)^{89}$ reaction.

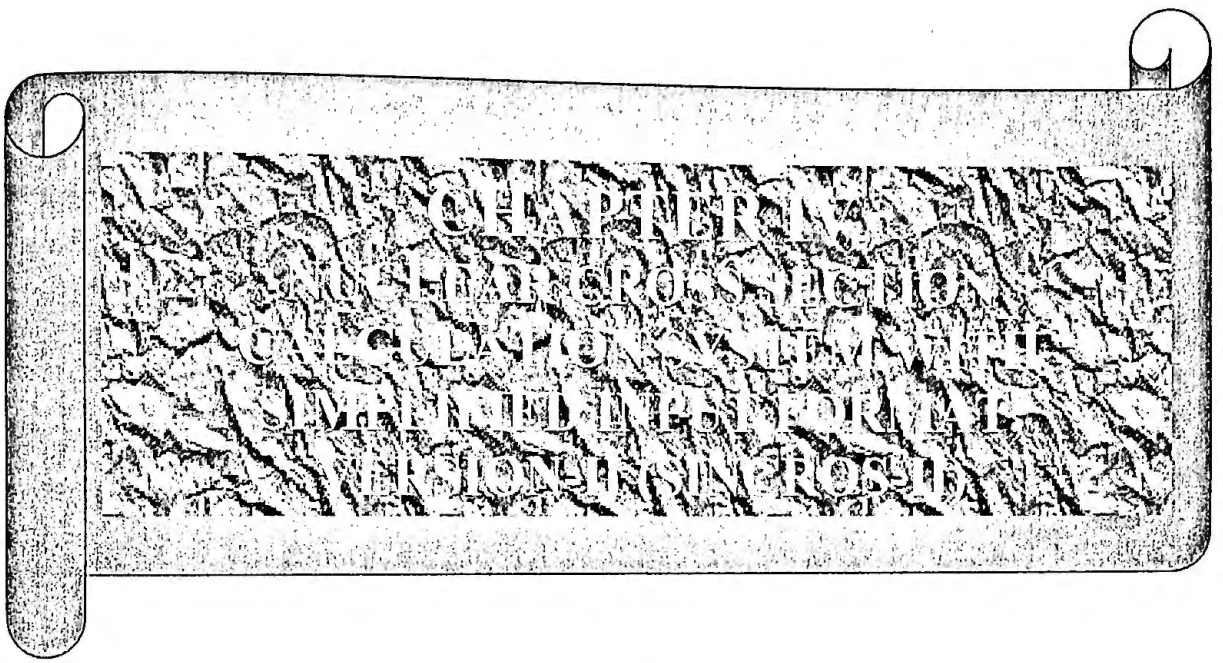

CHAPTER IV

NUCLEAR CROSS SECTION CALCULATION SYSTEM WITH SIMPLIFIED INPUT FORMAT, VERSION-II (SINCROS-II)

In order to describe the measured cross sections, nuclear model calculations were performed using the computer code SINCROS-II[35], which is based on the statistical model, incorporating pre-equilibrium emission. The SINCROS-II has been developed by improving the functions of the program in SINCROS-I[74] and preparing some process codes for the cross section applications. The input format of this new version is more simplified than that of version I. The level density of nuclei is represented by defining only the Fermi-gas model parameter "a", and "a" for about 200 nuclei were stored in the code as the data initialization statement. The relative widths Γ_γ for 200 nuclei were also stored, although some of them have tentative values.

Model calculations using SINCROS-II were done on target nuclides ^{64}Zn, ^{70}Zn, ^{70}Ge, ^{74}Ge, ^{76}Ge, ^{45}Sc and ^{90}Zr. Neutron, proton and alpha-particle emissions were taken into account from every compound nucleus and the necessary data for all nuclei were supplied. In the new version, the total neutron, proton, deuteron, alpha-particle and gamma-ray production cross sections are shown in the table. Instead of the excited state productions, the isomeric state production cross sections are directly out-put. It is not necessary, then, to find out the isomeric cross section within the excited state production cross sections. The isomer, of which the excitation function is intended to be given, can be designated in the last row of the input data.

In the present experiment, the neutron activation cross section values in the energy range of 13 to 15 MeV were measured theoretically using code SINCROS-II. The

theories, models, assumptions and parameters on which SINCROS-II code is based are briefly explained below.

4.1 Composition of SINCROS-II

The main codes of the SINCROS-II are the ELIESE[75] – GNASH[76] joint program (EGNASH2) and simplified input version of DWUCK4[77] (DWUCKY). EGNASH2 calculates the nuclear cross sections over the wide mass region using the built-in optical-model potential parameters. In DWUCKY, the same accepted neutron potentials are programmed as in EGNASH2. The discrete level data--excitation energy, spin, parity and branching ratios of gamma ray decay channels are prepared from the ENSDF through the format conversion and the editorial work. It is not necessary that too many levels are quoted from the ENSDF, rather it should be assured that the number of levels approximately increases as an exponential function of the excitation energy.

EGNASH2 reads the discrete level data, the direct inelastic scattering cross sections calculated with DWUCKY and the input data for the nuclear reactions. In addition to the output lists, the results of calculation can be stored into several files which are selected according to the object of calculation. The composition of SINCROS-II and the flow of data processing are shown in Fig. 4.1. The particle and gamma-ray total production cross sections and the production cross sections for reaction products, including isomeric states, are held in file 12.

4.2 Input and Output Format of EGNASH2

When we used the GNASH code, the transmission coefficients for neutrons, protons and alpha particles calculated from ELIESE3 were provided as input data to GNASH. Since many of the parameters were predetermined and stored in the program, the parameters which should be input are a small number. For the isomeric states, data are given in the last row of the input file. A sample input is given in Table 4.1. The inputs are arranged according to the requirement of the programming language.

In addition to the output of the original GNASH, the present code has a table of reaction cross sections to examine the results of calculation as soon as possible. The table includes the compound, direct, rate of pre-equilibrium processes and particles and gamma- ray total production cross sections. The ground and isomeric states production

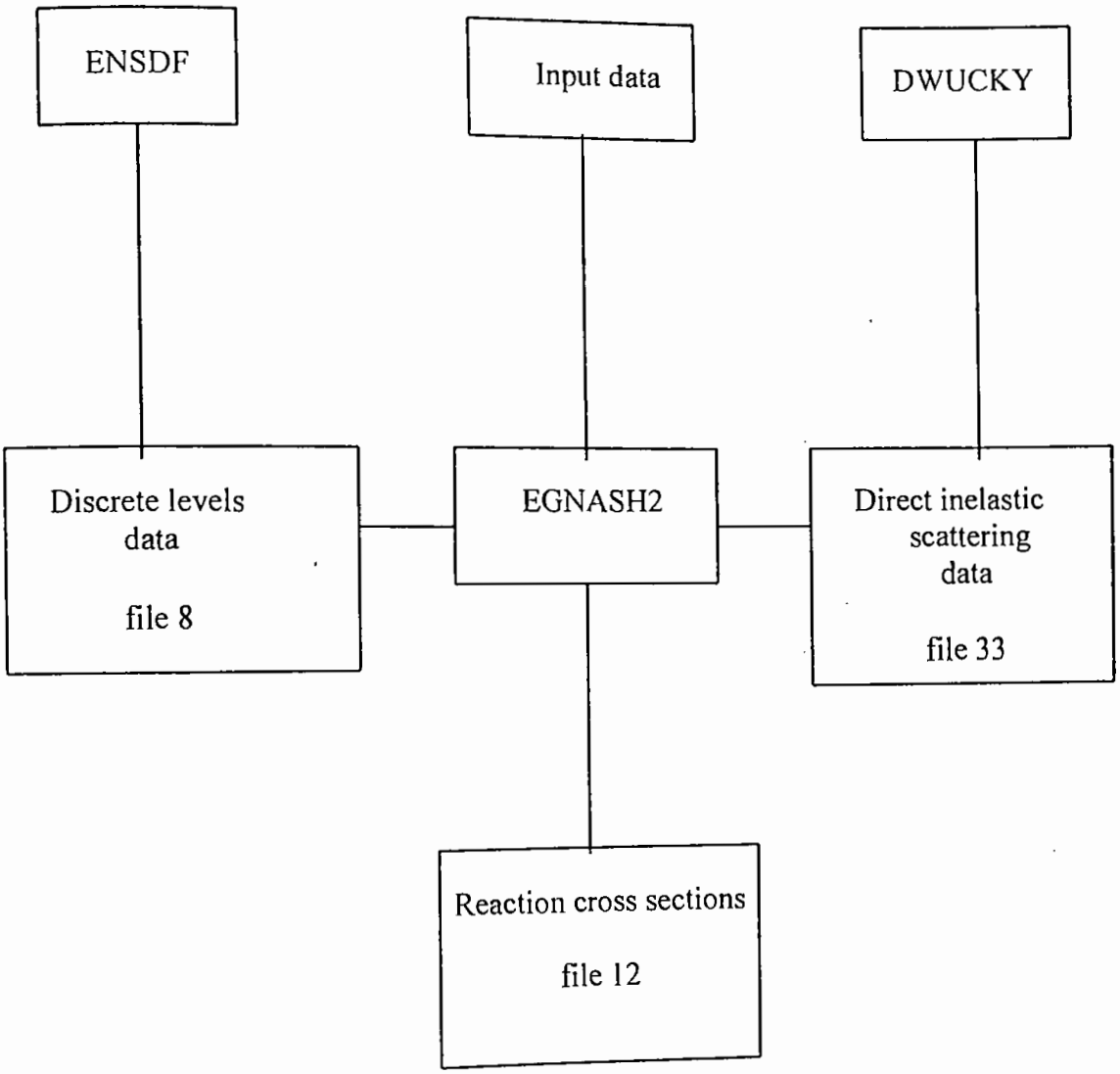

Fig. 4.1. Composition of SINCROS-II and the flow of data processing. Only relevant blocks are shown.

cross sections of isotopes and level inelastic scattering cross sections are also shown. A sample of output data of reaction cross section are shown in Table 4.2.

4.3 Optical Model Potential Parameters

A sequential evaporation is assumed for the particles and gamma-rays emitted in the nuclear reactions. Considering the conservation of the angular momentum, parity, each evaporation step is treated within the framework of the statistical model. The particle transmission coefficients are generated using parameters chosen from a global optical model parameter set. For neutron, the optical model parameter set of Walter-Guss[78] and Wilmore-Hodgson[79] are built into the EGNASH2. Walter-Guss recommended their potential to be applied above 53 in mass number and 10 to 80 MeV in energy range.

4.4 Parameters for Level Density and Gamma-ray Transitions

In the continuum level region, the Fermi-gas and the constant temperature model are used to represent the level density of nucleus. The Fermi-gas model formula as a function of energy E and spin J is

$$\rho(E,J) = \frac{\mathrm{Exp}[2\{a(E-\Delta)\}^{1/2}]}{C_0\,(E-\Delta)^2} R(J,E) \qquad (4.1)$$

Where $C_0 = 24\sqrt{2}\,(0.146)^{3/2} a\, A$ and the spin term is given by

$$R(J,E) = (2J+1)\exp[-(J+1/2)^2/\{2\sigma^2(E)\}] \qquad (4.2)$$

Where $\sigma^2(E)$ is the spin cutoff factor defined by

$$\sigma^2(E) = 0.146[a(E- \Delta)]^{1/2}A^{2/3} \qquad (4.3)$$

The pairing correction Δ was quoted from the Gilbert and Cameron's paper[80]. In the lower excitation, the constant temperature formula expressed by

$$\rho(E,J) = \rho(E_x)\exp[(E - E_x)/T]R(J,E), \qquad E<E_x, \qquad (4.4)$$

is used, where E_x is the energy at which both densities are smoothly connected and $\rho(E_x)$ is the energy term of level density at the energy E_x. If the spin dependent level density $\rho(E, J)$ is summed over the spin J, we get the density $\rho(E)$ of levels of all J, which has a different form from the constant temperature formula of Gilbert and Cameron as the spin cut off factor is energy dependent.

The GNASH code is able to automatically determine the nuclear temperature, T, if the discrete levels in the low energy region and the Fermi-gas level density parameter "a" were suitably input. Then the level density of nucleus in the continuum can be described by the parameter "a" only. In some cases, however, the code is unable to match discrete level and thus the temperature, which connects smoothly between the Fermi-gas and discrete levels, is not determined. For those cases, the temperature is calculated with a systematic relation between the level density parameter and temperature,

$$T = 7.50\, a^{-0.84} \qquad (4.5)$$

in the code EGNASH2. At the beginning of the calculation, when the experimental value of the average spacing D_0 of s-wave neutron resonance at the neutron binding energy E_B is known[81], the parameter "a" was assumed to have a value which is calculated from the spacing D_0 by inversely solving the equation[82],

$$D_0 = C_0 (E_B - \Delta)/(2I+1) \exp[\{3 + (2I+1)^2\} / \{8\sigma^2(E_B)\} - 2\sqrt{a(E_B - \Delta)}] \qquad (4.6)$$

Where I is the spin of target nucleus. And a set of parameters "a" of isotopes in the nuclear decaying processes has practically been selected through the cross section calculation to agree with the various experimental data which could be considered to be reliable. The procedure of the parameter determination is described in section 4.5.

With the cross section calculations for about 50 nuclei, the level density parameters "a" of about 200 isotopes were determined and stored into the EGNASH2 as the data initialization statement. The relation between these "a" and the total shell corrections S is given by Gilbert and Cameron. The tentative formula,

$$a/A = 0.008\ S + 0.17 \tag{4.7}$$

is programmed to give the initial value of "a" for the undeformed nuclei for which the cross section is not yet calculated. Here S is the shell correction energy.

To provide gamma-ray transmission coefficients, the Brink-Axel giant dipole resonance form was used. The defaulted energy and width of the giant resonance are $E_R = 40\ A^{-1/5}$ MeV and $\Gamma_\gamma = 6$ MeV , respectively. The normalization constant is obtained from the ratio of the average radiative width Γ_γ to the observed resonance spacing D_o for s-wave neutrons at the neutron binding energy E_B , which is derived in the code from the level density parameter "a" used in the cross section calculation by the formula (4.6).

4.5 Determination of the Value of Parameters

In SINCROS, the global optical-model potential parameters are employed to calculate the transmission coefficients as mentioned in section 4.3. The nonelastic cross sections for neutron and the reaction cross sections for proton calculated with the built-in potentials agreed with experimental data. The key points of the cross section calculation, therefore, are the determination of level density parameters of daughter nuclei and the rate of contribution of pre-equilibrium and direct processes to the statistical process. In the following, the method of parameter determination for the pre-equilibrium process and for the level density is described in detail at subsections 4.5.1 and 4.5.2 respectively.

4.5.1 Parameter Determination of the Pre-equilibrium Process

In the code EGNASH2, the pre-equilibrium and direct processes of particle emission are treated with the code PRECO developed by Kalbach[83], which is coupled with GNASH, and with the code DWUCKY for inelastic scattering. In the GNASH, the single particle state density and the normalization factor for excitation-model were free parameters. In contrast with this, the single-particle state density constant is not free, but related to the level density parameter "a" by the formula,

$$g = (6/\pi^2)a \tag{4.8}$$

in the EGNASH2. In addition, the normalization factor F2, which is equal to the Kalbach constant divided by 100, the adjusting factors F3 and F4 are introduced for pick-up and knock-out processes, respectively. The factor F2 and the contribution of direct inelastic scattering are so determined that the calculated neutron emission spectrum is in agreement with the high energy part of the experimental neutron spectrum, when the experimental data at 14 MeV are available.

4.5.2 Parameter Determination of the Level Density

After the parameters for the pre-equilibrium and direct processes were selected, the free parameter to be determined is only the level density parameter "a" in the Fermi-gas model, because the nuclear temperature used in the constant temperature model can be determined automatically or by the equation (4.5). Since the total emission of various kinds of particles from the compound nucleus is controlled by a set of level density parameters for daughter nuclei, it is better that the level density parameter of each daughter nucleus is so practically determined that the calculated cross sections for reactions (n,2n), (n,p), and (n,α) agree with the experimental data of respective reactions.

The first step to fix the level density parameters is the calculation of them using the experimental value of mean level spacing for s-wave neutron resonance at the neutron binding energy. The calculation was made by solving inversely equation (4.6), with the spin cut off factor defined by equation (4.3) and the pairing correction quoted from Gilbert and Cameron.

The second step to determine the level density parameters is the cross section calculation in the mass region where the reliable experimental data exist. Several test calculations of cross sections around 14 MeV were carried out, referring to the experimental data for the (n,2n), (n,p), and (n,α) reactions. In this stage, the measurement of cross sections of Mo isotopes performed by Ikeda et al. and Katoh et al. are very useful for the determination of level density parameters.

Table 4.1 Input data file for ^{64}Zn as target nucleus.

```
zn64n2
   ZN-64 + NEUTRON REACTION   (ELIESE-GNASH JOINT PROGRAM EGNASH2A)
                                        2001 01 09  Shuza Uddin
    9     0    11     0     0     1     2    -1     0
 1.         30064.     0.5          0.5                          0.1
 0.028
   05
 13.0       13.5         14.0         14.5         15.0
 30065.     5.
 30064.     3.
 30063.     1.
 29064.     3.
 29063.     1.
 28063.     2.
 28062.     2.
 28061.     2.
 28060.     1.
 0.
 0.
 0.
```

Table 4.2 Portion of output data for ^{64}Zn as target nucleus.

GROUND STATE PRODUCTION CROSS SECTIONS (MB)

ENERGY(MEV)	30065	30064	30063	29064	29063
1.30E+01	4.720E-01	6.768E+02	3.976E+01	2.641E+02	4.650E+02
1.35E+01	4.389E-01	6.069E+02	8.726E+01	2.387E+02	5.142E+02
1.40E+01	4.083E-01	5.445E+02	1.393E+02	2.140E+02	5.487E+02
1.45E+01	3.808E-01	4.895E+02	1.895E+02	1.912E+02	5.746E+02
1.50E+01	3.567E-01	4.434E+02	2.320E+02	1.713E+02	5.984E+02

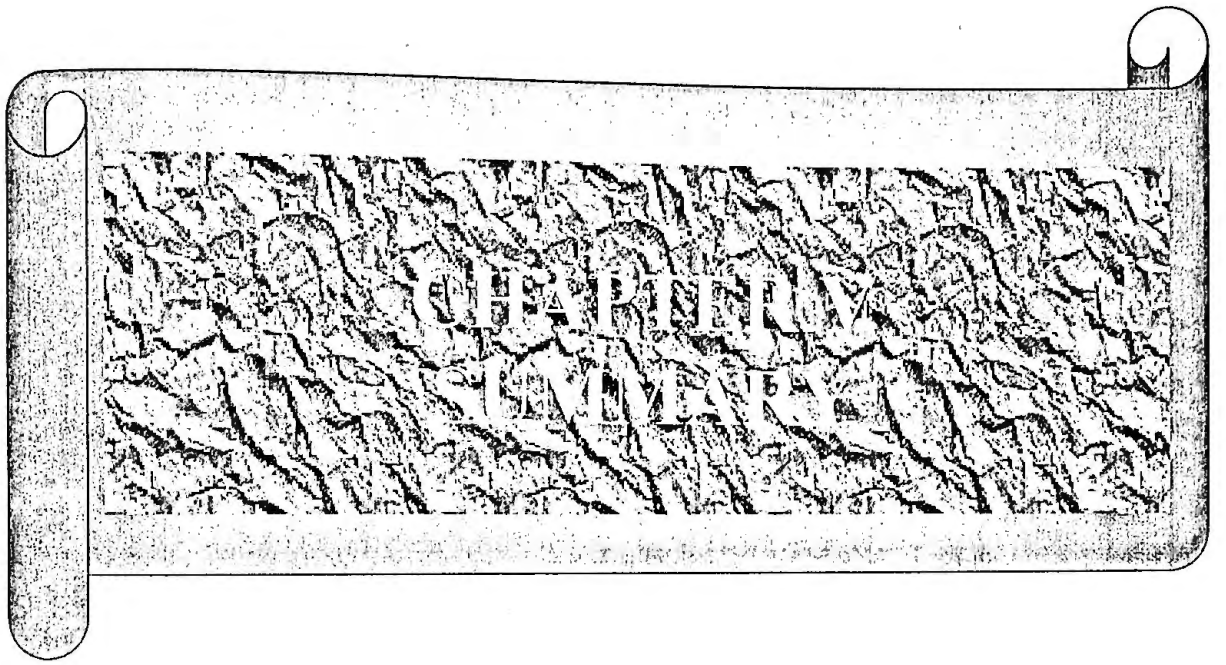

CHAPTER V

SUMMARY

In the present experiment, the cross sections of (n,2n), (n, p) and (n,α) reactions on the isotopes of zinc, germanium, scandium and zirconium were determined through identification of the activation products via γ–ray spectrometry.

Samples of zinc (as ZnO), germanium metal powder and scandium (as Sc_2O_3) in the form of pellet with dimension of 1.2 cm diameter and ~0.15 cm thickness, of zirconium foil of 1cm ×1 cm were prepared. All of the samples were sandwiched between Al-foils of the same size of sample separately. Aluminium foils were used to measure the neutron flux at the sample positions.

Five zinc samples with Al-foils were irradiated by neutrons at 0°, 30°, 60°, 90° and 120° angle with respect to the deuteron beam direction in a ring geometry arrangement over a period of 3 hrs. Neutrons were produced at the J-25 Neutron Generator of the Institute of Nuclear Science and Technology, AERE, Savar, Dhaka via $^3H(d,n)^4He$ reaction with 110 keV deuterons of 200 μA beam current.

Five germanium samples were irradiated by neutrons at 10°, 50°, 70°, 90° and 110° with respect to the deuteron beam direction. In this case, the neutron generator operation parameter : beam current 100 μA, deuteron energy 110 keV and irradiation time 1 hr and 7 minutes. Four scandium and four zirconium samples were also irradiated by neutrons for 3 hrs in the same experimental configuration. The angular positions for scandium samples were 10°, 30°, 80°, 110° and for zirconium were 0°, 50°, 70°, 100° with respect to deuteron beam of 110 keV energy and 100 μA current.

After irradiation, the radioactivities of the reaction products were measured by using a high resolution HPGe-detector. The gamma-ray spectra were accumulated and analyzed in Canberra S-100 Multi Channel Analyzer (MCA) master board package based on personal computer. The measured counts under photo peak were subjected to usual correction for dead time loss, pileup loss, coincidence effects etc. The counts of 511 keV gamma-ray energy were corrected by subtracting background counts and separating the counts of this energy from two different radionuclides establishing composite decay curve. The background correction was also performed for 909.1 keV gamma-ray energy emitted from the product nuclide ^{89}Zr.

The count rates were converted to decay rates by well known equation :

$$DPS = \frac{CPS}{\varepsilon \times I_\gamma} \times e^{\lambda_d}$$

as mentioned in previous section. From the decay rates, the cross sections were determined using well known activation formula that are shown in section 2.3.7. The uncertainty in cross sections was determined by considering both the systematic and statistical errors. The overall uncertainties for the present work were in the range of 7-15 %. The maximum errors in the cross sections are due to the poor counting statistics.

The cross sections of the ^{64}Zn(n,2n)^{63}Zn, ^{64}Zn(n,p)^{64}Cu and ^{70}Zn(n,2n)^{69m}Zn reactions were measured at 13.82, 14.10, 14.41, 14.63, 14.71 MeV neutron energies.

The cross sections of the ^{70}Ge(n,2n)^{69}Ge, ^{74}Ge(n,α)^{71m}Zn and ^{76}Ge(n,2n)$^{75m+g}$Ge reactions were measured at 13.90, 14.10, 14.31, 14.51 and 14.70 MeV neutron energies.

The cross sections at 13.90, 14.21, 14.63, 14.70 MeV neutron energies for ^{45}Sc(n,2n)^{44m}Sc reaction and at 14.00, 14.31, 14.51, 14.71 MeV neutron energies for ^{90}Zr(n,2n)^{89}Zr reaction were measured in the same experimental configuration.

The measured cross sections along with the values obtained from available literature were plotted as a function of neutron energy. The cross sections of all the (n,2n) reactions on the isotopes investigated in present work increase with the increasing neutron energy whereas the cross section of (n,p) reaction decreases with increasing neutron energy. Again (n,α) reaction cross section increases with increasing neutron energy.

In order to describe the measured excitation functions of the selected reactions, theoretical calculations of the cross section have been done using the statistical code SINCROS-II in the range of 13-15 MeV neutron energy for four(4) elements in the mass region A= 45-90.

Up to now, there have been very limited numbers of available data for the activation cross sections of $^{64}Zn(n,2n)^{63}Zn$, $^{64}Zn(n,p)^{64}Cu$, $^{70}Zn(n,2n)^{69m}Zn$, $^{70}Ge(n,2n)^{69}Ge$, $^{74}Ge(n,\alpha)^{71m}Zn$, $^{76}Ge(n,2n)^{75m+g}Ge$, $^{45}Sc(n,2n)^{44m}Sc$ and $^{90}Zr(n,2n)^{89}Zr$ reactions even at 14 MeV. The cross section data of these reactions measured in present work showed significant improvement in accuracy in comparison with previously reported data. Hence, the cross section data obtained from the present investigation based on unified experimental condition have provided nuclear data base and removed large previous discrepancies for some of the reactions in the energy range of 13.82 to 14.71 MeV. The agreement between experiment and theory is fairly satisfactory in most of the cases.

It is hoped that our measured and calculated cross section data provide real data base for fusion reactor technology design, semiconductor technology development, new evaluations of activation cross sections and to a detailed future theoretical calculation and testing nuclear models.

SUGGESTIONS FOR FURTHER WORK

Fast neutron reactions with materials produce energetic atoms emerge from the metal surface. I have measured the first neutron induced reaction cross sections at different energies in the range 13.82 to 14.71 MeV of the following reactions using the J-25 neutron generator facility, $^{64}Zn(n,2n)^{63}Zn$, $^{64}Zn(n,p)^{64}Cu$, $^{70}Zn(n,2n)^{69m}Zn$, $^{70}Ge(n,2n)^{69}Ge$, $^{74}Ge(n,\alpha)^{71m}Zn$, $^{76}Ge(n,2n)^{75m+g}Ge$, $^{45}Sc(n,2n)^{44m}Sc$ and $^{90}Zr(n,2n)^{89}Zr$. The reaction products in the observed cases viz. ^{69m}Zn, ^{71m}Zn, $^{75m+g}Ge$ are β^- emitters and ^{44m}Sc, ^{63}Zn, ^{69}Ge, ^{89}Zr are β^+ emitters. On the other hand ^{64}Cu is both β^+ and β^- emitter. Of particular interest is the $^{92}Zr(n, \alpha)^{89}Sr$ reaction which leads to a pure β^- emitting radioisotope. These studies may be enabled one in developing and promoting his understanding towards some mechanistic information, the nuclear data research for pure and applied science programs.

It is worth mentioning here that our existing nuclear data research facility is somewhat limited to a narrow neutron energy range (13-15 MeV). Mention is made that monoenergetic neutron energy in the range of 5 to 12 MeV available at compact cyclotron via $^{2}H(d,n)^{3}He$ reaction.

In view of the above consideration, it may be carried out the further extension of research work on measurement of excitation functions of the above mentioned reactions to other neutron energies and other important neutron activated reactions via radiochemical separation technique followed by γ and β counting. It is expected that many more measurement will be done radiochemically. Nuclear model calculations using statistical codes EXIFON, SINCROS-II, STAPRE, etc. will be done to validate the experimentally measured cross section data. It is hoped that the proposed work might be an important addition towards neutron activated reactions.

REFERENCES

1. R. Wolfle and S. M. Qaim, J. Radiochim. Acta 27, 65-69 (1980).

2. J. Csikai, Proc. advisor group meeting on nuclear data for fusion reactor technology, Viena (1978), IAEA-TECDOC-223, 199 (1979).

3. V.M.Bychkov, V.N.Manokhin, A.B.Pashchenko, V.I.Plyaskin, Report INDC(CCP)-146 / LJ, 1-149 (1980).

4. E.Steiner, P.Huber, W. Salathe and R.Wagner, Hel. Phys. Acti. 43, 17 (1970).

5. D.J.Rose and R.Carruthers, Proc. of an IAEA Workshop Culham, United Kingdom, 3,9, 29 Jan.-15 Feb. (1974).

6. F.H.Tenney, Proc. of an IAEA Workshop Culham, United Kingdom, 17, 29 Jan.-15 Feb. (1974).

7. Y. Seki and T. Hiraoka, in preparation.

8. K.Sako, M.Ohta, Y.Seki, H.Yamato, T.Hiraoka, K.Tanaka, N.Asami and S.Mori, Proc. of an IAEA Workshop Culham, United Kingdom, 27, 29 Jan.-15 Feb. (1974).

9. J.T.E.Nihoul, S.C.K.-C.E.N., Mol, Belgium, Proc. of a Symposium, VIENNA, 2-6 June (1969).

10. R.Vojan, Phys. Stat. Sol. 6, 925 (1964); 7, 299 (1964); and 8, 331 (1965).
11. W.Kohler and W.Schilling, Nukleonik 71, 384 (1965).

12. G.Burger et al., Phys. Stat. Sol. 4, 281 (1964).

13. K.Dettmann, Phys. Stat. Sol. 10, 269 (1965).

14. G.Luck and R.Sizmann, Phys. Stat. Sol.5, 683 (1964).

15. M.Balarin and O.Havser, Phys. Stat. Sol. 10, 475 (1965).

16. G.W.Iseler et al., Phys. Rev. 146, 468 (1966).

17. G.M.Mccracken, First–wall protection, Proc. of an IAEA Workshop Culham, United Kingdom, 29 Jan.-15 Feb. (1974).

18. G.L.Kulcinski, Proc. of an IAEA Workshop Culham, United Kingdom, 483, 29 Jan.-15 Feb. (1974).

19. Status reviews of 14 MeV neutron induced cross sections; measurements and calculations, INDC(NDS)-173/GJ, IAEA Nuclear data section, Vienna Sept. (1985).

20. i) N.Rohr, Nature 137, 344 (1936).

ii) A.Rohr and B.R.Mottelson, Ann. Rev. Nucl. Sci. 23, 363 (1973).

iii) C.Mahaux and H.A.Weidemuller, Ann. Rev. Nucl. Sci. 29, 1 (1979).

21. G.Friedlander,J.W.Kenneday,E.S.Macias and J.M.Miller, Nuclear and radiochemistry, John Willey and Sons., Inc.N.Y., 133, 3rd ed. (1981).

22. C.F.Von, Naturwissenschaften, 24, 813 (1936).

23. Merit Student's Encyclopaedia 13, 561 (1985).

24. R.A.Forrest, Harwell Report No. AERE-R-12419 (1986).

25. N. Banu, M.Sc Thesis, Dept. of Physics, Jahangirnagar University (1999).

26. C. Nesariya, K.H. Linse, S.Spellerberg, S. Sudar, A. Suhaimi and S.M. Qaim, J. Radiochim. Acta 86, 1-9 (1999).

27. R.U. Miah, Ph.D Thesis, Dhaka University (1996).

28. H.Kalka, A model for statistical multistep reactions (code EXIFON) INDC(GDR)-060/L, Sept. (1990).

29. Z.Wenrong, L.Hanlin, Y.Weixiang and Y.Xialin, INDC (CPR)-16 (1989).

30. M.Belgaid and M.Asghar, J. App. Radi. And Isotopes, No. 12, Vol. 49, 1497-1503, Dec. (1998).

31. D.E.Cullen, N.Kocherov, P.K.Mclaughlen, IRDF[9], Internal report, IAEA-NDS-48, IAEA, Vienna (1982).

32. V.M.Bychkov, K.I.Zolotarey, A.B.Pashchenko, V.I.Plyaskin, Rept. INDC (CCP)-183/L (1982).

33. Ikeda et al., Activation cross section measurements for fusion reactor structural materials at neutron energy from 13.3 to 15.0 MeV using FNS facility, JAERI 1312, Japan atomic energy research inst., March (1988).

34. G. Erdtman, Neutron Act. Tables, Kernchemic in Einzeldarstellungen, Vol. 6 (1976).

35. N.Yamamuro, A Nuclear Cross Section Calculation System with Simplified Input Format, Version-II, SINCROS-II, JAERI-M, 90-006, NEANDC (J)-146/U, INDC (JPN)-133/L, Feb. (1990).

36. B.K.Sharma, Instrumental method of analysis, 219,14th ed. (1994).

37. Proc. of specialist's meeting on nuclear data for fusion neutronics, JAERI-M 86-029, Japan atomic energy research inst., March (1986).

38. M.S.Uddin, M.R.Zaman, R.U.Miah and N.I.Molla, Bangl. Chem. Soci. 23rd Conf., 32, 26-28 Jan. (2001).

39. M.S.Uddin, R.U.Miah, SK.A.Latif, S.M.Hossain, N.I.Molla and M.R.Zaman, J. Nucl. Sci. and App. (2001) (accepted).

40. M.S.Uddin, SK.A.Latif, M.Hossain, R.U.Miah, N.I.Molla, M.R.Zaman and M.D.Hossain, Jahan. Univ. Jour. Sci. Vol.24 (2001).

41. Handbook on nuclear activation data, IAEA, Vienna, Technical report series no. 273.

42. J.C.Laul, Neutron activaton analysis of geological materials, Atomic energy review 17, 2 (1979).

43. Manual of troubleshooting and upgrading of neutron generators, IAEA-TECDOC-913, International atomic energy agency, Nov. (1996).

44. Certificate of tritium source, Radioisotope center, POLATOM, Poland.

45. G.F.Knoll, Radiation detection and measurement, 2nd ed., John Wiley and Sons., New York (1989).

46. S.Nargolwalla and E.P.Przybylowicz, Activation analysis with neutron generators, 23, John Wiley and Sons, New York (1973).

47. S.Cierjacks (editor), Neutron sources for basic physics and applications, Pergamon press (1983).

48. J.Csikai, Handbook of fast neutron generators, Vol. I, CRC Press, Inc. (1987).

49. S.Glastone and A.Sesonske, Nuclear reactor eng., 3rd ed., CBS publisher and distributors, Dhelhi (1986).

50. H.J.Arnikar, Essential of nuclear chemistry, 434, 4th ed., Jan. (1995).

51. I.Kaplan, Nuclear physics, 129, 2nd ed., copyright (1962).

52. H.J.Arnikar, Essentials of nuclear chemistry, 318, 4th ed., Jan. (1995).

53. I.Kaplan, Nuclear physics, 411, 2nd ed., copyright (1962).

54. S.S.Kapoor and V.S.Ramamurthy, Nuclear radiation detectors, Wiley Eastern limited, New Delhi (1986).

55. H.A.Enge, Introduction to nuclear physics.

56. CANBERRA Product cataloge, 4, 10th ed., Addition Wisely.

57. A.P.Malvino, Electronic principles, Tata McGraw-Hill publishing company limited, New Delhi (1984).

58. D. De Soete, R.Gijbels and J.Hoste, Neutron activation analysis, John Wiley, New York (1972).

59. G.Bertolini and A.Coche, Semiconductor detectors, North-Holand, Amsterdam (1968)

60. CANBERRA Germanium detectors, User's Manual (1991).

61. R.L.Health, Gamma-ray spectrum catalogue, Ge and Si detector spectra, 4th ed., Original work published- March (1974), Electronic version with updated nuclear data and decay schemes added Sept. (1998).

62. G.Friedlander, J.W.Kenneday, E.S.Macias and J.M.Miller, Nuclear and radiochemistry, 610, 3rd ed. (1981).

63. H.Vonach, Nuclear data standards for nuclear measurements, Technical report series 227, 59 IAEA (1983).

64. Catalog, J-25 Neutron Generator.

65. KFA, FORSCHUNGSZENTRUM, Julich GmbH, Abteilung, Sicherheil and Strahlenschut, ASS-Bericht Nr. O510, 21, 4th ed. April (1990).

66. A.Martin and S.A.Harbison, An introduction to radiation protection, 159, 2nd ed. (1979).

67. Hand book on nuclear activation cross sections, Technical report series no. 156, IAEA, Vienna (1974).

68. M.Bormann and B.Lammers, Nucl. Phys., 195, A130(1969).

69. V.M.Bychkov, V.N.Manokhin, A.B.Pashchenko and V.I.Plyaskin, Cross section for the (n,p), (n,α) and (n,2n) threshold reactions, Rept. INDC (CCP)-146 / L J (1980).

70. S.Okumura, Nucl. Phys., 74, A93 (1967).

71. J.L.Perkin, Private communication, Quoted in rept. BNL-325, Suppl. 2 (1966).

72. D.M.Arnold and L.A.Rayburn, Bull. Am. Phys. Soc. 352, 9 (1964).

73. C.Philis, Dosimetry data file ENDF/B-5 (1979).

74. N.Ymamuro, A nuclear cross section calculation system with simplified Input-Format Version-I (SINCROS-I), JAERI-M, 88-140 (1988).

75. S.Igarashi, Program ELIESE-3 ; Program for calculation of the nuclear cross section by using local and non-local optical models and statistical model, JAERI 1224 (1977).

76. P.G.Young and E.D.Arther, GNASH ; A preequilibrium, Statistical nuclear- model code for calculation of cross sections and emission spectra, LA-6947 (1977).

77. P.D.Kunz, Distored wave code DWUCK4, University of Colorado (1974).

78. R.L.Walter and P.P.Guss, A global optical model for neutron scattering for $A > 53$ and 10 MeV $< E <$ 80 MeV, Proc. Int. Conf., Nuclear data for basic and applied sciences, Santa Fe, New Mexico, 1079 (1985).

79. D.Wilmore and P.E.Hodgson, Nucl. Phys. 673, 55 (1964).

80. A.Gilbert and A.G.W.Cameron, Can. J. Phys., 1446, 43 (1965).

81. S.F.Mughabghab, M.Divadeenam and N.E.Holden, Neutron cross sections, Vol. 1, Neutron resonance parameters and thermal cross sections, Part A, Z= 1-60 (1981).

82. S.Ijima, T.Yoshida, T.Aoki, T.Watanable and M.Sasaki, J. Nucl. Sci. Tech., 10, 21 (1984).

83. C.Kalbach and Z.Physik, 401, A 283 (1977).

APPENDICES

The essential steps and necessary data for the determination of neutron flux, cross sections and errors in cross section values only for zinc samples are as follows.

1 Neutron flux determination

The neutron flux at each sample position was determined using monitor reaction

$$^{27}Al(n,\alpha)^{24}Na$$

Where, half life of ^{24}Na = 15.02 hrs., E_γ= 1369 keV, I_γ= 100 %.

The cross sections of the monitor reaction at different energies were taken from the work of H. Vonach.

1.1 Data for determination of DPS needed to neutron flux measurement.

Sample position	Neutron energy (MeV)	Net area	Live time (sec)	$CPS = \frac{Area}{Live\ \ time}$	Gamma Ray Intensity I_γ	Efficiency ε	Half Life $T_{1/2}$ (sec)	$\lambda = \frac{0.693}{T_{1/2}}$ (s^{-1}) $\times 10^{-5}$	Decay time T_d (sec)	$DPS = \frac{CPS \times e^{\lambda t_d}}{\varepsilon \times I_\gamma}$
0°	14.71±0.11	9294	3600	2.5817	1	0.0143	54072	1.2816	19426	231.57
30°	14.63±0.11	9251	3600	2.5697	1	0.0143	54072	1.2816	23160	241.79
60°	14.41±0.08	8583	3600	2.3841	1	0.0143	54072	1.2816	26820	235.11
90°	14.10±0.04	2761	1500	1.8406	1	0.0143	54072	1.2816	29477	187.79
120°	13.82±0.06	1829	1500	1.2193	1	0.0143	54072	1.2816	31170	127.13

1.2 Data for determination of neutron flux.

Neutron energy (MeV)	DPS	Known cross section of monitor reaction (cm^2) $\times 10^{-27}$	Weight of Al-foil W (g)	Isotopic abundance F	Atomic Weight of Al M	Irradiation time t_i (sec)	Decay constant λ (s^{-1}) $\times 10^{-5}$	Number of target nuclide, ^{27}Al $N = \frac{W \times F \times 6.023 \times 10^{23}}{M}$ (atoms / mole)	Neutron Flux $\varphi = \frac{DPS}{N\sigma(1-e^{-\lambda t_i})}$ ($n\ cm^{-2}s^{-1}$)
14.71±0.11	231.5768	113.100	0.3828	1	26.98	10800	1.2816	8.545×10^{21}	1.854×10^{6}
14.63±0.11	241.7981	114.530	0.4143	1	26.98	10800	1.2816	9.248×10^{21}	1.766×10^{6}
14.41±0.08	235.1074	117.540	0.4074	1	26.98	10800	1.2816	9.094×10^{21}	1.702×10^{6}
14.10±0.04	187.7975	121.907	0.3408	1	26.98	10800	1.2816	7.608×10^{21}	1.566×10^{6}
13.82±0.06	127.1347	122.725	0.2451	1	26.98	10800	1.2816	5.471×10^{21}	1.465×10^{6}

2 Cross section determination for $^{64}Zn(n,p)^{64}Cu$ reaction.

2.1 Data for determination of corrected CPS related to cross section measurement.

Sample position	Neutron energy (MeV)	Live time t (sec)	Total area A	Background area B	Net area C=A-B	CPS correction factor D	Corrected $CPS = \frac{C}{t} \times D$
0°	14.71±0.11	3600	5607	292	5315	0.71875	1.0611
30°	14.63±0.11	7200	3853	584	3269	-	0.4540
60°	14.41±0.08	7200	3582	584	2997	-	0.4162
90°	14.10±0.04	3600	11467	292	11175	0.38235	1.1868
120°	13.82±0.06	3600	5326	292	5034	0.65789	0.9199

2.2 Data for determination of DPS needed to cross section measurements.

Neutron Energy (MeV)	CPS	Efficiency at 511 keV gamma energy ε	Gamma-ray Intensity I_γ	Half life of product nuclide, ^{64}Cu $T_{1/2}$ (sec)	Decay time of ^{64}Cu t_d (sec)	Decay constant $\lambda = \frac{0.693}{T_{1/2}}$ (s^{-1})	$e^{\lambda t_d}$	$DPS = \frac{CPS \times e^{\lambda t_d}}{\varepsilon \times I_\gamma}$
14.71±0.11	1.0611	0.03002	0.37	45864	15660	1.511×10^{-5}	1.266	120.930
14.63±0.11	0.4540	0.03002	0.37	45864	75228	1.511×10^{-5}	3.116	127.362
14.41±0.08	0.4162	0.03002	0.37	45864	82485	1.511×10^{-5}	3.477	130.222
14.10±0.04	1.1868	0.03002	0.37	45864	8340	1.511×10^{-5}	1.134	121.186
13.82±0.06	0.9199	0.03002	0.37	45864	12030	1.511×10^{-5}	1.199	99.310

2.3 Data for determination of cross section of $^{64}Zn(n,p)^{64}Cu$ reaction.

Neutron Energy (MeV)	Weight of sample W (g)	Mole-cular weight of ZnO M	Isotopic abundance of ^{64}Zn F	No. of target nuclide $N = \frac{W \times F \times 6.023 \times 10^{23}}{M}$	Decay const. λ (s^{-1}) $\times 10^{-5}$	DPS	Neutron flux φ $ncm^{-2}s^{-1}$ $\times 10^{6}$	Irrad-iation time t_i (sec)	Cross section $\sigma = \frac{DPS}{N\varphi(1-e^{-\lambda t_i})}$ (mb)
14.71±0.11	0.7366	81.37	0.489	2.666×10^{21}	1.511	120.930	1.854	10800	162.491
14.63±0.11	0.7835	81.37	0.489	2.835×10^{21}	1.511	127.362	1.766	10800	168.951
14.41±0.08	0.7761	81.37	0.489	2.809×10^{21}	1.511	130.222	1.702	10800	180.900
14.10±0.04	0.7708	81.37	0.489	2.789×10^{21}	1.511	121.186	1.566	10800	184.279
13.82±0.06	0.7216	81.37	0.489	2.612×10^{21}	1.511	99.310	1.465	10800	172.364

3 Error calculation

The errors in measured cross section values were determined considering both systematic and statistical errors. The systematic errors of the investigated reactions are given in Table 2.10. As an example, the error calculation only for $^{64}Zn(n,p)^{64}Cu$ reaction at 14.71 MeV is shown below.

Total error in quadrature = [(statistical error)^2 + (systematic error)^2]$^{1/2}$

The statistical error is given by

$$E_{st} = \sqrt{\frac{(\sigma_i - \bar{\sigma})}{N-1}}$$

Where, σ_i = Cross section value

$\bar{\sigma}$ = Average cross section

N = Number of cross section values

We have taken three cross section values from three times counting and obtained statistical error 5.835 % for the cross section 162.491 mb at 14.71 MeV neutron energy.

Systematic error

$$= [2^2 + 1^2 + (2.56)^2 + (2.25)^2 + (0.5)^2 + (0.5)^2 + 1^2 + 1^2 + (0.65)^2 + (0.65)^2 + (0.75)^2]^{\frac{1}{2}}$$

=4.530 %

Total error =$[(5.835)^2 + (4.530)^2]^{\frac{1}{2}}$

= 7.387 %

$$\text{Error for } 162.491 \text{ mb} = \frac{162.491}{100} \times 7.387$$

$$= 12.0032 \text{ mb}$$

For all of the investigated reactions, the similar procedure was followed to determine errors in measured cross section values of the selected neutron energy.

List of Papers Accepted for Publication Based on the Present Work

1. M.S. Uddin, Sk. A. Latif, M. Hossain, R.U. Miah, N.I. Molla, M.R. Zaman and M.D. Hossain, Excitation Function Measurement of the $^{70}Ge(n,2n)^{69}Ge$ Reaction over the Neutron Energy Range 13.90-14.70 MeV, Jahan. Univer. Jour. Science, Vol. 24, 2001.

2. M.S. Uddin, R.U. Miah, Sk. A. Latif, S. M. Hossain, N. I. Molla and M.R. Zaman, Excitation Function of Neutron Induced Reaction $^{64}Zn\ (n,p)^{64}Cu$ in the Energy Range 13.82 to 14.71 MeV, J. Nuel. Sci. and App., 2001.